Chapter 3
Resonances and Threshold Behaviour

We consider in this chapter the theory of resonance reactions and the closely related behaviour of cross sections near threshold. Our treatment will concentrate on theoretical methods that have found wide applicability in atomic and molecular collision processes. For example, we will see in Chap. 5 that resonances play a crucial role in low-energy electron collisions with multi-electron atoms and atomic ions, where effective collision strengths can be increased by an order of magnitude or more at low temperatures by resonance processes. We will also see in later chapters that resonances are important in electron impact ionization, in single- and multiphoton ionization processes, in photorecombination and in electron–molecule collisions. Hence, understanding and interpreting resonances in collision processes are important goals for theory and their detailed and accurate prediction provides a challenge for computational methods.

A fundamental approach to the study of resonances and threshold behaviour is through an analysis of the analytic properties of the S-matrix or collision matrix introduced by Wheeler [961] and Heisenberg [452]. We have already defined the S-matrix in Chaps. 1 and 2 in terms of the asymptotic form of the radial wave function describing electron collisions with atoms and atomic ions. We have also considered in Sect. 1.3 the analytic properties of the single-channel S-matrix which arises in potential scattering. We found in that section that bound states and resonances are closely related to poles in the S-matrix in the complex momentum plane. In this chapter we extend our discussion of S-matrix theory to multichannel resonances and threshold behaviour.

We commence in Sect. 3.1 by generalizing our discussion of the analytic properties of the S-matrix in Sect. 1.3 by defining multichannel Jost functions in terms of the solutions of coupled second-order integrodifferential equations (2.63) which describe electron collisions with multi-electron atoms and atomic ions. By expressing the S-matrix in terms of Jost functions we can then relate the analytic properties of the S-matrix in the multi-Riemann-sheeted complex energy plane to the simpler analytic properties of the Jost functions. This provides the basis for discussing the distribution of bound-state and resonance poles in the S-matrix in the complex energy plane.

In Sect. 3.2 we derive explicit expressions for the K-matrix and S-matrix in the neighbourhood of an isolated resonance pole using a theoretical approach

P.G. Burke, *R-Matrix Theory of Atomic Collisions*, Springer Series on Atomic, Optical, and Plasma Physics 61, DOI 10.1007/978-3-642-15931-2_3,

introduced by Brenig and Haag [137] and Fano [301]. In this approach, a zero-order Hamiltonian is defined which can be solved exactly in terms of discrete and continuum states. The full Hamiltonian then mixes these states giving rise to resonances in the S-matrix and we obtain expressions for the individual eigenphases and the eigenphase sum in the neighbourhood of a resonance. We also discuss the time-delay matrix, first introduced by Smith [881], and we relate the trace of this matrix to the derivative of the eigenphase sum with respect to energy. We then show that this quantity can often provide an accurate procedure for analysing overlapping resonances. We also consider in this section, the projection operator approach of Feshbach [320, 321], which provides a powerful framework for describing resonance phenomena in a wide range of atomic, molecular and nuclear collision processes. Finally, we discuss the hyperspherical system of coordinates which has been important in the analysis of resonances and threshold behaviour of three-body systems, such as two electrons in a Coulomb field and three-nucleon molecules such as H_3^+, as well as in the general description of the three-body problem.

In Sect. 3.3, we consider the threshold behaviour of excitation and ionization cross sections. This behaviour was investigated in a fundamental paper by Wigner [970] who showed that the analytic behaviour of cross sections near threshold depends, apart from a constant, on the form of the long-range interaction between the particles. We consider first two-body collision processes where we use the analytic properties of the multichannel R-matrix, discussed in Chap. 5, to derive a multichannel effective range theory for short-range potentials, following the work of Ross and Shaw [798]. We then extend this theory to treat long-range dipole potentials considered by Gailitis and Damburg [359] and a Coulomb potential considered by Gailitis [357]. We also discuss multichannel quantum defect theory (MQDT) introduced, developed and reviewed by Seaton [859], and we summarize the extension of MQDT to molecular collision processes first considered by Fano [303]. Finally, we consider the threshold law of electron impact ionization of atoms and positive ions first derived by Wannier [954, 955]. In this analysis we adopt the hyperspherical system of coordinates, introduced in Sect. 3.2.6.

3.1 Analytic Properties of the S-Matrix

In this section we generalize our discussion of the analytic properties of the S-matrix in potential scattering given in Sect. 1.3 to multichannel collisions. As in Chap. 2 we illustrate this discussion by considering low-energy elastic and inelastic electron collisions with multi-electron atoms and atomic ions described by

$$e^- + A_i \rightarrow A_j + e^-, \tag{3.1}$$

where A_i and A_j are the initial and final bound states of the target. We consider the solution of the n coupled second-order integrodifferential equations (2.63), which describe these collisions for a given set of conserved quantum numbers. We rewrite

these equations using matrix notation as follows:

$$\left(\frac{\mathrm{d}^2}{\mathrm{d}r^2} - \frac{\boldsymbol{\ell}(\boldsymbol{\ell}+\mathbf{I})}{r^2} + \frac{2(Z-N)}{r} - \mathbf{U}(r) + \mathbf{k}^2\right)\mathbf{F}(r) = 0, \tag{3.2}$$

where Z is the nuclear charge number, N is the number of target electrons, $\mathbf{U}$ is an $n \times n$-dimensional matrix representing the sum of the local direct, non-local exchange and non-local correlation potentials $2(\mathbf{V}+\mathbf{W}+\mathbf{X})$ in (2.63), $\mathbf{I}$ is the $n \times n$-dimensional unit matrix and $\boldsymbol{\ell}$ and $\mathbf{k}^2$ are $n \times n$-dimensional diagonal matrices representing the channel orbital angular momenta and wave numbers squared, respectively. We note that in (3.2) we have not imposed the orthogonality constraints defined by (2.62). Hence the Lagrange multiplier terms in (2.63) and the additional quadratically integrable functions included in the original expansion (2.57) for completeness are not required. However, as pointed out following (2.87), the relaxation of these constraints does not affect the K-matrix, S-matrix and scattering amplitudes and hence the analytic properties of the S-matrix considered here.

We find it convenient, as in Sect. 2.4, to order the target eigenstates and pseudostates retained in expansion (2.57) so that their energies defined by (2.5) are in increasing order. It follows that the corresponding channel wave numbers squared k_i^2, defined by (2.7), satisfy (2.78) when the total energy E is real. Initially we limit our discussion to neutral atomic targets where the nuclear charge number Z equals the number of target electrons N. It then follows from (2.73) that the leading term in the long-range potential experienced by the scattered electron is $\sim r^{-2}$. Later in this chapter we will consider electron collisions with atomic ions where a long-range Coulomb potential is also present.

In analogy with our consideration of the analytic properties of the S-matrix in potential scattering, discussed in Sect. 1.3, we define, following Jost [515], two linearly independent matrix solutions $\mathbf{f}(\pm\mathbf{k}, r)$ of (3.2) by the asymptotic boundary conditions

$$\lim_{r\to\infty} \exp(\pm \mathrm{i}\mathbf{k}r)\mathbf{f}(\pm\mathbf{k}, r) = \mathbf{I}, \tag{3.3}$$

where the diagonal elements of $\mathbf{k}$ are defined by (2.7) and where the total energy E can now be complex. Also $\mathbf{f}(\pm\mathbf{k}, r)$ are diagonal $n \times n$-dimensional matrices in the limit $r \to \infty$ but, as shown below, are in general non-diagonal for finite values of r. For potentials which occur in electron–atom collisions, the boundary conditions (3.3) define $\mathbf{f}(\mathbf{k}, r)$ uniquely for $\mathrm{Im}\, k_i < 0$ and $\mathbf{f}(-\mathbf{k}, r)$ uniquely for $\mathrm{Im}\, k_i > 0$ for $i = 1, \ldots, n$. If we can impose stronger conditions on the potentials V_{ij}, W_{ij} and X_{ij} in (2.63) then the functions $\mathbf{f}(\pm\mathbf{k}, r)$ can be analytically continued outside of these regions, as discussed in Sect. 1.3 in the case of potential scattering.

The physical solutions of (3.2) which vanish at the origin can be expressed as linear combinations of the functions $\mathbf{f}(\pm\mathbf{k}, r)$. Let us normalize these physical solutions so that they satisfy the following boundary condition at the origin:

$$\lim_{r\to 0} r^{-\boldsymbol{\ell}-\mathbf{I}}\mathbf{F}(\mathbf{k}, r) = \mathbf{I}, \tag{3.4}$$

where $\boldsymbol{\ell}$ is the $n \times n$-dimensional diagonal matrix whose diagonal elements are ℓ_i, $i = 1, \ldots, n$ and where we have introduced the $n \times n$-dimensional solution matrix $\mathbf{F}(\mathbf{k}, r)$ which is diagonal in the limit $r \to 0$ but is in general non-diagonal for non-zero values of r. The second subscript k on this solution matrix F_{ik} runs from 1 to n and denotes the n linearly independent solutions of (3.2) which are defined by the boundary conditions (3.4). These solutions form a complete set of solutions which vanish at the origin. The boundary condition (3.4), which does not depend on $\mathbf{k}$, then ensures that, as in potential scattering, $\mathbf{F}(\mathbf{k}, r)$ is an entire function of $\mathbf{k}$. We then define the multichannel Jost function matrices $\tilde{\mathbf{f}}(\pm\mathbf{k})$ by the Wronskian

$$\tilde{\mathbf{f}}(\pm\mathbf{k}) = W[\mathbf{f}(\pm\mathbf{k}, r), \mathbf{F}(\mathbf{k}, r)], \tag{3.5}$$

where $\tilde{\mathbf{f}}(\pm\mathbf{k})$ are $n \times n$-dimensional matrices. Also in (3.5) we have defined the Wronskian of any two solution vectors $\mathbf{u}$ and $\mathbf{v}$ by

$$W[\mathbf{u}, \mathbf{v}] = \mathbf{u}^{\mathrm{T}}\mathbf{v}' - \mathbf{u}'^{\mathrm{T}}\mathbf{v}, \tag{3.6}$$

where $\mathbf{u}^{\mathrm{T}}$ is the transpose of $\mathbf{u}$ and the prime denotes the derivative with respect to r. It is straightforward to show that the Wronskian is independent of r.

We now use the relations

$$W[\mathbf{f}(\pm\mathbf{k}, r), \mathbf{f}(\mp\mathbf{k}, r)] = \pm 2\mathrm{i}\mathbf{k} \tag{3.7}$$

and

$$W[\mathbf{f}(\pm\mathbf{k}, r), \mathbf{f}(\pm\mathbf{k}, r)] = 0, \tag{3.8}$$

which follow from (3.3), to write $\mathbf{F}(\mathbf{k}, r)$ in the form

$$\mathbf{F}(\mathbf{k}, r) = (2\mathrm{i})^{-1}[\mathbf{f}(-\mathbf{k}, r)\mathbf{k}^{-1}\tilde{\mathbf{f}}(\mathbf{k}) - \mathbf{f}(\mathbf{k}, r)\mathbf{k}^{-1}\tilde{\mathbf{f}}(-\mathbf{k})]. \tag{3.9}$$

If we compare this equation with the asymptotic form (2.110), we find that the S-matrix can be defined in terms of the Jost functions by

$$\mathbf{S}_n(\mathbf{k}) = \exp\left(\tfrac{1}{2}\mathrm{i}\pi\boldsymbol{\ell}\right)\mathbf{k}^{-1/2}\tilde{\mathbf{f}}(\mathbf{k})\tilde{\mathbf{f}}^{-1}(-\mathbf{k})\mathbf{k}^{1/2}\exp\left(\tfrac{1}{2}\mathrm{i}\pi\boldsymbol{\ell}\right), \tag{3.10}$$

where the subscript n on $\mathbf{S}_n$ refers to the dimension of the S-matrix and where in the following discussion we assume that all channels are open so that the number of open channels $n_a = n$ in (2.110). This equation enables the analytic properties of the S-matrix to be related to the simpler analytic properties of the Jost functions.

In order to study the analytic properties of the Jost functions we return to (3.2) satisfied by $\mathbf{f}(\pm\mathbf{k}, r)$. We assume that $\mathbf{f}(-\mathbf{k}, r)$ satisfies the equation

$$\left(\frac{\mathrm{d}^2}{\mathrm{d}r^2} - \frac{\boldsymbol{\ell}(\boldsymbol{\ell} + \mathbf{I})}{r^2} + \frac{2(Z - N)}{r} - \mathbf{U}(r) + \mathbf{k}^2\right)\mathbf{f}(-\mathbf{k}, r) = 0. \tag{3.11}$$

We then take the complex conjugate of this equation yielding

$$\left(\frac{\mathrm{d}^2}{\mathrm{d}r^2} - \frac{\boldsymbol{\ell}(\boldsymbol{\ell}+\mathbf{I})}{r^2} + \frac{2(Z-N)}{r} - \mathbf{U}(r) + \mathbf{k}^{*2}\right)\mathbf{f}^*(-\mathbf{k}, r) = 0, \tag{3.12}$$

where we assume that r, $\boldsymbol{\ell}$, Z, N and $\mathbf{U}$ are real but $\mathbf{k}$, which is defined in terms of the total energy E by (2.7), can be complex. In addition it follows, by replacing $-\mathbf{k}$ by $\mathbf{k}^*$ in (3.11), that $\mathbf{f}(\mathbf{k}^*, r)$ is a solution of

$$\left(\frac{\mathrm{d}^2}{\mathrm{d}r^2} - \frac{\boldsymbol{\ell}(\boldsymbol{\ell}+\mathbf{I})}{r^2} + \frac{2(Z-N)}{r} - \mathbf{U}(r) + \mathbf{k}^{*2}\right)\mathbf{f}(\mathbf{k}^*, r) = 0. \tag{3.13}$$

Hence $\mathbf{f}^*(-\mathbf{k}, r)$ and $\mathbf{f}(\mathbf{k}^*, r)$ satisfy the same differential equation and from (3.3) they satisfy the same boundary condition. Hence

$$\mathbf{f}^*(-\mathbf{k}, r) = \mathbf{f}(\mathbf{k}^*, r) \tag{3.14}$$

is satisfied for all points in the upper half k-plane with $\operatorname{Im} k_i > 0,\ i = 1, \ldots, n$, and for all other points in the complex k-plane for which the potential admits an analytic continuation from the upper half k-plane.

In a similar way, we can show from (3.11) and the boundary condition (3.4) satisfied by $\mathbf{F}(\mathbf{k}, r)$ that

$$\mathbf{F}^*(\mathbf{k}, r) = \mathbf{F}(\mathbf{k}^*, r) \tag{3.15}$$

and

$$\mathbf{F}(\mathbf{k}, r) = \mathbf{F}(-\mathbf{k}, r). \tag{3.16}$$

Using (3.14), (3.15) and (3.16), we find from (3.5) that the Jost functions satisfy

$$\tilde{\mathbf{f}}^*(-\mathbf{k}) = \tilde{\mathbf{f}}(\mathbf{k}^*). \tag{3.17}$$

Hence we obtain from (3.10)

$$\mathbf{S}_n^*(\mathbf{k}^*) = \exp(-\tfrac{1}{2}\mathrm{i}\pi\boldsymbol{\ell})\mathbf{k}^{-1/2}\tilde{\mathbf{f}}(-\mathbf{k})\tilde{\mathbf{f}}^{-1}(\mathbf{k})\mathbf{k}^{1/2}\exp(-\tfrac{1}{2}\mathrm{i}\pi\boldsymbol{\ell}). \tag{3.18}$$

Combining this equation with (3.10) gives

$$\mathbf{S}_n(\mathbf{k})\mathbf{S}_n^*(\mathbf{k}^*) = \mathbf{I}. \tag{3.19}$$

Also, as we have shown in Sect. 2.4, the K-matrix is symmetric and hence from (2.112) the S-matrix is also symmetric so that

$$\mathbf{S}_n(\mathbf{k}) = \mathbf{S}_n^{\mathrm{T}}(\mathbf{k}), \tag{3.20}$$

where $\mathbf{S}_n^{\mathrm{T}}$ denotes the transpose of $\mathbf{S}_n$. Hence it follows from (3.19) and (3.20) that

$$\mathbf{S}_n(\mathbf{k})\mathbf{S}_n^{\dagger}(\mathbf{k}^*) = \mathbf{I}, \tag{3.21}$$

where $\mathbf{S}_n^{\dagger}$ denotes the hermitian conjugate of $\mathbf{S}_n$. This is the generalization of the unitarity relation given by (1.97) for potential scattering.

A further analytic property of the S-matrix can be obtained by considering $\mathbf{S}_n^*(-\mathbf{k}^*)$. From (3.10) and (3.17) we obtain

$$\mathbf{S}_n^*(-\mathbf{k}^*) = \exp\left(-\tfrac{1}{2}\mathrm{i}\pi\boldsymbol{\ell}\right)\mathbf{k}^{-1/2}\tilde{\mathbf{f}}(\mathbf{k})\tilde{\mathbf{f}}^{-1}(-\mathbf{k})\mathbf{k}^{1/2}\exp\left(-\tfrac{1}{2}\mathrm{i}\pi\boldsymbol{\ell}\right). \tag{3.22}$$

Combining this equation with (3.10) and (3.20) yields

$$\mathbf{S}_n(\mathbf{k}) = \exp(\mathrm{i}\pi\boldsymbol{\ell})\mathbf{S}_n^{\dagger}(-\mathbf{k}^*)\exp(\mathrm{i}\pi\boldsymbol{\ell}), \tag{3.23}$$

which is the generalization of the reflection relation given by (1.98) in potential scattering.

It is useful at this point to discuss the continuation paths in the complex energy plane implied by relations (3.21) and (3.23). Since the k_i occur in the definition of the Jost functions given by (3.3) and (3.5) and hence in the S-matrix given by (3.10), the value of $\mathbf{S}_n(\mathbf{k})$ is only defined uniquely in terms of the total energy E of the electron–atom system if the sign ambiguities

$$k_i = \pm[2(E - e_i)]^{1/2}, \quad i = 1, \ldots, n, \tag{3.24}$$

which follow from (2.7), are resolved. These signs can be chosen in 2^n different ways and consequently the S-matrix can only be made single valued, or uniformized, by introducing 2^n Riemann sheets in the complex E-plane. We define these sheets in Fig. 3.1, by introducing n branch points $e_i, i = 1, \ldots, n$, with their associated branch cuts chosen to run in each case from $E = e_i$ along the real energy axis to $E = +\infty$. The physical sheet, which we denote by P, is defined by the condition

$$\operatorname{Im} k_i > 0, \quad i = 1, \ldots, n, \tag{3.25}$$

and the physical scattering region, which is illustrated in Fig. 3.1 by arrows, lies on the real energy axis, along the upper edge of the n branch cuts.

Following Eden and Taylor [283], we let U_m denote the unphysical sheet reached from the physical sheet by crossing the branch cuts in Fig. 3.1 which originate from the branch points e_i, $i = 1, \ldots, m$, where $1 \leq m \leq n$. We then find using (3.24) that on U_m

$$\begin{aligned} &\operatorname{Im} k_i < 0, \quad i = 1, \ldots, m, \\ &\operatorname{Im} k_i > 0, \quad i = m+1, \ldots, n. \end{aligned} \tag{3.26}$$

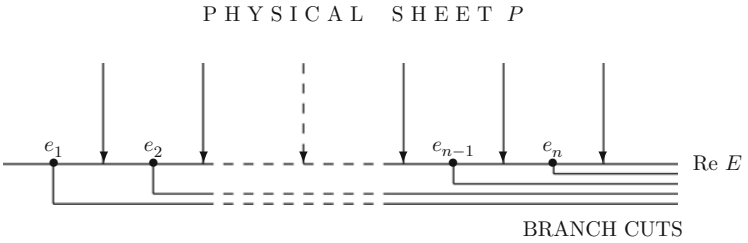

Fig. 3.1 The analytic properties of the multichannel S-matrix in the complex energy plane E, showing the branch points e_i, $i = 1, \ldots, n$, and the associated branch cuts starting from the branch points e_i (where the branch cuts are displaced from the real energy axis for clarity). Also shown is the physical sheet P and the paths, denoted by (*arrows*), from this sheet to reach the physical scattering region on the real energy axis

Furthermore, on the real energy axis between e_m and e_{m+1} k_i is real for $i = 1, \ldots, m$ and positive imaginary for $i = m + 1, \ldots, n$. Other unphysical sheets can be reached by following more complicated paths from the physical sheet so that all combinations of the signs of $\mathrm{Im}\, k_i$ can be achieved on these sheets.

As an example, when $n = 2$ there are $2^n = 4$ Riemann sheets, or three unphysical sheets in addition to the physical sheet. We show in Fig. 3.2 four continuation paths which enable E^* on the unphysical sheets and on the physical sheet to be reached from E on the physical sheet, where E^* denotes the complex conjugate of E. The path labelled (1) goes from E on P to E^* on U_1, the path labelled (2) goes from E on P to E^* on U_2, the path labelled (1,2) goes from E on P to E^* on $U_{1,2}$ and the path labelled (0) goes from E to E^* on the physical sheet P. It is clear from Fig. 3.2 that on $U_{1,2}$, $\mathrm{Im}\, k_1 > 0$ and $\mathrm{Im}\, k_2 < 0$. The signs of $\mathrm{Im}\, k_1$ and $\mathrm{Im}\, k_2$ for E^* on U_1 and U_2 are given by (3.26), while $\mathrm{Im}\, k_1 > 0$ and $\mathrm{Im}\, k_2 > 0$ on P.

Returning to the general case illustrated in Fig. 3.3 where there are n channels, we see that if the point represented by $\mathbf{k}$ in (3.21) and (3.23) lies on the physical sheet defined by (3.25) then the point represented by $\mathbf{k}^*$ lies on U_n defined by (3.26) with $m = n$. In addition, the point represented by $-\mathbf{k}^*$ lies on the physical sheet. Hence the unitarity relation (3.21) can be rewritten as

$$\mathbf{S}_n(E \text{ on } P)\mathbf{S}_n^\dagger(E^* \text{ on } U_n) = \mathbf{I}, \tag{3.27}$$

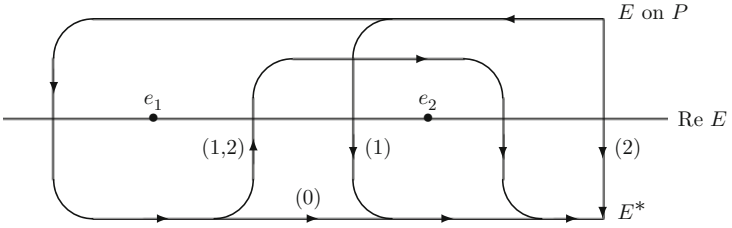

Fig. 3.2 The four continuation paths in the complex energy plane when $n = 2$ which enable E^* on the three unphysical sheets and on the physical sheet to be reached from E on the physical sheet denoted by P. The branch points are denoted by e_1 and e_2

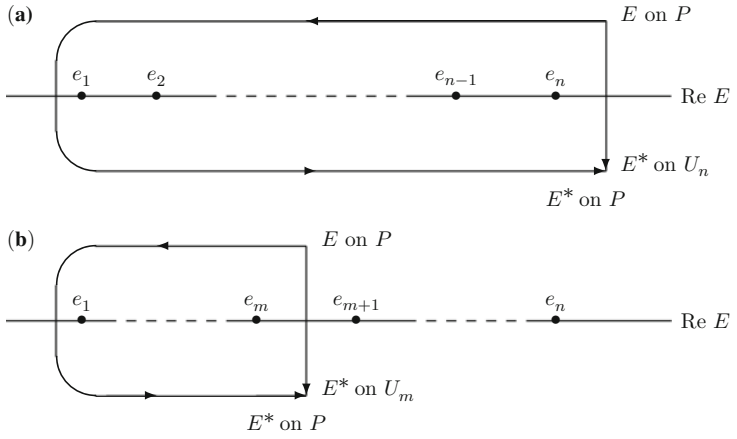

Fig. 3.3 Continuation paths in the complex energy plane when there are n non-degenerate channels, where P denotes the physical sheet and U_n and U_m denote unphysical sheets as explained in the text. The branch points are denoted by $e_i,\ i = 1, \ldots, n$

where E^* on U_n is reached by the path indicated in Fig. 3.3a. In a similar way, the reflection relation (3.23) can be rewritten as

$$\mathbf{S}_n(E \text{ on } P) = \exp(\mathrm{i}\pi\ell)\mathbf{S}_n^{\dagger}(E^* \text{ on } P)\exp(\mathrm{i}\pi\ell), \tag{3.28}$$

where E^* on P is reached by the path also indicated in Fig. 3.3a.

The above discussion can be generalized to determine the analytic properties of the S-matrix under the continuation paths indicated in Fig. 3.3b. Under the continuation from E on P to E^* on U_m we see from (3.26) that the k_i transform according to

$$\begin{aligned} k_i &\to k_i^*, \qquad i = 1, \ldots, m, \\ k_i &\to -k_i^*, \qquad i = m+1, \ldots, n. \end{aligned} \tag{3.29}$$

Hence (3.17) and (3.18) are no longer valid under this continuation and the unitarity relation (3.27) is not satisfied if U_n is replaced by U_m with $m < n$. However, we can show that the $m \times m$-dimensional leading submatrix of $\mathbf{S}_n$ which we call $\mathbf{S}_m$ does satisfy a generalized unitarity relation analogous to (3.27).

To prove this, we introduce an $n \times m$-dimensional solution matrix $\mathbf{G}(\mathbf{k}, r)$ of (3.11) by the equation

$$\mathbf{G}(\mathbf{k}, r) = \mathbf{F}(\mathbf{k}, r)\mathbf{A}(\mathbf{k}), \tag{3.30}$$

where $\mathbf{F}$ is the $n \times n$-dimensional solution matrix defined by (3.4) and $\mathbf{A}$ is an $n \times m$-dimensional matrix which is chosen so that $\mathbf{G}$ is real on the real energy axis in the range between e_m and e_{m+1} and so that in this energy range the exponentially increasing components in the last $n - m$ channels of $\mathbf{F}(\mathbf{k}, \mathbf{r})$ are eliminated. $\mathbf{G}(\mathbf{k}, r)$

thus corresponds to the physical solutions in the energy range $e_m \leq \mathrm{Re}E < e_{m+1}$, where m channels are open and $n-m$ channels are closed. It is then straightforward to show that (3.15), which can be rewritten as

$$\mathbf{F}(E \text{ on } P) = \mathbf{F}^*(E^* \text{ on } U_n), \tag{3.31}$$

is replaced by

$$\mathbf{G}(E \text{ on } P) = \mathbf{G}^*(E^* \text{ on } U_m). \tag{3.32}$$

We now introduce an $m \times m$-dimensional Jost function matrix by the equation

$$\tilde{\mathbf{f}}_m(\pm\mathbf{k}) = W[\mathbf{f}_m(\pm\mathbf{k}, r), \mathbf{G}(\mathbf{k}, r)], \tag{3.33}$$

where $\mathbf{f}_m(\pm\mathbf{k}, r)$ are the first m columns of the solutions defined by (3.3). Hence, in analogy with (3.9) we can write

$$\mathbf{G}(\mathbf{k}, r) = (2\mathrm{i})^{-1}[\mathbf{f}_m(-\mathbf{k}, r)\mathbf{k}_m^{-1}\tilde{\mathbf{f}}_m(\mathbf{k}) - \mathbf{f}_m(\mathbf{k}, r)\mathbf{k}_m^{-1}\tilde{\mathbf{f}}_m(-\mathbf{k})], \tag{3.34}$$

where $\mathbf{k}_m$ is an $m \times m$ diagonal matrix with diagonal elements $k_i, \quad i = 1, \ldots, m$. Comparing this equation with the asymptotic form (2.110) where $n_a = m$ gives immediately

$$\mathbf{S}_m(\mathbf{k}) = \exp\left(\tfrac{1}{2}\mathrm{i}\pi\boldsymbol{\ell}_m\right)\mathbf{k}_m^{-1/2}\tilde{\mathbf{f}}_m(\mathbf{k})\tilde{\mathbf{f}}_m^{-1}(-\mathbf{k})\mathbf{k}_m^{1/2}\exp\left(\tfrac{1}{2}\mathrm{i}\pi\boldsymbol{\ell}_m\right), \tag{3.35}$$

where $\boldsymbol{\ell}_m$ is the $m \times m$ diagonal matrix with diagonal elements $\ell_i, i = 1, \ldots, m$. We can then show from the analytic properties of $\mathbf{f}_m(\pm\mathbf{k}, r)$ and $\mathbf{G}(\pm\mathbf{k}, r)$ that

$$\mathbf{S}_m(E \text{ on } P)\mathbf{S}_m^\dagger(E^* \text{ on } U_m) = \mathbf{I}. \tag{3.36}$$

This is the generalization of the unitarity relation given by (3.27). Equation (3.36), together with the generalization of the reflection relation (3.28), which can be written as

$$\mathbf{S}_m(E \text{ on } P) = \exp(\mathrm{i}\pi\boldsymbol{\ell}_m)\mathbf{S}_m^\dagger(E^* \text{ on } P)\exp(\mathrm{i}\pi\boldsymbol{\ell}_m), \tag{3.37}$$

defines the analytic properties of the $m \times m$-dimensional submatrix $\mathbf{S}_m$.

3.2 Bound States and Resonances

In this section we commence our discussion of bound-state and resonance poles in the S-matrix for multichannel collisions by considering their distribution in the multi-Riemann-sheeted complex energy plane. We then derive an explicit

expression for the multichannel K-matrix and S-matrix in the neighbourhood of an isolated resonance pole using a theoretical approach introduced by Brenig and Haag [137] and Fano [301]. We also derive an expression for the behaviour of the eigenphases near this resonance. We then introduce the projection operator approach of Feshbach [320, 321], used initially to describe nuclear resonance reactions, which has provided a powerful framework for describing resonance phenomena in atomic and molecular collision processes. Finally, we mention that early applications of these theories in electron and photon collisions with atoms and molecules were reviewed by Burke [151, 153].

3.2.1 Bound-State and Resonance Poles in the S-Matrix

In order to discuss the distribution of bound-state and resonance poles in the complex energy plane we consider (3.9) and (3.10) which express, respectively, the physical solution and the S-matrix in terms of the Jost function matrices $\mathbf{f}(\pm\mathbf{k}, r)$ and $\tilde{\mathbf{f}}(\pm\mathbf{k})$. We first diagonalize the $n\times n$-dimensional matrix $\tilde{\mathbf{f}}(-\mathbf{k})$ by the similarity transformation

$$\mathbf{X}^{-1}\tilde{\mathbf{f}}(-\mathbf{k})\mathbf{X} = \mathbf{D}, \tag{3.38}$$

where $\mathbf{D}$ is a diagonal $n \times n$-dimensional matrix. Let us assume that one of the diagonal elements of $\mathbf{D}$, say the first $d_1(E)$, has a simple zero at some energy E_p. It follows that $\tilde{\mathbf{f}}^{-1}(-\mathbf{k})$ and, hence from (3.10), $\mathbf{S}_n(\mathbf{k})$ are both singular with simple poles at $E = E_p$. We substitute (3.38) into (3.9) and postmultiply by $\mathbf{X}$ yielding

$$\mathbf{F}\mathbf{X} = (2\mathrm{i})^{-1}[\mathbf{f}(-\mathbf{k}, r)\mathbf{k}^{-1}\tilde{\mathbf{f}}(\mathbf{k})\mathbf{X} - \mathbf{f}(\mathbf{k}, r)\mathbf{k}^{-1}\mathbf{X}\mathbf{D}]. \tag{3.39}$$

Since $d_1(E_p) = 0$, the first column of $\mathbf{f}(\mathbf{k}, r)\mathbf{k}^{-1}\mathbf{X}\mathbf{D}$ vanishes when $E = E_p$. Hence the corresponding solution can be written as

$$\mathbf{F}\mathbf{x}_1 = (2\mathrm{i})^{-1}\mathbf{f}(-\mathbf{k}, r)\mathbf{k}^{-1}\tilde{\mathbf{f}}(\mathbf{k})\mathbf{x}_1, \quad E = E_p, \tag{3.40}$$

where the vector $\mathbf{x}_1$ is the first column of $\mathbf{X}$. It follows from (3.3) that at a pole in the S-matrix

$$\mathbf{F}\mathbf{x}_1 \underset{r\to\infty}{\sim} \mathrm{e}^{\mathrm{i}\mathbf{k}r}\mathbf{N}, \quad E = E_p, \tag{3.41}$$

where the normalization vector $\mathbf{N} = (2\mathrm{i}\mathbf{k})^{-1}\tilde{\mathbf{f}}(\mathbf{k})\mathbf{x}_1$. This equation is the multichannel generalization of (1.100).

If the energy E_p lies on the physical sheet of the complex energy plane then conditions (3.25) are satisfied. Consequently, the physical solution (3.41) vanishes asymptotically and hence is normalizable. Since the Hamiltonian is Hermitian, all normalizable wave functions must belong to real energy eigenvalues. Hence poles in

the S-matrix on the physical sheet must lie on the real energy axis. If this real energy lies below the first threshold $E < e_1$, then it follows from (3.24) and (3.25) that

$$k_i = +\mathrm{i}\kappa_i = +\mathrm{i}[2(e_i - E)]^{1/2}, \quad i = 1, \ldots, n, \tag{3.42}$$

where the κ_i are real and positive. Hence the solution defined by (3.41) has the asymptotic form

$$\mathbf{F}\mathbf{x}_1 \underset{r\to\infty}{\sim} \mathrm{e}^{-\boldsymbol{\kappa} r}\mathbf{N}, \quad E = E_p, \tag{3.43}$$

where $\boldsymbol{\kappa}$ is an $n \times n$-dimensional diagonal matrix with diagonal elements κ_i, $i = 1, \ldots, n$. Since the solution corresponding to (3.43) is normalizable it clearly corresponds to a bound state. We illustrate the position of such bound-state poles by crosses in Fig. 3.4.

In certain circumstances poles in the S-matrix can lie on the real energy axis with $E > e_1$. Consider, for example, real energies in the range $e_m < E < e_{m+1}$. Poles can lie in this range of energies if the channels with threshold energies e_i, $i = 1, \ldots, m$, are not coupled to the channels with threshold energies e_i, $i = m+1, \ldots, n$. This occurs, for example, if these two sets of channels have a different conserved quantum number such as parity and hence are not coupled by the Hamiltonian. In this case the $n \times n$-dimensional S-matrix $\mathbf{S}_n$ can be partitioned into disconnected sub-matrices as follows:

$$\mathbf{S}_n = \begin{bmatrix} \mathbf{S}_m & 0 \\ 0 & \mathbf{S}_{n-m} \end{bmatrix}, \tag{3.44}$$

where $\mathbf{S}_m$ has dimension $m \times m$ and $\mathbf{S}_{n-m}$ has dimension $(n-m) \times (n-m)$. From the generalized unitarity relation (3.36), $\mathbf{S}_m$ must be unitary and hence non-singular in this range of energies. However, a pole can occur in $\mathbf{S}_{n-m}$. A pole of this type corresponds to a bound state lying in the continuum and is denoted by an open circle in Fig. 3.4.

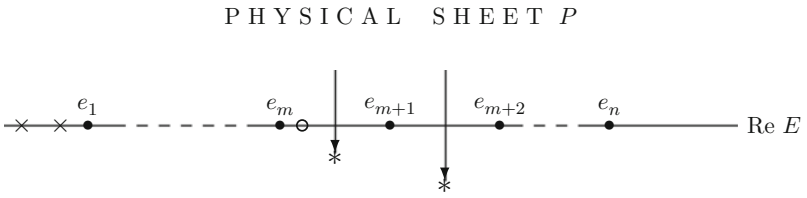

Fig. 3.4 Distribution of S-matrix poles in the complex energy plane. $\times$, bound-state poles lying on the physical sheet; $\circ$, bound-state pole lying in the continuum on the real energy axis; $*$, resonance poles lying on unphysical sheets U_m and U_{m+1}. The *arrows* denote the continuation paths from the physical sheet P to the resonance poles. The branch points are denoted by e_i, $i = 1, \ldots, n$

In the general case, when all n channels are coupled by the Hamiltonian, poles cannot occur in the S-matrix for real energies with $E > e_1$ corresponding to the physical scattering region, except in very exceptional circumstances. This is because the unitarity equation (3.36) would then be violated. However poles can occur on any of the unphysical sheets U_m since the sign of at least one $\mathrm{Im}\, k_i,\ i = 1, \ldots, n$, is then negative and hence from (3.41) the corresponding wave function is then not normalizable. If such poles lie close to the physical scattering region they give rise to observable effects and are called resonance poles and the corresponding wave functions, which satisfy outgoing wave boundary conditions, are often called Siegert states [876]. We define the real and imaginary parts of the energy of such a pole by

$$E_p = E_r - \frac{1}{2}\mathrm{i}\Gamma, \quad \text{on } U_m, \tag{3.45}$$

where E_r and Γ are both real and Γ is small and positive. Poles of this type are denoted by an asterisk in Fig. 3.4. We also denote by arrows in this figure the continuation paths from the physical sheet to these resonance poles. The generalized unitarity relation (3.36) shows that at the corresponding energies

$$E_p^* = E_r + \frac{1}{2}\mathrm{i}\Gamma, \quad \text{on } P, \tag{3.46}$$

one of the eigenvalues of $\mathbf{S}_m$ has a simple zero, that is the rank of $\mathbf{S}_m$ is $m - 1$. Eden and Taylor [283] have shown that the presence of a resonance pole on U_m usually also implies the presence of "shadow poles" on other Riemann sheets of the complex energy plane which are further removed from the physical scattering region. These shadow poles can play a role in a number of applications such as dissociative attachment and multiphoton ionization discussed in later chapters in this monograph.

Finally, we note that the preceding discussion was based on the assumption that bound-state and resonance poles in the S-matrix are simple. Although there is no general principle that guarantees that all such poles are simple, in practice this is usually the case. However, in atomic multiphoton processes, discussed in Chap. 9, laser induced degenerate states, or LIDS, corresponding to double poles in the S-matrix have been found in detailed calculations (see Sect. 9.2.3). If the S-matrix does contain a double pole in the complex energy plane then the main effects will be to distort the shape of the associated resonance profile from that considered in the next section and to produce a decay which deviates from the usual exponential behaviour. These effects have been considered by Goldberger and Watson [387], Newton [683] and Kylstra and Joachain [557].

3.2.2 Behaviour of the S-Matrix Near a Resonance

In this section we derive explicit expressions for the behaviour of the multichannel K-matrix and S-matrix in the physical scattering region near an isolated resonance pole lying on an adjacent unphysical sheet of the complex energy plane. We also

derive expressions for the behaviour of the eigenphases in the neighbourhood of a resonance. This was originally discussed by Brenig and Haag [137] and by Fano [301] and we consider here the configuration interaction theory of Fano.

Following Sect. 3.1, we consider low-energy elastic and inelastic electron collisions with multi-electron atoms and atomic ions containing N electrons and we analyse the interaction of one discrete state with n continuum states. We sub-divide configuration space into a zero-order discrete state, represented by a quadratically integrable function $\chi_0^0(\mathbf{X}_{N+1})$, which gives rise to the resonance, and n zero-order continuum states $\psi_{jE}^0(\mathbf{X}_{N+1})$, $j = 1, \ldots, n$, which do not have resonances or thresholds in the energy range of interest. We can expand these zero-order continuum states as

$$\begin{aligned}\psi_{jE}^0(\mathbf{X}_{N+1}) = \mathcal{A}\sum_{i=1}^{n}\overline{\Phi}_i(\mathbf{X}_N;\hat{\mathbf{r}}_{N+1}\sigma_{N+1})r_{N+1}^{-1}F_{ij}^0(r_{N+1}) \\ + \sum_{i=1}^{m}\chi_i^0(\mathbf{X}_{N+1})b_{ij}^0, \quad j = 1, \ldots, n,\end{aligned} \tag{3.47}$$

where we have adopted a notation analogous to expansion (2.57) and where the superscript Γ, which denotes the conserved quantum numbers, has been omitted for notational convenience. It is convenient in the following analysis to include only the n open channels in the first expansion in (3.47). The χ_i^0, $i = 1, \ldots, m$, in the second expansion are then zero-order quadratically integrable functions, which represent the effect of the closed channels whose thresholds lie above the energy range of interest.

We can now assume, without approximation, that these zero-order states satisfy the orthonormality relations

$$\begin{aligned}\langle\chi_0^0|\chi_0^0\rangle &= 1, \\ \langle\chi_0^0|\psi_{jE}^0\rangle &= 0, \quad j = 1, \ldots, n, \\ \langle\psi_{jE}^0|\psi_{j'E'}^0\rangle &= \delta_{jj'}\delta(E - E'), \quad j, j' = 1, \ldots, n.\end{aligned} \tag{3.48}$$

We also define the matrix elements of the $(N + 1)$-electron Hamiltonian H_{N+1} in this zero-order basis by the equations

$$\begin{aligned}\langle\chi_0^0|H_{N+1}|\chi_0^0\rangle &= E_0, \\ \langle\chi_0^0|H_{N+1}|\psi_{jE}^0\rangle &= V_j(E), \quad j = 1, \ldots, n, \\ \langle\psi_{jE}^0|H_{N+1}|\psi_{j'E'}^0\rangle &= E\delta_{jj'}\delta(E - E'), \quad j,\ j' = 1, \ldots, n,\end{aligned} \tag{3.49}$$

where we choose real asymptotic boundary conditions for the radial functions $F_{ij}^0(r)$ in (3.47) so that the $V_j(E)$ are real. The assumption made in the last of Eqs. (3.49), that the Hamiltonian is prediagonalized in the subspace spanned by the zero-order continuum states, is inessential and has been relaxed by Fano and Prats [309].

We introduce n new continuum basis states θ_{jE}, $j = 1, \ldots, n$, which are linear combinations of the basis ψ^0_{jE}, chosen so that only the first, θ_{1E}, interacts through the Hamiltonian with the discrete state χ^0_0. We define

$$\theta_{iE} = \sum_{j=1}^{n} \psi^0_{jE} U_{ji}(E), \quad i = 1, \ldots, n, \tag{3.50}$$

where $\mathbf{U}$ is an orthogonal matrix whose first column is defined by

$$U_{j1}(E) = V_j(E) \left[\sum_{i=1}^{n} V_i(E)^2 \right]^{-1/2}, \quad j = 1, \ldots, n, \tag{3.51}$$

while the remaining $n - 1$ columns are orthonormal and are orthogonal to the first column but are otherwise arbitrary. In terms of this new basis, Eqs.(3.49) are replaced by

$$\begin{aligned} \langle \chi^0_0 | H_{N+1} | \chi^0_0 \rangle &= E_0, \\ \langle \chi^0_0 | H_{N+1} | \theta_{jE} \rangle &= V(E)\delta_{j1}, \quad j = 1, \ldots, n, \\ \langle \theta_{jE} | H_{N+1} | \theta_{j'E'} \rangle &= E\delta_{jj'}\delta(E - E'), \quad j, j' = 1, \ldots, n, \end{aligned} \tag{3.52}$$

where we have introduced the real quantity

$$V(E) = \left[\sum_{i=1}^{n} V_i(E)^2 \right]^{1/2}, \tag{3.53}$$

which is a measure of the strength of the interaction of the discrete state with the continuum.

The eigensolutions of the Schrödinger equation which diagonalize the Hamiltonian can now be expanded in terms of these new zero-order states as follows:

$$\begin{aligned} \Psi_{1E} &= \int \theta_{1E'} a(E, E') \mathrm{d}E' + \chi^0_0 b(E), \\ \Psi_{jE} &= \theta_{jE}, \quad j = 2, \ldots, n, \end{aligned} \tag{3.54}$$

where the coefficients $a(E, E')$ and $b(E)$ are determined by projecting the Schrödinger equation

$$(H_{N+1} - E)\Psi_{1E} = 0 \tag{3.55}$$

onto the zero-order basis states θ_{1E} and χ^0_0. We obtain

$$\begin{aligned} \langle \theta_{1E'} | H_{N+1} - E | \Psi_{1E} \rangle &= 0, \\ \langle \chi^0_0 | H_{N+1} - E | \Psi_{1E} \rangle &= 0. \end{aligned} \tag{3.56}$$

Substituting for Ψ_{1E} from (3.54) into (3.56) and using (3.48) and (3.52), then gives

$$E'a(E,E') + V(E')b(E) = Ea(E,E'),$$
$$\int V(E')a(E,E')\mathrm{d}E' + E_0 b(E) = Eb(E). \tag{3.57}$$

The first equation in (3.57) can be formally solved for $a(E, E')$ yielding

$$a(E,E') = \left[\frac{\mathcal{P}}{E-E'} + z(E)\delta(E-E')\right]V(E')b(E), \tag{3.58}$$

where $\mathcal{P}$ is the principal value integral and $z(E)$ is then obtained by substituting (3.58) for $a(E, E')$ into the second equation in (3.57). We obtain

$$z(E) = \frac{E - E_0 - \Delta(E)}{V(E)^2}, \tag{3.59}$$

where we have introduced the quantity

$$\Delta(E) = \mathcal{P}\int \frac{V(E')^2}{E-E'}\mathrm{d}E', \tag{3.60}$$

which is called the resonance shift.

In order to determine the K-matrix and S-matrix for the interacting system, we assume that the zero-order reduced radial wave function matrix $\mathbf{F}^0$ in (3.47) satisfies the real K-matrix asymptotic boundary conditions

$$\mathbf{F}^0(r) \underset{r\to\infty}{\sim} \left(\frac{2}{\pi\mathbf{k}}\right)^{1/2}(\sin\boldsymbol{\theta} + \cos\boldsymbol{\theta}\mathbf{K}_0)(\mathbf{I}+\mathbf{K}_0^2)^{-1/2}. \tag{3.61}$$

In this equation $\mathbf{F}^0$ is an $n \times n$-dimensional matrix, $\mathbf{k}$ and $\boldsymbol{\theta}$ are diagonal matrices, where the diagonal elements of $\boldsymbol{\theta}$ are defined by (2.82), (2.83) and(2.84), and $\mathbf{K}_0$ is the multichannel zero-order $n \times n$-dimensional K-matrix obtained in the absence of the interaction between the zero-order discrete state and the continuum states. In analogy with our discussion in Sect. 1.1, see (1.21), the coefficient $(2/\pi\mathbf{k})^{1/2}$ and the factor $(1+\mathbf{K}_0^2)^{-1/2}$ in (3.61) are included so that the δ-function orthonormality relation in the last equation in (3.48) is satisfied. It follows from (3.47), (3.50) and (3.54) that Ψ_{jE} can be expanded as follows:

$$\Psi_{jE}(\mathbf{x}_1,\ldots,\mathbf{x}_{N+1}) = \mathcal{A}\sum_{i=1}^{n}\overline{\Phi}_i(\mathbf{x}_1,\ldots,\mathbf{x}_N;\hat{\mathbf{r}}_{N+1}\sigma_{N+1})r_{N+1}^{-1}G_{ij}(r_{N+1})$$
$$+\sum_{i=0}^{m}\chi_i(\mathbf{x}_1,\ldots,\mathbf{x}_N)c_{ij}, \quad j=1,\ldots,n, \tag{3.62}$$

where the reduced radial wave function matrix $\mathbf{G}$ in this equation is obtained by substituting (3.58) into (3.54), using (3.61) and carrying out the integration over E'.

We find that $\mathbf{G}$ satisfies the asymptotic boundary conditions

$$\begin{aligned}\mathbf{G}_1(r) &\underset{r\to\infty}{\sim} \left(\frac{2}{\pi\mathbf{k}}\right)^{1/2} \{\sin\boldsymbol{\theta}[z(E)+\pi\mathbf{K}_0]+\cos\boldsymbol{\theta}[-\pi+z(E)\mathbf{K}_0]\} \\ &\quad\times(1+\mathbf{K}_0^2)^{-1/2}\mathbf{U}_1, \\ \mathbf{G}_j(r) &\underset{r\to\infty}{\sim} \left(\frac{2}{\pi\mathbf{k}}\right)^{1/2} (\sin\boldsymbol{\theta}+\cos\boldsymbol{\theta}\mathbf{K}_0)(1+\mathbf{K}_0^2)^{-1/2}\mathbf{U}_j, \\ &\quad j=2,\ldots,n, \end{aligned} \tag{3.63}$$

where $\mathbf{G}_j$ and $\mathbf{U}_j$ are the jth columns of the $n\times n$-dimensional matrices $\mathbf{G}$ and $\mathbf{U}$, respectively. Also the quadratically integrable functions $\chi_i,\ i=0,\ldots,m$, in (3.62) are linear combinations of the zero-order discrete state represented by the quadratically integrable function χ_0^0 and the zero-order quadratically integrable functions $\chi_i^0,\ i=1,\ldots,m$, in (3.47).

Equations (3.63) can be written in a more convenient form by post-multiplying by $\mathbf{U}^{-1}$ and substituting for $z(E)$ from (3.59). This gives

$$\begin{aligned}\mathbf{G}(r)\mathbf{U}^{-1} \underset{r\to\infty}{\sim} \left(\frac{2}{\pi\mathbf{k}}\right)^{1/2} \Bigg[&\sin\boldsymbol{\theta}\left((1+\mathbf{K}_0^2)^{-1/2}+\mathbf{K}_0(1+\mathbf{K}_0^2)^{-1/2}\frac{1}{2}\Gamma\frac{\boldsymbol{\gamma}\times\boldsymbol{\gamma}}{E-E_r}\right) \\ &+\cos\boldsymbol{\theta}\left(\mathbf{K}_0(1+\mathbf{K}_0^2)^{-1/2}-(1+\mathbf{K}_0^2)^{-1/2}\frac{1}{2}\Gamma\frac{\boldsymbol{\gamma}\times\boldsymbol{\gamma}}{E-E_r}\right)\Bigg], \end{aligned} \tag{3.64}$$

where the partial width amplitudes γ_i are defined by

$$\gamma_i = V_i V^{-1}, \quad i=1,\ldots,n, \tag{3.65}$$

and the resonance energy E_r and total width Γ are defined by

$$\begin{aligned} E_r &= E_0+\Delta, \\ \Gamma &= 2\pi V^2. \end{aligned} \tag{3.66}$$

The quantity $\boldsymbol{\gamma}\times\boldsymbol{\gamma}$ in (3.64) is a real symmetric $n\times n$-dimensional matrix with matrix elements $\gamma_i\gamma_j$ where we note that the real K-matrix boundary condition (3.61) implies that $V_j(E),\ j=1,\ldots,n$, defined by (3.49), are real and hence the partial width amplitudes γ_i are real.

By taking linear combinations of the solutions defined by (3.64), we can choose the reduced radial wave functions to have the following asymptotic form analogous to that given by (3.61)

$$\mathbf{F}(r) \underset{r\to\infty}{\sim} \left(\frac{2}{\pi\mathbf{k}}\right)^{1/2} (\sin\boldsymbol{\theta}+\cos\boldsymbol{\theta}\mathbf{K})(\mathbf{I}+\mathbf{K}^2)^{-1/2}, \tag{3.67}$$

where the K-matrix is defined by

$$\mathbf{K} = \mathbf{K}_0 - \frac{1}{2}\Gamma \frac{(1+\mathbf{K}_0^2)^{1/2}\boldsymbol{\gamma} \times \boldsymbol{\gamma}(1+\mathbf{K}_0^2)^{1/2}}{E - E_r + \frac{1}{2}\Gamma \boldsymbol{\gamma}^{\mathrm{T}}\mathbf{K}_0\boldsymbol{\gamma}}. \tag{3.68}$$

The S-matrix, which is related to the K-matrix by (2.112), can then be written as

$$\mathbf{S} = \mathbf{S}_0 - \mathrm{i}\Gamma \frac{\mathbf{S}_0^{1/2}\boldsymbol{\gamma} \times \boldsymbol{\gamma}\mathbf{S}_0^{1/2}}{E - E_r + \frac{1}{2}\mathrm{i}\Gamma}, \tag{3.69}$$

where the zero-order S-matrix $\mathbf{S}_0$ is defined by

$$\mathbf{S}_0 = \frac{\mathbf{I} + \mathrm{i}\mathbf{K}_0}{\mathbf{I} - \mathrm{i}\mathbf{K}_0}. \tag{3.70}$$

Equations (3.68) and (3.69) are the basic expressions which describe the behaviour of the K-matrix and S-matrix in the neighbourhood of an isolated resonance. We see that all elements of the S-matrix are singular at the complex energy $E = E_r - \frac{1}{2}\mathrm{i}\Gamma$ while the K-matrix elements are singular at the shifted real energy $E = E_r - \frac{1}{2}\Gamma\boldsymbol{\gamma}^{\mathrm{T}}\mathbf{K}_0\boldsymbol{\gamma}$. Equation (3.68), which is discussed further by Burke [153], forms the basis of a computer program written by Bartschat and Burke [64] which enables the resonance position and its total and partial widths to be determined from K-matrix elements calculated at a few energy values in the neighbourhood of an isolated resonance.

Finally, using the definition of $V_j(E)$ given by (3.49) together with the definitions of γ_j and Γ given by (3.65) and (3.66), we find that

$$\gamma_j \Gamma^{1/2} = (2\pi)^{1/2}\langle \chi_0^0 | H_{N+1} | \psi_{jE}^0 \rangle, \tag{3.71}$$

where the reduced radial wave functions $F_{ij}^0(r)$ in ψ_{jE}^0 satisfy the real K-matrix boundary conditions (3.61). Squaring (3.71), summing over j and using (3.53) and (3.65) then yields

$$\Gamma = 2\pi \sum_{j=1}^{n} \left[\langle \chi_0^0 | H_{N+1} | \psi_{jE}^0 \rangle \right]^2. \tag{3.72}$$

This expression has often been used to calculate an approximate value for the total resonance width Γ given approximate representations for the zero-order discrete state χ_0^0 and the zero-order continuum states ψ_{jE}^0, $j = 1, \ldots, n$.

3.2.3 *Behaviour of Eigenphases Near a Resonance*

We have shown in Sect. 1.3 that in the case of potential scattering the phase shift increases by approximately π radians as the energy increases through the resonance

energy, as described by (1.105) and (1.106). In this section we show that the eigenphase sum

$$\delta_{\text{sum}} = \sum_{i=1}^{n} \delta_i, \tag{3.73}$$

where the eigenphases δ_i are defined by (2.113) and (2.114), satisfies a generalization of these equations. In addition, we will derive an equation satisfied by the individual eigenphases near a resonance. As in Sect. 3.2.2, we assume that n channels are open.

Following (2.113), we diagonalize the S-matrix defined by (3.69) giving

$$\begin{aligned} \mathbf{S} &= \mathbf{A} \exp(2\mathrm{i}\boldsymbol{\Delta})\mathbf{A}^{\mathrm{T}} \\ &= \mathbf{A}_0 \exp(\mathrm{i}\boldsymbol{\Delta}_0)\mathbf{A}_0^{\mathrm{T}} \left[1 - \mathrm{i}\Gamma \frac{\boldsymbol{\gamma} \times \boldsymbol{\gamma}}{E - E_r + \frac{1}{2}\mathrm{i}\Gamma} \right] \mathbf{A}_0 \exp(\mathrm{i}\boldsymbol{\Delta}_0)\mathbf{A}_0^{\mathrm{T}}, \end{aligned} \tag{3.74}$$

where $\mathbf{A}$ and $\mathbf{A}_0$ are the real orthogonal matrices which diagonalize $\mathbf{S}$ and $\mathbf{S}_0$, respectively, and $\boldsymbol{\Delta}$ and $\boldsymbol{\Delta}_0$ are diagonal matrices whose diagonal elements are the eigenphases $\delta_i, i = 1, \ldots, n$ and the zero-order non-resonant eigenphases $\delta_i^0, i = 1, \ldots, n$, respectively. We now take the determinant of both sides of (3.74) yielding

$$\exp\left(2\mathrm{i}\delta_{\text{sum}}\right) = \exp(2\mathrm{i}\delta_{\text{sum}}^0) \det \left[1 - \mathrm{i}\Gamma \frac{\boldsymbol{\gamma} \times \boldsymbol{\gamma}}{E - E_r + \frac{1}{2}\mathrm{i}\Gamma} \right], \tag{3.75}$$

where in analogy with (3.73) we have defined

$$\delta_{\text{sum}}^0 = \sum_{i=1}^{n} \delta_i^0. \tag{3.76}$$

We now observe from (3.53) and (3.65) that $\boldsymbol{\gamma}^{\mathrm{T}}\boldsymbol{\gamma} = 1$. Hence by diagonalizing the matrix in square brackets in (3.75) we find that

$$\det \left[1 - \mathrm{i}\Gamma \frac{\boldsymbol{\gamma} \times \boldsymbol{\gamma}}{E - E_r + \frac{1}{2}\mathrm{i}\Gamma} \right] = \exp \left[2\mathrm{i} \tan^{-1} \frac{\frac{1}{2}\Gamma}{E_r - E} \right]. \tag{3.77}$$

Combining (3.75) and (3.77) then yields the equation

$$\delta_{\text{sum}} = \delta_{\text{sum}}^0 + \tan^{-1} \frac{\frac{1}{2}\Gamma}{E_r - E}. \tag{3.78}$$

This equation, obtained by Hazi [446], is the multichannel generalization of (1.105) and (1.106) describing the behaviour of the phase shift near a resonance in potential

scattering. We see that the resonant part of $\delta_{\rm sum}$, given by the second term on the right-hand side of (3.78), increases by π radians as the energy increases through the resonance, while the non-resonant term $\delta^0_{\rm sum}$ is smoothly varying with energy. Equation (3.78) is often used to determine the position and width of a multichannel resonance from the calculated S-matrix (e.g. [918]). Also, Quigley et al. [761, 762] combined this equation with the analytic properties of the R-matrix to obtain an accurate "QB" procedure for analysing resonances.

In order to determine the behaviour of the individual eigenphases in the neighbourhood of a resonance we follow Macek [620] by diagonalizing the S-matrix defined by (3.69) in two stages. We first transform $\mathbf{S}$ by the real orthogonal matrix $\mathbf{A}_0$ which diagonalizes $\mathbf{S}_0$ giving

$$\mathbf{S}' = \mathbf{A}_0^{\rm T}\mathbf{S}\mathbf{A}_0 = \exp(2{\rm i}\boldsymbol{\Delta}) - {\rm i}\Gamma\frac{\exp({\rm i}\boldsymbol{\Delta}_0)\mathbf{y}\times\mathbf{y}\exp({\rm i}\boldsymbol{\Delta}_0)}{E-E_r+\frac{1}{2}{\rm i}\Gamma}, \tag{3.79}$$

where $\mathbf{y} = \mathbf{A}_0^{\rm T}\boldsymbol{\gamma}$ is a vector whose elements give the amplitudes for the decay of the resonance into the eigenchannels of $\mathbf{S}_0$. We then substitute (3.79) into the eigenvalue equation

$$\mathbf{S}'\mathbf{b}_j = \exp(2{\rm i}\delta_j)\mathbf{b}_j, \quad j = 1,\ldots,n, \tag{3.80}$$

where δ_j is the jth eigenphase of $\mathbf{S}$. We obtain

$$\exp(2{\rm i}\delta_j)\mathbf{b}_j = \exp(2{\rm i}\boldsymbol{\Delta}_0)\mathbf{b}_j - {\rm i}\Gamma\frac{\exp({\rm i}\boldsymbol{\Delta}_0)\mathbf{y}}{E-E_r+\frac{1}{2}{\rm i}\Gamma}a_j, \tag{3.81}$$

where a_j is defined by

$$a_j = \mathbf{y}^{\rm T}\exp({\rm i}\boldsymbol{\Delta}_0)\mathbf{b}_j. \tag{3.82}$$

Equation (3.81) defines the vector $\mathbf{b}_j$ in terms of the quantity a_j. Substituting this expression for $\mathbf{b}_j$ into (3.82) then yields the consistency relation

$$a_j = -\frac{{\rm i}\Gamma}{E-E_r+\frac{1}{2}{\rm i}\Gamma}\sum_{i=1}^{n} y_i^2\frac{\exp(2{\rm i}\delta_i^0)}{\exp(2{\rm i}\delta_j)-\exp(2{\rm i}\delta_i^0)}a_j, \quad j = 1,\ldots,n. \tag{3.83}$$

In order for (3.83) to have a non-trivial solution, the coefficients of a_j on both sides must be equal. Using the condition $\mathbf{y}^{\rm T}\mathbf{y} = \boldsymbol{\gamma}^{\rm T}\boldsymbol{\gamma} = 1$ we obtain the required relation

$$E - E_r = \frac{1}{2}\Gamma\sum_{i=1}^{n} y_i^2\cot(\delta_i^0-\delta_j), \quad j = 1,\ldots,n. \tag{3.84}$$

When $n = 1$ this equation reduces to

$$\delta = \delta^0 + \tan^{-1} \frac{\frac{1}{2}\Gamma}{E_r - E}, \tag{3.85}$$

which corresponds to (3.78) obtained earlier.

Equations (3.84) define the behaviour of the eigenphases δ_j as a function of E. For any given energy this equation has n solutions, each solution δ_j lying between adjacent values of the non-resonant eigenphases δ_i^0. As the energy increases from a value well below the resonance energy E_r to a value well above E_r, the corresponding eigenphases increase from close to and just above each non-resonant eigenphase δ_i^0 to close to and just below the next higher non-resonant eigenphase δ_{i+1}^0. Taking the derivative of (3.84) with respect to the energy E and assuming that the δ_i^0 are independent of energy we obtain

$$1 = \frac{1}{2}\Gamma \frac{\mathrm{d}\delta_j}{\mathrm{d}E} \sum_{i=1}^{n} y_i^2 \mathrm{cosec}^2(\delta_i^0 - \delta_j), \quad j = 1, \ldots, n, \tag{3.86}$$

which shows that each eigenphase δ_j increases monotonically with energy. It also follows from this equation that the eigenphases δ_j increase most rapidly near E_r.

As an illustration of (3.84), we show in Fig. 3.5 the calculated eigenphase sum δ_{sum} and the three eigenphases δ_1, δ_2 and δ_3 in radians for e^-–H collisions, plotted as a function of the incident electron energy in Rydbergs in the neighbourhood of the $^1S^e$ resonance lying between the $n = 2$ and 3 thresholds at ~ 0.862 Rydbergs. The

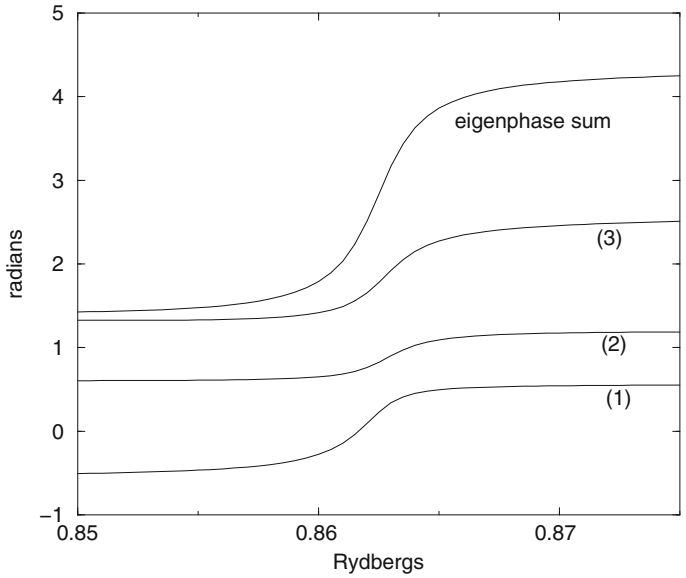

Fig. 3.5 The behaviour of the eigenphase sum δ_{sum} and the eigenphases δ_1, δ_2 and δ_3, labelled (*1*), (*2*) and (*3*), respectively, for e^-–H collisions in the neighbourhood of the $^1S^e$ resonance lying below the $n = 3$ thresholds at an incident electron energy ~ 0.862 Rydbergs

calculation, carried out using the R-matrix method discussed in Chap. 5, retained the six atomic hydrogen target states 1s, 2s, 2p, 3s, 3p and 3d in the close coupling expansion (2.57) for the conserved quantum numbers $L = 0$, $S = 0$ and $\pi =$ even. This results in six coupled channels in (2.63), where three channels, corresponding to the 1s, 2s and 2p states, are open and the three remaining channels, corresponding to the 3s, 3p and 3d states, are closed. Hence $n = 6$, $n_a = 3$ and $n_b = 3$ in (2.79) and the corresponding K- and S-matrices have dimensions 3×3. The eigenphase sum and the three eigenphases are seen to be continuous functions of energy through the resonance which was achieved by adding or subtracting the appropriate multiple of π radians at each calculated energy. As expected $\delta_{\rm sum}$, which is given by (3.78), increases by approximately π radians as the energy increases through the resonance. Also the individual eigenphases behave as described in the preceding paragraph. Further details of e^-–H collision calculations and the resonances that occur are given in Sect. 5.6.1 where we discuss the results of solving (2.63) using the R-matrix method.

3.2.4 Time-Delay Matrix

In the previous sections we have shown that the presence of poles in the S-matrix, lying on unphysical sheets of the complex energy plane close to the physical scattering region, gives rise to resonance effects in the corresponding eigenphases and scattering amplitudes. It was shown by Wigner [971] that a resonance not only gives a sharp peak or dip in the cross section but also gives rise to a time delay in the collision. In this section we consider the time delay caused by these resonances and, following the work of Smith [881], we introduce the time-delay matrix $\mathbf{Q}(E)$[1] on the real energy axis. We also relate the trace of this matrix to the derivative of the eigenphase sum with respect to energy and we show that this quantity often provides an accurate procedure for analysing overlapping resonances.

It was shown in early work by Eisenbud [288], Bohm [121] and Wigner [971], using wave-packet analyses, that the time delay Δt which arises in a single-channel collision can be described in terms of the derivative of the phase shift δ with respect to energy E by

$$\Delta t = 2\frac{\mathrm{d}\delta}{\mathrm{d}E}, \tag{3.87}$$

in atomic units. Remembering that the single-channel S-matrix is related to the phase shift δ by $S = \exp(2\mathrm{i}\delta)$ we find that

$$\Delta t = \mathrm{i}S\frac{\mathrm{d}S^*}{\mathrm{d}E} \quad = -\mathrm{i}\frac{\mathrm{d}S}{\mathrm{d}E}S^*, \tag{3.88}$$

where S^* is the complex conjugate of S.

[1] In the original work of Smith [881] $\mathbf{Q}(E)$ was called the lifetime matrix.

In the analysis of Smith [881], which was considered further by Celenza and Tobocman [206], the time delay was analysed using a steady-state wave function describing the collision. In this analysis, the lifetime is determined by considering the excess number of particles in an interaction region, after subtracting the number of particles that would have been present in the absence of the interaction. This excess number will remain finite even if the integration is taken to infinity, provided that the interaction vanishes rapidly enough at large distances. This excess, divided by the total flux in (or out) through a closed surface at large distances from the centre of the interaction region, gives the required lifetime. Using this independent analysis of the time delay yields the same results as the wave-packet analysis which leads to (3.88).

Smith [881] also generalized (3.88) to multichannel collisions by introducing a time-delay matrix $\mathbf{Q}$. In this analysis (3.88) becomes

$$\mathbf{Q} = \mathrm{i}\mathbf{S}\frac{\mathrm{d}\mathbf{S}^\dagger}{\mathrm{d}E} \quad = -\mathrm{i}\frac{\mathrm{d}\mathbf{S}}{\mathrm{d}E}\mathbf{S}^\dagger, \tag{3.89}$$

where $\mathbf{Q} = \mathbf{Q}^\dagger$ is hermitian and, like the S-matrix $\mathbf{S}$, has dimension $n \times n$, where n is the number of open channels at the energy E. Following Igarashi and Shimamura [486] we can relate the trace of the time-delay matrix $\mathbf{Q}$ to the eigenphase sum δ_{sum}, defined by (3.78). We first diagonalize the S-matrix by a real orthogonal transformation $\mathbf{A}$. Following (2.113) we write

$$\mathbf{A}^{\mathrm{T}}\mathbf{S}\mathbf{A} = \exp(2\mathrm{i}\boldsymbol{\Delta}) = \boldsymbol{\Lambda}, \tag{3.90}$$

where the diagonal elements of $\boldsymbol{\Lambda}$ can be expressed in terms of the eigenphases δ_i, as follows:

$$\Lambda_{ii} = \exp(2\mathrm{i}\delta_i), \quad i = 1, \ldots, n. \tag{3.91}$$

We find using (3.90) that

$$2\frac{\mathrm{d}\boldsymbol{\Delta}}{\mathrm{d}E} = \mathrm{i}\boldsymbol{\Lambda}\frac{\mathrm{d}\boldsymbol{\Lambda}^\dagger}{\mathrm{d}E}, \tag{3.92}$$

and

$$\frac{\mathrm{d}\boldsymbol{\Lambda}^\dagger}{\mathrm{d}E} = \mathbf{A}^{\mathrm{T}}\frac{\mathrm{d}\mathbf{S}^\dagger}{\mathrm{d}E}\mathbf{A} + \frac{\mathrm{d}\mathbf{A}^{\mathrm{T}}}{\mathrm{d}E}\mathbf{S}^\dagger\mathbf{A} + \mathbf{A}^{\mathrm{T}}\mathbf{S}^\dagger\frac{\mathrm{d}\mathbf{A}}{\mathrm{d}E}. \tag{3.93}$$

Substituting (3.93) into (3.92) and using (3.90) gives

$$2\frac{\mathrm{d}\boldsymbol{\Delta}}{\mathrm{d}E} = \mathrm{i}\left(\mathbf{A}^{\mathrm{T}}\mathbf{S}\frac{\mathrm{d}\mathbf{S}^\dagger}{\mathrm{d}E}\mathbf{A} + \mathbf{A}^{\mathrm{T}}\mathbf{S}\mathbf{A}\frac{\mathrm{d}\mathbf{A}^{\mathrm{T}}}{\mathrm{d}E}\mathbf{S}^\dagger\mathbf{A} + \mathbf{A}^{\mathrm{T}}\frac{\mathrm{d}\mathbf{A}}{\mathrm{d}E}\right). \tag{3.94}$$

Taking the trace of this equation then gives

$$\mathrm{Tr}\left(2\frac{\mathrm{d}\boldsymbol{\Delta}}{\mathrm{d}E}\right) = \mathrm{iTr}\left(\mathbf{S}\frac{\mathrm{d}\mathbf{S}^{\dagger}}{\mathrm{d}E}\right) + \mathrm{iTr}\left(\mathbf{A}\frac{\mathrm{d}\mathbf{A}^{\mathrm{T}}}{\mathrm{d}E} + \mathbf{A}^{\mathrm{T}}\frac{\mathrm{d}\mathbf{A}}{\mathrm{d}E}\right), \tag{3.95}$$

since the trace of a matrix is unaltered by an orthogonal transformation. It follows from (3.89) that the first term on the right-hand-side of (3.95) is Tr($\mathbf{Q}$) and the second term can be written as

$$\mathrm{iTr}\left(\mathbf{A}\frac{\mathrm{d}\mathbf{A}^{\mathrm{T}}}{\mathrm{d}E} + \mathbf{A}^{\mathrm{T}}\frac{\mathrm{d}\mathbf{A}}{\mathrm{d}E}\right) = \mathrm{iTr}\left(\frac{\mathrm{d}\left(\mathbf{A}^{\mathrm{T}}\mathbf{A}\right)}{\mathrm{d}E}\right) = 0. \tag{3.96}$$

Hence it follows from (3.95) that

$$\mathrm{Tr}\mathbf{Q} = 2\mathrm{Tr}\left(\frac{\mathrm{d}\boldsymbol{\Delta}}{\mathrm{d}E}\right). \tag{3.97}$$

Finally, we see from (3.90) and (3.91) that the diagonal elements of $\boldsymbol{\Delta}$ are the eigenphases δ_i and, therefore, using (3.73) we obtain

$$\mathrm{Tr}\mathbf{Q} = 2\frac{\mathrm{d}\delta_{\mathrm{sum}}}{\mathrm{d}E}. \tag{3.98}$$

This result generalizes the single-channel result given by (3.87) to multichannel collisions.

So far we have not made any assumption concerning the functional form of the S-matrix or the eigenphase sum. If we assume that δ_{sum} in (3.98) satisfies (3.78), then we find that (3.98) can be rewritten as

$$\mathrm{Tr}\mathbf{Q} = 2\frac{\mathrm{d}\delta_{\mathrm{sum}}}{\mathrm{d}E} = \frac{\Gamma}{(E-E_r)^2 + \left(\frac{1}{2}\Gamma\right)^2} + 2\frac{\mathrm{d}\delta^0_{\mathrm{sum}}}{\mathrm{d}E}. \tag{3.99}$$

In the case of N resonances, which may be overlapping, it follows immediately from (3.99) that

$$\frac{\mathrm{d}\delta_{\mathrm{sum}}}{\mathrm{d}E} = \sum_{i=1}^{N} \frac{\frac{1}{2}\Gamma_i}{(E-E_i)^2 + \left(\frac{1}{2}\Gamma_i\right)^2} + \frac{\mathrm{d}\delta^0_{\mathrm{sum}}}{\mathrm{d}E}, \tag{3.100}$$

where in this equation E_i are the resonance positions and Γ_i are the resonance widths.

Equation (3.100) has been used by a number of workers to determine the positions and widths of resonances. For example, this approach has been used by Stibbe and Tennyson [889] to analyse R-matrix calculations of resonances in e^-–H_2 and e^-–H_2^+ collisions, by Igarashi and Shimamura [486, 487] to analyse hyperspherical coordinate calculations of resonances in e^+–He^+ collisions, by Igarashi and Shimamura [488] and Shimamura et al. [873] to analyse hyperspherical coordinate calculations of resonances in e^-–Ps collisions and by Aiba et al. [5] to

analyse hyperspherical coordinate calculations of resonances in e^-–He and e^-–Ps collisions.

As an example of these calculations we consider results obtained by Aiba et al. [5] for overlapping resonances in electron–positronium atom collisions at energies below the $n = 5$ Ps threshold. In this case the scattered electron moves in a long-range dipole potential, discussed in Sect. 3.3.2, which gives rise to infinite series of overlapping resonances converging to the $n = 5$ and 6 thresholds. We show in Fig. 3.6 the results of calculations in a small energy region just below the $n = 5$ Ps threshold. We see in Fig. 3.6a that the $^1P^o$ eigenphase sum $\delta_{sum}(E)$ increases by about 3π in this energy region, suggesting that there may be three resonances. However, an appreciable change of slope in $\delta_{sum}(E)$ occurs only twice. Also, we see in Fig. 3.6b that Tr$\mathbf{Q}(E)$ exhibits only two peaks. However, by examining the individual eigenvalues $q_i(E)$ of the time-delay matrix in Fig. 3.6b we see that there is a strongly avoided crossing between the two largest eigenvalues and we observe a broad resonance peak corresponding to the third eigenvalue. This third

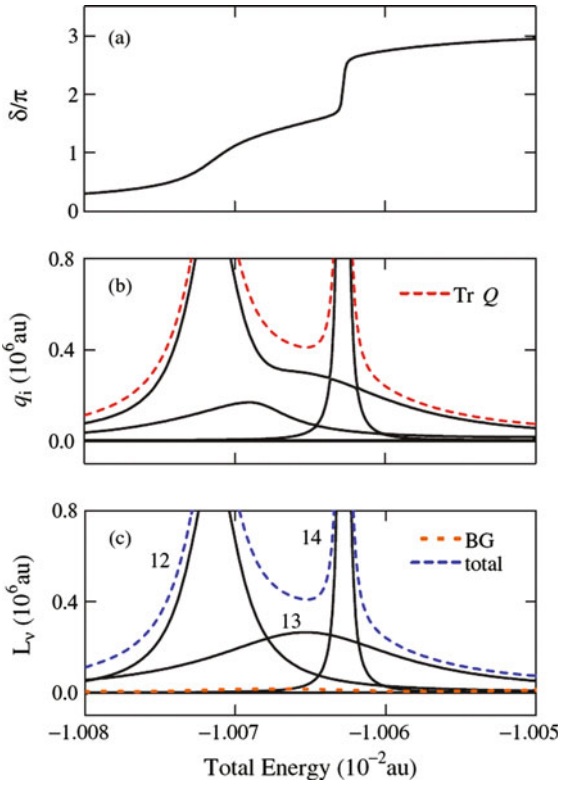

Fig. 3.6 A small energy region just below the Ps $n = 5$ threshold in electron–positronium atom collisions showing Ps^- ($^1P^o$) overlapping resonances. (**a**) The eigenphase sum $\delta_{sum}(E)$. (**b**) The eigenvalues $q_i(E)$ of the time-delay matrix and their sum Tr$\mathbf{Q}(E)$. (**c**) The three Lorentzians $L_i(E)$ representing the three resonances, the background $d\delta^0_{sum}/dE$ (BG) and their sum (Fig. 5 from [5])

resonance would be very difficult to find and analyse using a resonance analysis of the eigenphase sum $\delta_{\rm sum}(E)$ based on (3.78). Finally, in Fig. 3.6c we show the result of fitting the calculated result for $\mathrm{d}\delta_{\rm sum}/\mathrm{d}E$ on the left-hand side of (3.100) to three Lorentzians, defined by the first summation on the right-hand side of (3.100), together with a smoothly varying background term $\delta^0_{\rm sum}/\mathrm{d}E$. We see that this procedure clearly shows the existence of three resonances in the energy region with an almost negligible background and enables accurate positions and widths for these resonances to be determined.

In conclusion, resonance analyses based on the time-delay matrix provide an accurate procedure for resolving overlapping resonances in atomic, molecular and nuclear physics.

3.2.5 Feshbach Projection Operator Theory

In this section we discuss the widely used theory of resonance reactions introduced by Feshbach [320, 321]. This theory is based on a projection operator formalism in which Hilbert space spanned by the eigensolutions of the Schrödinger equation describing the collision process is sub-divided into two mutually orthogonal spaces by two projection operators P and Q. In this application bound states in Q-space, in the absence of coupling between P- and Q-spaces, evolve into resonances when the interaction with the open channels in P-space is included. This theory, which was first used to describe nuclear resonance reactions, has provided a powerful framework for describing resonance phenomena in atomic and molecular collision processes.

In Feshbach theory, the projection operators P and Q are chosen to satisfy the equations

$$\begin{aligned} P + Q &= 1, \\ P^2 = P,\ \ Q^2 &= Q, \\ PQ = QP &= 0. \end{aligned} \tag{3.101}$$

Using these definitions, the Schrödinger equation (2.2), describing multichannel collisions, can be formally rewritten as

$$P(H_{N+1} - E)(P + Q)\Psi = 0 \tag{3.102}$$

and

$$Q(H_{N+1} - E)(P + Q)\Psi = 0. \tag{3.103}$$

We can solve (3.103) for $Q\Psi$ yielding

$$Q\Psi = Q\frac{1}{Q(E - H_{N+1})Q}QH_{N+1}P\Psi. \tag{3.104}$$

Substituting this result for $Q\Psi$ into (3.102) then gives

$$P(H_{N+1} + V_{\text{opt}} - E)P\Psi = 0, \tag{3.105}$$

where V_{opt}, referred to as the "optical potential", is defined here as

$$V_{\text{opt}} = PH_{N+1}Q\frac{1}{Q(E - H_{N+1})Q}QH_{N+1}P. \tag{3.106}$$

We see that the optical potential describes collisions through the Hamiltonian H_{N+1} out of P-space into Q-space, propagation in Q-space and then collisions through the Hamiltonian back from Q-space into P-space. The optical potential contains all the complexity resulting from coupling Q-space to P-space. It is clear from the above derivation that the solution of (3.105) for $P\Psi$ yields identical results to that obtained by solving the original Schrödinger equation (2.2) for Ψ and then projecting this solution onto P-space.

Equations (3.105) and (3.106) hold for any projection operators P and Q satisfying (3.101). We now consider an explicit realization of these operators which has been particularly useful in studies of resonances in atomic and molecular collision processes. We choose P to project onto all the open channels at a particular value of the total energy E and Q to project onto the remaining closed channels at this energy. That is we assume that the wave function Ψ can be expanded in the form given by (2.45) where $P\Psi$ includes all the open channels in this expansion with the corresponding k_i^2 satisfying $k_i^2 \geq 0, \quad i = 1, \ldots, n$. We now introduce the eigenfunctions ξ_s of the operator $QH_{N+1}Q$ by the equation

$$QH_{N+1}Q\ \xi_s = \epsilon_s\ \xi_s, \tag{3.107}$$

where, since $Q = 1 - P$, this operator has a discrete spectrum in the energy range of interest below the lowest threshold in Q-space, plus a continuum spectrum starting from this threshold. The optical potential V_{opt} defined by (3.106) can be written as

$$V_{\text{opt}} = \sum_s \int \frac{PH_{N+1}Q|\xi_s\rangle\langle\xi_s|QH_{N+1}P}{E - \epsilon_s}\,\mathrm{d}\epsilon_s, \tag{3.108}$$

where the summation in this equation goes over the discrete spectrum and the integral over the continuum spectrum of $QH_{N+1}Q$. It is the discrete spectrum, which corresponds physically to an electron bound in the field of an excited atom or ion in Q-space, that gives rise to closed-channel resonance solutions of (3.105).

We now consider the solution of (3.105) for a given set of conserved quantum numbers, when the total energy E lies in the neighbourhood of an isolated eigenvalue ϵ_s of $QH_{N+1}Q$. We can then rewrite (3.105) as

$$P\left[H_{N+1}+\sum_{j\neq s}\int\frac{PH_{N+1}Q|\xi_j\rangle\langle\xi_j|QH_{N+1}P}{E-\epsilon_j}\,\mathrm{d}\epsilon_j-E\right]P\Psi$$
$$=-\frac{PH_{N+1}Q|\xi_s\rangle\langle\xi_s|QH_{N+1}P}{E-\epsilon_s}\,P\Psi, \tag{3.109}$$

where we have separated out on the right-hand side of this equation the rapidly varying pole term in the optical potential, corresponding to the isolated eigenvalue ϵ_s. In order to solve (3.109) we rewrite it as

$$(H'-E)P\Psi=-\frac{\mathcal{H}_{PQ}\xi_s\rangle\langle\xi_s\mathcal{H}_{QP}}{E-\epsilon_s}\,P\Psi, \tag{3.110}$$

where

$$\mathcal{H}_{PQ}=PH_{N+1}Q\quad\text{and}\quad\mathcal{H}_{QP}=QH_{N+1}P. \tag{3.111}$$

We also introduce a quantity Λ_s defined by

$$\Lambda_s=\frac{\langle\xi_s\mathcal{H}_{QP}\Psi\rangle}{E-\epsilon_s}. \tag{3.112}$$

Hence (3.110) can be rewritten as

$$(H'-E)P\Psi=-\Lambda_s\,\mathcal{H}_{PQ}\,\xi_s. \tag{3.113}$$

The solution of (3.113) can be obtained by introducing outgoing and ingoing wave solutions, Ψ_{iE}^{+} and Ψ_{iE}^{-}, of the equation

$$(H'-E)P\;\Psi_{iE}^{\pm}=0, \tag{3.114}$$

where the reduced radial wave functions corresponding to Ψ_{iE}^{+} and Ψ_{iE}^{-} satisfy the outgoing wave

$$\mathbf{F}^{+}(r)\underset{r\to\infty}{\sim}\frac{2}{\sqrt{\mathbf{k}}}\left(\sin\boldsymbol{\theta}+\frac{1}{2\mathrm{i}}\mathrm{e}^{\mathrm{i}\boldsymbol{\theta}}\mathbf{T}_0\right) \tag{3.115}$$

and ingoing wave

$$\mathbf{F}^{-}(r)\underset{r\to\infty}{\sim}\frac{2}{\sqrt{\mathbf{k}}}\left(\sin\boldsymbol{\theta}-\frac{1}{2\mathrm{i}}\mathrm{e}^{-\mathrm{i}\boldsymbol{\theta}}\mathbf{T}_0^{\dagger}\right), \tag{3.116}$$

boundary conditions, respectively. In analogy with our discussion in Sect. 1.1, see (1.21), $\Psi_{iE}^{\pm}$ in (3.114) then satisfy the δ-function orthonormality relation

$$\langle \Psi^{\pm}_{iE} | \Psi^{\pm}_{i'E'} \rangle = \delta_{ii'}\, \delta(E - E'), \tag{3.117}$$

where we remember from Sect. 2.5 that the T-matrix in (3.115) and (3.116) is related to the S-matrix by

$$\mathbf{T}_0 = \mathbf{S}_0 - \mathbf{I}. \tag{3.118}$$

We can then formally solve (3.113) yielding

$$P\Psi = \Psi^{+}_{iE} + \Lambda_s \frac{1}{E + \mathrm{i}\eta - H'} \mathcal{H}_{PQ}\, \xi_s, \tag{3.119}$$

where η is a positive infinitesimal quantity. Substituting (3.119) into (3.112) and collecting terms in Λ_s then gives

$$\Lambda_s = \frac{\langle \xi_s \mathcal{H}_{QP} \Psi^{+}_{iE} \rangle}{E - \epsilon_s - \langle \xi_s \mathcal{H}_{QP} (E + \mathrm{i}\eta - H')^{-1} \mathcal{H}_{PQ} \xi_s \rangle}. \tag{3.120}$$

Using this result for Λ_s, (3.119) becomes

$$P\Psi = \Psi^{+}_{iE} + \frac{1}{E + \mathrm{i}\eta - H'} \frac{\mathcal{H}_{PQ}\xi_s \langle \xi_s \mathcal{H}_{QP} \Psi^{+}_{iE} \rangle}{E - \epsilon_s - \langle \xi_s \mathcal{H}_{QP} (E + \mathrm{i}\eta - H')^{-1} \mathcal{H}_{PQ} \xi_s \rangle}. \tag{3.121}$$

In order to simplify (3.121) we consider the term appearing in the denominator on the right-hand side of this equation. We can write

$$\left\langle \xi_s \mathcal{H}_{QP} \frac{1}{E + \mathrm{i}\eta - H'} \mathcal{H}_{PQ} \xi_s \right\rangle = \sum_j \int \frac{|\langle \xi_s \mathcal{H}_{QP} \Psi^{+}_{jE'} \rangle|^2}{E - E' + \mathrm{i}\eta} \mathrm{d}E', \tag{3.122}$$

where we have expanded the inverse operator $(E + \mathrm{i}\eta - H')^{-1}$ in terms of the complete set of outgoing wave solutions of (3.114). The right-hand side of (3.122) can be written as a sum of its real and imaginary parts. The real part corresponds to the resonance shift Δ_s which is given by

$$\Delta_s = \sum_j \mathcal{P} \int \frac{|\langle \xi_s \mathcal{H}_{QP} \Psi^{+}_{jE'} \rangle|^2}{E - E'} \mathrm{d}E', \tag{3.123}$$

where $\mathcal{P}$ denotes the principal value integral. The imaginary part of (3.122) arises from the pole at $E = E'$ and is related to the resonance width Γ_s by the equation

$$\frac{1}{2} \mathrm{i} \Gamma_s = \mathrm{i}\pi \sum_j |\langle \xi_s \mathcal{H}_{QP} \Psi^{+}_{jE} \rangle|^2, \tag{3.124}$$

which gives

$$\Gamma_s = 2\pi \sum_j |\langle \xi_s \mathcal{H}_{QP} \Psi^+_{jE} \rangle|^2, \tag{3.125}$$

where the summation is taken over all final states. We see that this result for the resonance width has the same form as that given by (3.72) derived in Sect. 3.2.2.

Finally, we operate on the left-hand side of (3.121) by $(E + \mathrm{i}\eta - H')$, project onto the ingoing wave solution Ψ^-_{fE} of (3.114) and use the results for the resonance shift and width given by (3.123) and (3.125). The transition amplitude $\mathcal{T}_{fi}$ from an initial state i to a final state f is then given by

$$\mathcal{T}_{fi} = \mathcal{T}_{0fi} + \frac{\langle \Psi^-_{fE} \mathcal{H}_{PQ} \xi_s \rangle \langle \xi_s \mathcal{H}_{QP} \Psi^+_{iE} \rangle}{E - \epsilon_s - \Delta_s + \frac{1}{2}\mathrm{i}\Gamma_s}, \tag{3.126}$$

where $\mathcal{T}_{0fi}$ is the transition amplitude describing non-resonant scattering in P-space in the absence of the isolated eigenfunction ξ_s of $QH_{N+1}Q$. We see that (3.126) has the same general form as (3.69) describing the S-matrix in the neighbourhood of an isolated resonance.

The above theory has been extended by Feshbach [320, 321] to treat overlapping resonances. In this case $\mathcal{T}_{0fi}$ in (3.126) varies rapidly over the width of one of the resonances and the separation of the transition amplitude into two parts, given by (3.126), is no longer appropriate. If only a few closely spaced resonances are involved, such that the remaining background transition amplitude omitting these resonances is slowly varying, then the above theory can be straightforwardly extended to include these resonances. Equation (3.110) then becomes

$$(H' - E)P\Psi = -\sum_s \frac{\mathcal{H}_{PQ}\xi_s\rangle\langle\xi_s \mathcal{H}_{QP}}{E - \epsilon_s} P\Psi, \tag{3.127}$$

where H' is the Hamiltonian omitting these closely spaced resonances, and the subsequent equations are modified accordingly.

However, we also have to consider the situation in electron collisions with positive ions, where infinite series of resonances converging to each excited state threshold occur. In this case resonance series may overlap and it is then necessary to include the interaction between resonance series in the theory. This is achieved using multichannel effective range theory or multichannel quantum defect theory which we discuss in Sect. 3.3.

3.2.6 *Hyperspherical Coordinates*

We conclude this section by discussing the hyperspherical system of coordinates which has been important in the analysis of resonances and threshold behaviour

of three-body systems. For example, Fock [326] and Demkov and Ermolaev [260] used these coordinates in variational calculations of bound states of helium, Delves [257, 258] used them to describe the nuclear three-body problem and Smith [882, 883] has given a general discussion of the three-body problem in terms of these coordinates. They have also played an important role in the analysis of doubly excited resonance states of helium and other two-electron atoms, for example, by Macek [618, 619], Lin [598, 599], Greene [416] and Fano [307] as well as in positron collisions calculations, for example, by Igarashi et al. [485–487]. These coordinates have also been used in the calculation of weakly bound levels of triatomic molecules such as the helium trimer $^4He_3$ and isotopomers of the He_3^+ ion discussed by Kokoouline and Masnou-Seeuws [546]. Finally, we will use these coordinates in our derivation of the Wannier [954] threshold law of ionization in Sect. 3.3.5

Hyperspherical coordinates for two electrons moving in the field of an infinitely heavy nucleus at the origin of coordinates are defined in terms of the electronic spherical polar coordinates (r_1, θ_1, ϕ_1) and (r_2, θ_2, ϕ_2) by

$$R = (r_1^2 + r_2^2)^{1/2}, \quad \alpha = \tan^{-1}\frac{r_2}{r_1}, \quad 0 \le \alpha \le \frac{\pi}{2}, \tag{3.128}$$

while the four remaining coordinates are usually chosen to be $(\theta_1, \phi_1, \theta_2, \phi_2)$. The Schrödinger equation, defined by (2.2) and (2.3) with $N = 1$ and nuclear charge number Z can be expressed in terms of these coordinates as (e.g. [664])

$$\left(\frac{\mathrm{d}^2}{\mathrm{d}R^2} + \frac{5}{R}\frac{\mathrm{d}}{\mathrm{d}R} - \frac{\Lambda^2}{R^2} + \frac{C}{R} + 2E\right)\Psi = 0. \tag{3.129}$$

In this equation the potential function C is given in terms of the electron–electron and electron–nuclear potentials by

$$\begin{aligned} C(\alpha, \theta_{12}) &= R\left(\frac{2Z}{r_1} + \frac{2Z}{r_2} - \frac{2}{r_{12}}\right) \\ &= \frac{2Z}{\cos\alpha} + \frac{2Z}{\sin\alpha} - \frac{2}{(1 - \sin 2\alpha \cos\theta_{12})^{1/2}}, \end{aligned} \tag{3.130}$$

where θ_{12} is the angle between the radial vectors $\mathbf{r_1}$ and $\mathbf{r_2}$. Also the operator Λ^2 in (3.129) is defined by

$$\Lambda^2 = -\frac{1}{\sin^2\alpha\cos^2\alpha}\frac{\mathrm{d}}{\mathrm{d}\alpha}\left(\sin^2\alpha\cos^2\alpha\frac{\mathrm{d}}{\mathrm{d}\alpha}\right) + \frac{\boldsymbol{\ell}_1^2}{\cos^2\alpha} + \frac{\boldsymbol{\ell}_2^2}{\sin^2\alpha}, \tag{3.131}$$

where $\boldsymbol{\ell}_1^2$ and $\boldsymbol{\ell}_2^2$ are the squared orbital angular momentum operators for electrons 1 and 2, defined in Appendix B.3, with eigenfunctions $Y_{\ell_1 m_1}(\theta_1, \phi_1)$ and $Y_{\ell_2 m_2}(\theta_2, \phi_2)$ belonging to the eigenvalues $\ell_1(\ell_1 + 1)$ and $\ell_2(\ell_2 + 1)$, respectively. Λ^2 is thus the square of the grand angular momentum operator in six dimensions

and is the Casimir operator for the O(6) group. Its eigenvalues are $\lambda(\lambda+4)$ where λ is a non-negative integer. It commutes with $\mathbf{L}^2$, $\mathbf{S}^2$ and the parity as well as with $\boldsymbol{\ell}_1^2$ and $\boldsymbol{\ell}_2^2$ but it does not commute with C.

Returning to (3.129), we transform this equation to a more familiar form which removes the first derivative with respect to R by the transformation

$$\Psi = R^{-5/2}\psi. \tag{3.132}$$

Equation (3.129) then becomes

$$\left(\frac{\mathrm{d}^2}{\mathrm{d}R^2} - \frac{\Lambda^2 + \frac{15}{4}}{R^2} + \frac{C}{R} + 2E\right)\psi = 0, \tag{3.133}$$

which resembles the Schrödinger equation for the motion of a particle moving in the reduced potential $-C/R$ with centrifugal potential energy given by $(\Lambda^2 + 15/4)/R^2$. However, unlike the similar equation for the hydrogen atom C, which depends on the angular coordinates α and θ_{12}, does not commute with Λ^2. It follows from (3.133) that at large R the dynamics of the motion of two electrons moving in the field of the nucleus depends on the form of C as a function of α and θ_{12}. In Fig. 3.7 we give a three-dimensional plot of $-C(\alpha, \theta_{12})$ in the range $0 \le \alpha \le \pi/2$ and $0 \le \theta_{12} \le \pi$ for the case where the nuclear charge $Z = 1$ which was determined by Lin [598]. At $\alpha = 0$ and $\pi/2$ the potential surface tends to $-\infty$ corresponding to the electron–nuclear attraction singularity, while at $\alpha = \pi/4$ and

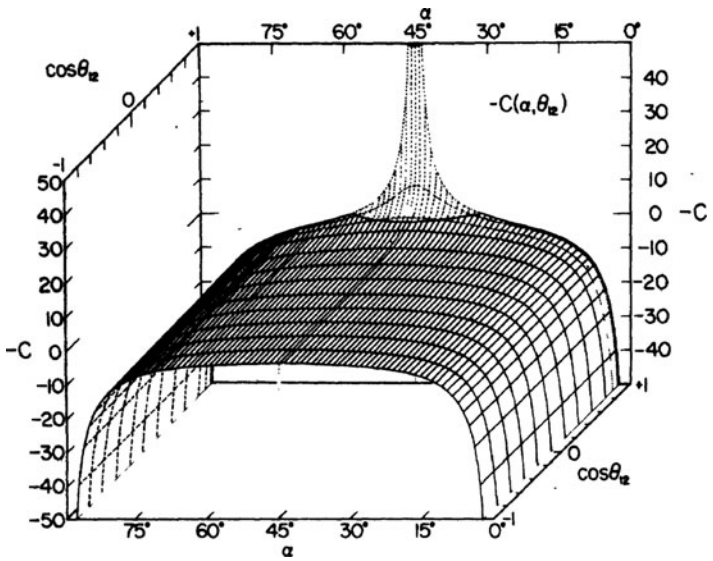

Fig. 3.7 Potential function $-C(\alpha, \theta_{12})$ as a function of α and $\cos\theta_{12}$ in Rydbergs for two electrons moving in the field of an H^+ ion (Fig. 1 from [598])

$\theta_{12} = 0$ there is a singularity corresponding to the electron–electron repulsion. The saddle point in the potential energy surface at $\alpha = \pi/4$ and $\theta_{12} = \pi$ corresponds to the situation where the two electrons are equidistant from and on opposite sides of the nucleus. We will see in Sect. 3.3.5 that it is this configuration of the outgoing electrons that Wannier [954] showed leads to the threshold behaviour of the electron impact ionization cross section.

In order to solve (3.133) it is convenient to introduce the eigenfunctions $U_K^\Gamma(\Omega)$ of the operator Λ^2. These hyperspherical harmonics, or K-harmonics, satisfy the equation

$$[\Lambda^2 - K(K+4)]U_K^\Gamma(\Omega) = 0, \tag{3.134}$$

where K is a non-negative integer which can be written as

$$K = \ell_1 + \ell_2 + 2m, \tag{3.135}$$

ℓ_1 and ℓ_2 being the usual orbital angular momentum quantum numbers and m a new non-negative integer quantum number associated with the motion in α. Also in (3.134), Ω specifies the angular variables

$$\Omega \equiv \alpha\ \theta_1\ \phi_1\ \theta_2\ \phi_2, \tag{3.136}$$

and Γ represents the conserved quantum numbers defined by (2.58).

We can eliminate the first derivative term in Λ^2 defined by (3.131) by introducing the eigenfunctions

$$\phi^\Gamma_{\ell_1\ell_2 m}(\Omega) = \sin\alpha\ \cos\alpha\ U_K^\Gamma(\Omega), \tag{3.137}$$

which satisfy the equation

$$\left[-\frac{\partial^2}{\partial\alpha^2} + \frac{\boldsymbol{\ell}_1^2}{\cos^2\alpha} + \frac{\boldsymbol{\ell}_2^2}{\sin^2\alpha} - (K+2)^2\right]\phi^\Gamma_{\ell_1\ell_2 m}(\Omega) = 0. \tag{3.138}$$

These eigenfunctions are given by

$$\phi^\Gamma_{\ell_1\ell_2 m}(\Omega) = \frac{1}{\sqrt{2}}\Big[f_{\ell_1\ell_2 m}(\alpha)Y_{\ell_1\ell_2 L M_L}(\hat{\mathbf{r}}_1,\hat{\mathbf{r}}_2) + (-1)^{\ell_1+\ell_2-L+S+m} \times\ f_{\ell_2\ell_1 m}(\alpha)Y_{\ell_2\ell_1 L M_L}(\hat{\mathbf{r}}_1,\hat{\mathbf{r}}_2)\Big], \quad \ell_1 \neq \ell_2 \tag{3.139}$$

and

$$\phi^\Gamma_{\ell_1\ell_2 m}(\Omega) = \frac{1}{\sqrt{2}}\left[1 + (-1)^{-L+S+m}\right] f_{\ell\ell m}(\alpha)Y_{\ell\ell L M_L}(\hat{\mathbf{r}}_1,\hat{\mathbf{r}}_2), \quad \ell_1 = \ell_2 = \ell, \tag{3.140}$$

where the functions $f_{\ell_1\ell_2 m}(\alpha)$ are defined in terms of Jacobi polynomials [618] and the functions $Y_{\ell_1\ell_2 LM_L}(\hat{\mathbf{r}}_1, \hat{\mathbf{r}}_2)$ are defined by (B.57).

The wave function ψ in (3.133) can now be expanded for each set of conserved quantum numbers Γ as

$$\psi^{\Gamma}(R; \Omega) = \sum_{i=1}^{n} \phi_i^{\Gamma}(\Omega) F_i^{\Gamma}(R), \tag{3.141}$$

where the subscript i represents the quantum numbers $\ell_1\ell_2 m$ and where the functions $F_i^{\Gamma}(R)$ depend only on R. Substituting this expansion into (3.133) and projecting onto the channel functions $\phi_i^{\Gamma}(\Omega)$ then gives after using (3.138)

$$\left(\frac{\mathrm{d}^2}{\mathrm{d}R^2} - \frac{(K_i+2)^2 - \frac{1}{4}}{R^2} + k^2\right) F_i^{\Gamma}(R) = -\frac{1}{R}\sum_{j=1}^{n} V_{ij}^{\Gamma} F_j^{\Gamma}(R), \quad i = 1, \ldots, n, \tag{3.142}$$

where $k^2 = 2E$. Also in (3.142) the potential matrix

$$V_{ij}^{\Gamma} = \langle \phi_i^{\Gamma}(\Omega) | C(\alpha, \theta_{12}) | \phi_j^{\Gamma}(\Omega) \rangle, \quad i,\ j = 1, \ldots, n, \tag{3.143}$$

where the integration which is over all angles Ω does not depend on R. We see that (3.142), unlike (2.63) which they replace for two electrons moving in the field of a nucleus, are a set of n coupled second-order differential equations rather than coupled second-order integrodifferential equations, where n is the number of terms retained in expansion (3.141). The Pauli exclusion principle is now represented by the form of the matrix V_{ij}^{Γ}, defined by (3.143), where the function C, defined by (3.130), satisfies the symmetry relation

$$C(\alpha, \theta_{12}) = C\left(\frac{\pi}{2} - \alpha, \theta_{12}\right), \quad 0 \le \alpha \le \frac{\pi}{2}, \tag{3.144}$$

as illustrated in Fig. 3.7. Equations (3.142) therefore partition into symmetric and antisymmetric sets corresponding to $S = 0$ and 1, respectively.

In spite of their formal simplicity, (3.142) are in principle still members of an infinite set of coupled second-order differential equations which have to be approximated in some way in practical applications. What makes the hyperspherical coordinate representation particularly useful is that in describing doubly excited resonance states of atoms, the motion in the variable R is approximately separable from the motion in other variables in a way which is analogous to the Born–Oppenheimer separation of the electronic and nuclear motion in the theory of molecular structure. This follows by examining the power series expansion of the solution $F_i^{\Gamma}(R)$ of (3.142) about $R = 0$, where we find that the leading term in the expansion does not depend on the coupling matrix V_{ij}^{Γ} on the right-hand side of (3.142) as discussed by Fano [307]. This leads us to introduce the adiabatic expansion

$$\psi^{\Gamma}(R;\Omega)=\sum_{i=1}^{n}\Phi_i^{\Gamma}(R;\Omega)G_i^{\Gamma}(R), \tag{3.145}$$

rather than expansion (3.141), where the functions $\Phi_i^{\Gamma}(R;\Omega)$ are chosen to diagonalize all the terms in (3.142) except $\mathrm{d}^2/\mathrm{d}R^2$ arising from the kinetic energy operator.

In order to determine the equations satisfied by $G_i^{\Gamma}(R)$ we introduce the symmetric matrix

$$X_{ij}^{\Gamma}(R)=\frac{(K_i+2)^2-\frac{1}{4}}{R^2}\delta_{ij}-\frac{1}{R}V_{ij}^{\Gamma},\quad i,\ j=1,\ldots,n, \tag{3.146}$$

which we diagonalize by an R-dependent orthogonal transformation as follows:

$$\left(\mathbf{A}^{\Gamma}\right)^{\mathrm{T}}\mathbf{X}^{\Gamma}\mathbf{A}^{\Gamma}=\mathbf{D}^{\Gamma}, \tag{3.147}$$

where $\mathbf{A}^{\Gamma}$ is an orthogonal matrix and $\mathbf{D}^{\Gamma}$ is a diagonal matrix, both of which are functions of R. Equations (3.142) can then be rewritten as

$$\left(\frac{\mathrm{d}^2}{\mathrm{d}R^2}-D_i^{\Gamma}(R)+k^2\right)G_i^{\Gamma}(R)=\sum_{j=1}^{n}W_{ij}^{\Gamma}(R)G_j^{\Gamma}(R),\quad i=1,\ldots,n, \tag{3.148}$$

where the functions Φ_i^{Γ} and G_i^{Γ} in (3.145) are defined in terms of the functions ϕ_i^{Γ} and F_i^{Γ} in (3.141) by the matrix equations

$$\boldsymbol{\Phi}^{\Gamma}(R;\Omega)=\left[\mathbf{A}^{\Gamma}(R)\right]^{\mathrm{T}}\boldsymbol{\phi}^{\Gamma}(\Omega) \tag{3.149}$$

and

$$\mathbf{G}^{\Gamma}(R)=\left[\mathbf{A}^{\Gamma}(R)\right]^{\mathrm{T}}\mathbf{F}^{\Gamma}(R). \tag{3.150}$$

Also the coupling potential matrix $\mathbf{W}^{\Gamma}$ on the right-hand side of (3.148) is defined by

$$\mathbf{W}^{\Gamma}(R)\mathbf{G}^{\Gamma}(R)=-2\left[\mathbf{A}^{\Gamma}(R)\right]^{\mathrm{T}}\frac{\mathrm{d}\mathbf{A}^{\Gamma}}{\mathrm{d}R}\frac{\mathrm{d}\mathbf{G}^{\Gamma}}{\mathrm{d}R}-\left[\mathbf{A}^{\Gamma}(R)\right]^{\mathrm{T}}\frac{\mathrm{d}^2\mathbf{A}^{\Gamma}}{\mathrm{d}R^2}\mathbf{G}^{\Gamma}(R). \tag{3.151}$$

The extreme adiabatic approximation is obtained by neglecting all coupling terms on the right-hand side of (3.148), while the adiabatic approximation is obtained by retaining in addition the diagonal terms $W_{ii}^{\Gamma}(R)$. If we retain all the terms in the coupling potential $W_{ij}^{\Gamma}(R)$ on the right-hand side of (3.148) then (3.142) and (3.148) give identical results.

3.3 Threshold Behaviour of Cross Sections

In this section we consider the behaviour of excitation and ionization cross sections in the neighbourhood of threshold. It was shown in a fundamental paper by Wigner [970] that the behaviour of cross sections near the threshold of a new reaction does not depend on the collision dynamics in the "reaction zone" where all the particles are close together and strongly interacting. Instead, Wigner showed that the threshold behaviour depends, apart from a constant multiple, only on the form of the potential between the reacting particles at large distances. This fundamental result is the basis of our treatment of both excitation and ionization scattering amplitudes and cross sections in the neighbourhood of threshold. We note that a review of collisions near threshold has been written by Sadeghpour et al. [804].

We commence our discussion of threshold behaviour by generalizing our treatment of effective range theory in potential scattering, to treat excitation processes involving many coupled two-body channels. In Sect. 3.3.1 we derive a multichannel effective range theory for the K-matrix and T-matrix for short-range potentials, following the work of Ross and Shaw [798], where in this derivation we make use of the analytic properties of the multichannel R-matrix introduced and discussed in Chap. 5 and later chapters. Then in Sect. 3.3.2, we extend this theory to treat excitation processes, where long-range dipole potentials are present, which was first considered by Gailitis and Damburg [359]. We conclude our treatment of threshold behaviour of excitation by considering in Sects. 3.3.3 and 3.3.4 the situation which arises in electron collisions with positive and negative ions where long-range Coulomb potentials between the interacting particles are present. We consider first in Sect. 3.3.3 an extension of multichannel effective range theory developed by Gailitis [357] using the analytic properties of the R-matrix. Then in Sect. 3.3.4 we discuss multichannel quantum defect theory (MQDT), introduced, developed and reviewed by Seaton [859] which has been widely used in the analysis of electron collisions with positive ions and photoionization processes in the neighbourhood of threshold. Also in this section we summarize extensions of MQDT to treat molecular collision processes. Finally, in Sect. 3.3.5 we consider the threshold behaviour of ionization with emphasis on single ionization of atoms and positive ions by electrons. The foundations of this subject were laid by Wannier [954, 955] and, in an introduction to this section, we summarize the threshold law of single ionization and the main theoretical and experimental developments that have been made since Wannier's fundamental analysis. We then derive the threshold law of single ionization adopting a classical analysis analogous to that used by Wannier, based on hyperspherical coordinates discussed in Sect. 3.2.6. Finally we mention some recent ab initio calculations of threshold behaviour of ionization which satisfy Wannier's threshold law.

3.3.1 Excitation: Short-Range Potentials

We commence our discussion of threshold behaviour by generalizing our treatment of effective range theory in potential scattering given in Sect. 1.4 to treat excitation

processes involving many coupled channels where the potential interactions are short range. In this way we derive a multichannel generalization of (1.120) which was first obtained by Ross and Shaw [798].

We consider the solution of n coupled second-order integrodifferential equations corresponding to electron collisions with neutral atoms, obtained by setting $N = Z$ in (3.2), which then becomes

$$\left(\frac{\mathrm{d}^2}{\mathrm{d}r^2} - \frac{\boldsymbol{\ell}(\boldsymbol{\ell}+\mathbf{I})}{r^2} - \mathbf{U}(r) + \mathbf{k}^2\right)\mathbf{F}(r) = 0, \tag{3.152}$$

where initially we assume that the potential $\mathbf{U}$ is short range satisfying

$$\mathbf{U}(r) = 0, \quad r \geq a, \tag{3.153}$$

for some finite radius $r = a$. This enables us to develop a multichannel effective range theory which forms the basis for later developments when long-range dipole and Coulomb potentials are present. In all of this work we assume that the target states are ordered so that (2.78) is satisfied.

In the energy region where all the channels are open, we showed in Sect. 2.4 that the matrix solution of (3.152), which vanishes at the origin, has the following asymptotic form:

$$\mathbf{F}(r) = \mathbf{k}^{-1/2}[\mathbf{s}_\ell(\mathbf{k}r) + \mathbf{c}_\ell(\mathbf{k}r)\mathbf{K}], \quad r \geq a, \tag{3.154}$$

where $\mathbf{K}$ is the $n \times n$-dimensional K-matrix. Also in (3.154), $\mathbf{s}_\ell(\mathbf{k}r)$ and $\mathbf{c}_\ell(\mathbf{k}r)$ are diagonal matrices which satisfy the following asymptotic boundary conditions

$$\mathbf{s}_\ell(\mathbf{k}r) = \mathbf{k}r j_\ell(\mathbf{k}r) = \left(\frac{\pi \mathbf{k}r}{2}\right)^{1/2} J_{\ell+\frac{1}{2}}(\mathbf{k}r) \underset{r\to\infty}{\sim} \sin\left(\mathbf{k}r - \tfrac{1}{2}\boldsymbol{\ell}\pi\right) \tag{3.155}$$

and

$$\mathbf{c}_\ell(\mathbf{k}r) = -\mathbf{k}r n_\ell(\mathbf{k}r) = (-1)^{\boldsymbol{\ell}}\left(\frac{\pi \mathbf{k}r}{2}\right)^{1/2} J_{-\boldsymbol{\ell}-\frac{1}{2}}(\mathbf{k}r) \underset{r\to\infty}{\sim} \cos\left(\mathbf{k}r - \tfrac{1}{2}\boldsymbol{\ell}\pi\right), \tag{3.156}$$

where the diagonal elements are expressed in terms of spherical Bessel functions of half-odd integer order defined in Appendix C.2. We previously encountered these functions in Sect. 1.1 where we observed that $\mathbf{c}_\ell(\mathbf{k}r)$ can also be expressed in terms of spherical Neumann functions.

In order to determine the analytic properties of the K-matrix we relate it to the analytic properties of the $n \times n$-dimensional R-matrix $\mathbf{R}(E)$, introduced in Sect. 5.1.2. In that section we show that the R-matrix, defined by (5.19), is a real meromorphic function of energy with simple poles only on the real energy axis. Hence the R-matrix does not contain threshold branch cuts, discussed in Sect. 3.1,

which arise from the solution of the coupled second-order integrodifferential equations (3.152) in the external and asymptotic regions.

The solution of (3.152) which vanishes at the origin $r = 0$ satisfies the following equation:

$$\mathbf{F}(a) = \mathbf{R}(E)\left(a\frac{\mathrm{d}\mathbf{F}}{\mathrm{d}r} - b\mathbf{F}\right)_{r=a}, \tag{3.157}$$

where b is an arbitrary constant and where we have chosen the boundary of the internal R-matrix region to be the range $r = a$ of the potential $\mathbf{U}(r)$. We then substitute the solution $\mathbf{F}(r)$, defined by (3.154), into (3.157) yielding

$$\mathbf{k}^{-1/2}(\mathbf{s}_\ell + \mathbf{c}_\ell\mathbf{K}) = \mathbf{R}(E)\mathbf{k}^{-1/2}[\boldsymbol{\rho}(\mathbf{s}'_\ell + \mathbf{c}'_\ell\mathbf{K}) - b(\mathbf{s}_\ell + \mathbf{c}_\ell\mathbf{K})], \tag{3.158}$$

where the diagonal matrix $\boldsymbol{\rho} = \mathbf{k}a$ and where the diagonal matrices $\mathbf{s}_\ell$, $\mathbf{c}_\ell$, $\mathbf{s}'_\ell$ and $\mathbf{c}'_\ell$ are defined by

$$\mathbf{s}_\ell = \mathbf{s}_\ell(\mathbf{k}a), \quad \mathbf{c}_\ell = \mathbf{c}_\ell(\mathbf{k}a), \quad \mathbf{s}'_\ell = \frac{1}{\mathbf{k}}\left.\frac{\mathrm{d}\mathbf{s}_\ell(\mathbf{k}r)}{\mathrm{d}r}\right|_{r=a}, \quad \mathbf{c}'_\ell = \frac{1}{\mathbf{k}}\left.\frac{\mathrm{d}\mathbf{c}_\ell(\mathbf{k}r)}{\mathrm{d}r}\right|_{r=a}. \tag{3.159}$$

Setting the arbitrary constant $b = 0$ in (3.157) and (3.158), using the Wronskian relation $\mathbf{s}'_\ell\mathbf{c}_\ell - \mathbf{c}'_\ell\mathbf{s}_\ell = \mathbf{I}$ and re-arranging the terms in (3.158), we obtain the following expression for the K-matrix in terms of the R-matrix evaluated at $r = a$:

$$\mathbf{K}^{-1} = -\frac{\mathbf{c}_\ell}{\mathbf{s}_\ell} + \frac{\mathbf{I}}{\mathbf{s}'_\ell\mathbf{s}_\ell} + \boldsymbol{\rho}^{-1/2}\mathbf{s}'^{-1}_\ell\left(\mathbf{R}(E) - \boldsymbol{\rho}^{-1}\frac{\mathbf{s}_\ell}{\mathbf{s}'_\ell}\right)^{-1}\mathbf{s}'^{-1}_\ell\boldsymbol{\rho}^{-1/2}. \tag{3.160}$$

The analytic behaviour of the K-matrix in the complex energy plane is therefore given in terms of the analytic properties of the matrices $\mathbf{s}_\ell$, $\mathbf{s}'_\ell$ and $\mathbf{c}_\ell$ together with that of the R-matrix $\mathbf{R}(E)$. We find, following our discussion in potential scattering which led to (1.117), that $\mathbf{k}^{-\ell-1}\mathbf{s}_\ell$, $\mathbf{k}^{-\ell}\mathbf{s}'_\ell$ and $\mathbf{k}^{\ell}\mathbf{c}_\ell$ are diagonal matrices whose elements are analytic functions of energy which do not contain threshold branch cuts. Hence, after substituting these results into (3.160) we find that $\mathbf{K}^{-1}$ can be written in the following form:

$$\mathbf{K}^{-1} = \mathbf{k}^{-\ell-\frac{1}{2}}\mathbf{M}(E)\mathbf{k}^{-\ell-\frac{1}{2}}, \tag{3.161}$$

where the $n \times n$-dimensional M-matrix $\mathbf{M}(E)$ is a real symmetric analytic function of energy E which does not contain threshold branch cuts.

We can also obtain an analogous expression for the T-matrix, introduced in Sect. 2.5, which is defined in terms of the K-matrix by

$$\mathbf{T} = \frac{2\mathrm{i}\mathbf{K}}{\mathbf{I} - \mathrm{i}\mathbf{K}}. \tag{3.162}$$

We find, after substituting (3.161) into (3.162), that

$$\mathbf{T} = \mathbf{k}^{\ell+\frac{1}{2}} \frac{2\mathrm{i}}{\mathbf{M}(E) - \mathrm{i}\mathbf{k}^{2\ell+1}} \mathbf{k}^{\ell+\frac{1}{2}}. \tag{3.163}$$

Equations (3.161) and (3.163) were first obtained by Ross and Shaw [798].

It follows from the above discussion that the M-matrix $\mathbf{M}(E)$ can be expanded as a power series in energy

$$\mathbf{M}(E) = \mathbf{M}_0 + \mathbf{M}_1 E + \mathbf{M}_2 E^2 + \cdots, \tag{3.164}$$

where $\mathbf{M}_0$, $\mathbf{M}_1$, $\mathbf{M}_2, \ldots$ are real symmetric energy-independent matrices. This expansion is valid through thresholds although the radius of convergence of the expansion will in general be finite. We see that (3.161), (3.163) and (3.164) reduce, when the number of channels $n = 1$, to (1.118), (1.119) and (1.120) which we obtained for potential scattering in Sect. 1.4.1.

The above effective range theory enables theoretical calculations or experimental measurements above and below thresholds to be related. For example, we have shown in Sect. 3.2.1 that bound states and resonances correspond to poles in the S-matrix and hence in the T-matrix. It follows from (3.163) that these poles occur when the denominator of this equation satisfies

$$\det\left[\mathbf{M}(E) - \mathrm{i}\mathbf{k}^{2\ell+1}\right] = 0. \tag{3.165}$$

Hence (3.161), (3.163) and (3.164) relate the scattering amplitudes and cross sections above threshold to the bound states and resonances below threshold through the analytic properties of the M-matrix.

We consider briefly an application of the above theory to two coupled channels. In this case we can relate the parameters of a resonance lying below the upper threshold to the two elastic scattering amplitudes, the inelastic scattering amplitude and the corresponding cross sections above this threshold. We see this most clearly if the elements of the M-matrix are slowly varying over this energy range so that we need to only consider the three independent elements of $\mathbf{M}_0$ in (3.164). These elements can be fitted to give the resonance position, resonance width and background phase shift which then enables the three scattering amplitudes and hence the cross sections to be determined over a limited energy range above this threshold. This relationship between resonances below threshold and cross sections above threshold in two-channel models has been considered by several workers. For example, Damburg and Peterkop [244] explored this relationship in a 1s–2s model e^-–H collision calculation, and Burke [151, 152] related the resonance parameters of the ^{2}S resonance at 19.37 eV, which lies below the $2\,^3$S threshold in e^-–He collisions, to the $1\,^1$S–$2\,^3$S excitation cross section in the ^{2}S state just above this threshold. Further discussions of resonances which arise in e^-–He collisions are given in Sect. 5.6.2.

Finally, we remark that, as in potential scattering, although the effective range expansion, defined by (3.161), (3.162), (3.163) and(3.164), has been derived for a finite range potential satisfying (3.153), it is also valid for potentials that fall off asymptotically as fast as or faster than an exponential, provided that the radius a is chosen so that these potentials are negligibly small for $r \geq a$.

3.3.2 Excitation: Dipole Potentials

In this section we extend our discussion of threshold behaviour of excitation to treat many coupled two-body channels where long-range dipole potentials are present. We obtain a multichannel effective range expression first derived by Gailitis and Damburg [358, 359] and we consider an application to electron–hydrogen atom collisions near the $n = 2$ threshold.

As in Sect. 3.3.1, we consider the solution of the n coupled second-order integro-differential equations (3.2) where we set $N = Z$ corresponding to electron collisions with neutral atoms. We have shown in Sect. 2.3.2 that we can choose a radius $r = a$ such that the local direct potential included in $\mathbf{U}(r)$ in (3.2) is represented by a sum of terms behaving as inverse powers of the radius r, while the non-local exchange and correlation potentials are negligibly small beyond this radius. It follows that for neutral atoms the leading term in the long-range potential has the form

$$\mathbf{U}(r) = \frac{\boldsymbol{\alpha}}{r^2}, \quad r \geq a, \tag{3.166}$$

where $\boldsymbol{\alpha}$ is a real symmetric matrix. Hence the coupled integrodifferential equations (3.2) corresponding to electron collisions with neutral atoms reduce to

$$\left(\frac{\mathrm{d}^2}{\mathrm{d}r^2} - \frac{\boldsymbol{\ell}(\boldsymbol{\ell}+\mathbf{I}) + \boldsymbol{\alpha}}{r^2} + \mathbf{k}^2\right)\mathbf{F}(r) = 0, \quad r \geq a, \tag{3.167}$$

where we have neglected higher order terms in the long-range potential. However, these terms can be included in the internal region, $r < a$, together with the non-local exchange and correlation potentials.

We now describe the modified multichannel effective range theory, developed by Gailitis and Damburg [358, 359], which is applicable to scattering by long-range potentials defined by (3.166). We will see that this theory describes the situation where the off-diagonal dipole terms retained in the calculation couple degenerate or almost degenerate channels. This includes the most important long-range potential terms in electron collisions with hydrogen atoms, where the degeneracy of the non-relativistic target states corresponding to principal quantum numbers $n \geq 2$ results in the target atom acquiring a non-zero dipole moment in the field of the scattered electron. This theory is also applicable to electron collisions with atoms in highly excited states which are almost degenerate and with polar molecules when the rotational splitting of the levels can be neglected.

We commence by introducing an r- and energy-independent orthogonal matrix $\mathbf{A}$ which diagonalizes the matrix coefficient of the r^{-2} term $\boldsymbol{\ell}(\boldsymbol{\ell}+\mathbf{I})+\boldsymbol{\alpha}$ in (3.167) giving

$$\mathbf{A}^{-1}[\boldsymbol{\ell}(\boldsymbol{\ell}+\mathbf{I})+\boldsymbol{\alpha}]\mathbf{A}=\boldsymbol{\lambda}(\boldsymbol{\lambda}+\mathbf{I}). \tag{3.168}$$

In accord with the above discussion, we only retain terms in $\boldsymbol{\alpha}$ which couple degenerate or almost degenerate channels. Hence $\boldsymbol{\ell}(\boldsymbol{\ell}+\mathbf{I})+\boldsymbol{\alpha}$ has block diagonal form, where each block corresponds to a set of degenerate channels. It follows that $\mathbf{A}$ has the same block diagonal form and consequently commutes with the diagonal matrix $\mathbf{k}^2$ in (3.167). We can therefore transform (3.167) to diagonal form by multiplying on the left by $\mathbf{A}^{-1}$ yielding

$$\left(\frac{\mathrm{d}^2}{\mathrm{d}r^2}-\frac{\boldsymbol{\lambda}(\boldsymbol{\lambda}+\mathbf{I})}{r^2}+\mathbf{k}^2\right)\mathbf{A}^{-1}\mathbf{F}(r)=0,\quad r\geq a. \tag{3.169}$$

We observe that while the elements of the diagonal matrix $\boldsymbol{\lambda}(\boldsymbol{\lambda}+\mathbf{I})$ are real the corresponding effective angular momentum components λ_i are non-integral and can become complex for sufficiently strong long-range dipole interactions represented by the matrix $\boldsymbol{\alpha}$. We will see below that this leads to new and anomalous threshold behaviour.

In order to determine the threshold behaviour we introduce a transformed K-matrix $\mathcal{K}$ in analogy with (3.154) by the asymptotic form

$$\mathbf{A}^{-1}\mathbf{F}(r)=\mathbf{k}^{-1/2}[\mathbf{s}_{\boldsymbol{\lambda}}(\mathbf{k}r)+\mathbf{c}_{\boldsymbol{\lambda}}(\mathbf{k}r)\mathcal{K}],\quad r\geq a, \tag{3.170}$$

where $\mathbf{s}_{\boldsymbol{\lambda}}(\mathbf{k}r)$ and $\mathbf{c}_{\boldsymbol{\lambda}}(\mathbf{k}r)$ are diagonal matrices which satisfy the following asymptotic boundary conditions

$$\mathbf{s}_{\boldsymbol{\lambda}}(\mathbf{k}r)=\mathbf{k}r\,j_{\boldsymbol{\lambda}}(\mathbf{k}r)=\left(\frac{\pi\mathbf{k}r}{2}\right)^{1/2}J_{\boldsymbol{\lambda}+\frac{1}{2}}(\mathbf{k}r)\underset{r\to\infty}{\sim}\sin\left(\mathbf{k}r-\tfrac{1}{2}\boldsymbol{\lambda}\pi\right) \tag{3.171}$$

and

$$\mathbf{c}_{\boldsymbol{\lambda}}(\mathbf{k}r)=-\mathbf{k}r\,n_{\boldsymbol{\lambda}}(\mathbf{k}r)=\left(\frac{\pi\mathbf{k}r}{2}\right)^{1/2}\frac{J_{-\boldsymbol{\lambda}-\frac{1}{2}}(\mathbf{k}r)}{\cos\boldsymbol{\lambda}\pi}\underset{r\to\infty}{\sim}\frac{\cos\left(\mathbf{k}r+\frac{1}{2}\boldsymbol{\lambda}\pi\right)}{\cos\boldsymbol{\lambda}\pi}. \tag{3.172}$$

These equations reduce to Eqs. (3.155) and (3.156) when the dipole potential matrix $\boldsymbol{\alpha}$ is zero and hence the diagonal elements of $\boldsymbol{\lambda}$ reduce to integer values given by $\boldsymbol{\ell}$. Also, as discussed in Appendix C.2, the spherical Bessel functions, defined by (3.171) and (3.172), have simple analytic properties in the complex energy plane for non-integral and complex values of $\boldsymbol{\lambda}$ which enables the development of the multichannel effective range theory described below.

The analytic properties of the transformed K-matrix $\boldsymbol{\mathcal{K}}$ can be determined by relating it to the analytic properties of the transformed R-matrix $\boldsymbol{\mathcal{R}}(E)$ corresponding to (3.169). In analogy with (3.157) the R-matrix is defined by

$$\mathbf{A}^{-1}\mathbf{F}(a) = \boldsymbol{\mathcal{R}}(E)\left(a\mathbf{A}^{-1}\frac{\mathrm{d}\mathbf{F}}{\mathrm{d}r} - b\mathbf{A}^{-1}\mathbf{F}\right)_{r=a}. \tag{3.173}$$

It follows from this definition that $\boldsymbol{\mathcal{R}}(E)$ is related to the R-matrix $\mathbf{R}(E)$, corresponding to the original coupled integrodifferential equations, defined by (3.152) and (3.167), by the transformation

$$\boldsymbol{\mathcal{R}}(E) = \mathbf{A}^{-1}\mathbf{R}(E)\mathbf{A}. \tag{3.174}$$

Since $\mathbf{R}(E)$ is an analytic function of energy with simple poles only on the real energy axis and since $\mathbf{A}$ does not depend on the energy, then $\boldsymbol{\mathcal{R}}(E)$ is also an analytic function of energy with poles only on the real energy axis. We set the arbitrary constant $b = 0$ in (3.173) and substitute the expression for $\mathbf{A}^{-1}\mathbf{F}(a)$ given by (3.170) into (3.173). After re-arranging the terms and using the Wronskian relation $\mathbf{s}'_{\boldsymbol{\lambda}}\mathbf{c}_{\boldsymbol{\lambda}} - \mathbf{c}'_{\boldsymbol{\lambda}}\mathbf{s}_{\boldsymbol{\lambda}} = \mathbf{I}$, we obtain

$$\boldsymbol{\mathcal{K}}^{-1} = -\frac{\mathbf{c}_{\boldsymbol{\lambda}}}{\mathbf{s}_{\boldsymbol{\lambda}}} + \frac{\mathbf{I}}{\mathbf{s}'_{\boldsymbol{\lambda}}\mathbf{s}_{\boldsymbol{\lambda}}} + \boldsymbol{\rho}^{-1/2}\mathbf{s}'^{-1}_{\boldsymbol{\lambda}}\left(\boldsymbol{\mathcal{R}}(E) - \boldsymbol{\rho}^{-1}\frac{\mathbf{s}_{\boldsymbol{\lambda}}}{\mathbf{s}'_{\boldsymbol{\lambda}}}\right)^{-1}\mathbf{s}'^{-1}_{\boldsymbol{\lambda}}\boldsymbol{\rho}^{-1/2}, \tag{3.175}$$

where $\boldsymbol{\rho} = \mathbf{k}a$ and $\mathbf{s}_{\boldsymbol{\lambda}}$, $\mathbf{s}'_{\boldsymbol{\lambda}}$, $\mathbf{c}_{\boldsymbol{\lambda}}$ and $\mathbf{c}'_{\boldsymbol{\lambda}}$ are defined by (3.159) with $\boldsymbol{\ell}$ replaced by $\boldsymbol{\lambda}$. We see that (3.175) has the same form as (3.160) where the diagonal elements of $\boldsymbol{\lambda}$ are replaced by integer values given by $\boldsymbol{\ell}$. The analytic behaviour of the K-matrix $\boldsymbol{\mathcal{K}}$ in the complex energy plane is then given in terms of the analytic properties of $\mathbf{s}_{\boldsymbol{\lambda}}$, $\mathbf{s}'_{\boldsymbol{\lambda}}$ and $\mathbf{c}_{\boldsymbol{\lambda}}$ together with those of the R-matrix $\boldsymbol{\mathcal{R}}(E)$.

Following our discussion which led to (3.161), we find that $\boldsymbol{\mathcal{K}}^{-1}$ can be written in the form

$$\boldsymbol{\mathcal{K}}^{-1} = \mathbf{k}^{-\boldsymbol{\lambda}-\frac{1}{2}}\boldsymbol{\mathcal{M}}(E)\mathbf{k}^{-\boldsymbol{\lambda}-\frac{1}{2}}, \tag{3.176}$$

where the M-matrix $\boldsymbol{\mathcal{M}}(E)$ is an analytic function of energy which does not contain threshold branch cuts. Also, it follows from (3.175) and (3.176) that $\boldsymbol{\mathcal{M}}(E)$ is symmetric and when all the elements of $\boldsymbol{\lambda}$ are real then $\boldsymbol{\mathcal{M}}(E)$ is also real. However, if some of the elements of $\boldsymbol{\lambda}$ are complex then $\boldsymbol{\mathcal{M}}(E)$ will also be complex. Hence $\boldsymbol{\mathcal{M}}(E)$ can be expanded as a power series in the energy

$$\boldsymbol{\mathcal{M}}(E) = \boldsymbol{\mathcal{M}}_0 + \boldsymbol{\mathcal{M}}_1 E + \boldsymbol{\mathcal{M}}_2 E^2 + \cdots, \tag{3.177}$$

where the coefficients $\boldsymbol{\mathcal{M}}_0$, $\boldsymbol{\mathcal{M}}_1$, $\boldsymbol{\mathcal{M}}_2, \ldots$ are in general complex symmetric energy-independent matrices.

In order to determine the corresponding multichannel effective range theory expressions for the S- and T-matrices we recombine the columns of (3.170) by multiplying on the right by a matrix $\mathbf{B}$ to give

$$\mathbf{A}^{-1}\mathbf{F}(r)\mathbf{B} = \mathbf{k}^{-1/2}\left\{\exp\left[-\mathrm{i}\left(\mathbf{k}r - \tfrac{1}{2}\boldsymbol{\lambda}\pi\right)\right] - \exp\left[\mathrm{i}\left(\mathbf{k}r - \tfrac{1}{2}\boldsymbol{\lambda}\pi\right)\right]\boldsymbol{\mathcal{S}}\right\}, \quad r \geq a, \tag{3.178}$$

where the transformed S-matrix $\boldsymbol{\mathcal{S}}$ is defined by

$$\boldsymbol{\mathcal{S}} = [\mathbf{I} + \mathrm{i}(\mathbf{I} + \mathrm{i}\tan\boldsymbol{\lambda}\pi)\boldsymbol{\mathcal{K}}]\,[\mathbf{I} - \mathrm{i}(\mathbf{I} - \mathrm{i}\tan\boldsymbol{\lambda}\pi)\boldsymbol{\mathcal{K}}]^{-1} \tag{3.179}$$

and $\mathbf{B}$ is defined by

$$\mathbf{B}^{-1} = -\frac{1}{2\mathrm{i}}\,[\mathbf{I} - \mathrm{i}(\mathbf{I} - \mathrm{i}\tan\boldsymbol{\lambda}\pi)\boldsymbol{\mathcal{K}}]\,. \tag{3.180}$$

We then transform (3.178) by multiplying this equation on the left by $\mathbf{A}$ and on the right by

$$\mathbf{C} = \exp\left(-\tfrac{1}{2}\mathrm{i}\boldsymbol{\lambda}\pi\right)\mathbf{A}^{-1}\exp\left(\tfrac{1}{2}\mathrm{i}\boldsymbol{\ell}\pi\right), \tag{3.181}$$

which yields

$$\mathbf{F}(r)\mathbf{B}\mathbf{C} = \mathbf{k}^{-1/2}\left\{\exp\left[-\mathrm{i}\left(\mathbf{k}r - \tfrac{1}{2}\boldsymbol{\ell}\pi\right)\right] - \exp\left[\mathrm{i}\left(\mathbf{k}r - \tfrac{1}{2}\boldsymbol{\ell}\pi\right)\right]\mathbf{S}\right\}, \quad r \geq a, \tag{3.182}$$

where the S-matrix $\mathbf{S}$ is defined by

$$\mathbf{S} = \exp\left(\tfrac{1}{2}\mathrm{i}\boldsymbol{\ell}\pi\right)\mathbf{A}\exp\left(-\tfrac{1}{2}\mathrm{i}\boldsymbol{\lambda}\pi\right)\boldsymbol{\mathcal{S}}\exp\left(-\tfrac{1}{2}\mathrm{i}\boldsymbol{\lambda}\pi\right)\mathbf{A}^{-1}\exp\left(\tfrac{1}{2}\mathrm{i}\boldsymbol{\ell}\pi\right). \tag{3.183}$$

Finally, we substitute for $\boldsymbol{\mathcal{S}}$ given by (3.179) into (3.183), where $\boldsymbol{\mathcal{K}}$ is written in terms of $\boldsymbol{\mathcal{M}}(E)$ using (3.176). We find that

$$\begin{aligned}\mathbf{T} = {} & \exp\left(\tfrac{1}{2}\mathrm{i}\boldsymbol{\ell}\pi\right)\mathbf{A}\exp\left(-\tfrac{1}{2}\mathrm{i}\boldsymbol{\lambda}\pi\right)\mathbf{k}^{\boldsymbol{\lambda}+\frac{1}{2}}\,\frac{2\mathrm{i}}{\boldsymbol{\mathcal{M}}(E) - \mathrm{i}(\mathbf{I} - \mathrm{i}\tan\boldsymbol{\lambda}\pi)\mathbf{k}^{2\boldsymbol{\lambda}+1}} \\ & \times \mathbf{k}^{\boldsymbol{\lambda}+\frac{1}{2}}\exp\left(-\tfrac{1}{2}\mathrm{i}\boldsymbol{\lambda}\pi\right)\mathbf{A}^{-1}\exp\left(\tfrac{1}{2}\mathrm{i}\boldsymbol{\ell}\pi\right) \\ & + \exp\left(\tfrac{1}{2}\mathrm{i}\boldsymbol{\ell}\pi\right)\mathbf{A}\exp(-\mathrm{i}\boldsymbol{\lambda}\pi)\mathbf{A}^{-1}\exp\left(\tfrac{1}{2}\mathrm{i}\boldsymbol{\ell}\pi\right) - \mathbf{I},\end{aligned} \tag{3.184}$$

which is the effective range expression for the T-matrix in the presence of long-range dipole potentials, where we remember that $\mathbf{T} = \mathbf{S} - \mathbf{I}$. We see that when the dipole potential matrix $\boldsymbol{\alpha}$ is zero then $\boldsymbol{\lambda} = \boldsymbol{\ell}$ and $\mathbf{A} = \mathbf{I}$ so that $\tan\boldsymbol{\lambda}\pi = 0$. Equation (3.184) then reduces to (3.163) valid for short-range potentials. It follows from (3.184) that the well-known symmetry of the S-matrix, and hence the T-matrix,

corresponds to the symmetry of the M-matrix $\boldsymbol{\mathcal{M}}(E)$ discussed above. In addition it should be noted that the unitarity of the S-matrix imposes further restrictions on $\boldsymbol{\mathcal{M}}(E)$.

We observe that, as in potential scattering discussed in Sect. 1.4.2, for a sufficiently strong long-range dipole potential $\mathbf{U}(r)$, defined by (3.166), individual components λ_i of the diagonal matrix $\boldsymbol{\lambda}$ defined by (3.168) can be complex and can be written as

$$\lambda_i = -\frac{1}{2} + \mathrm{i}\,\mathrm{Im}\,\lambda_i, \tag{3.185}$$

where $\mathrm{Im}\,\lambda_i$ can be positive or negative. It follows that the corresponding components of the factor $\mathbf{k}^{\lambda+\frac{1}{2}}$ in the T-matrix defined by (3.184) can be written as

$$k_i^{\lambda_i+\frac{1}{2}} = k_i^{\mathrm{i}\,\mathrm{Im}\lambda_i} = \exp(\mathrm{i}\,\mathrm{Im}\,\lambda_i \ln k_i), \tag{3.186}$$

which gives rise to an infinite number of oscillations in the cross section as the energy tends to threshold from above. Also, an infinite number of bound states or resonances converge to this threshold from below.

As an example of the above analysis we consider electron collisions with atomic hydrogen for total orbital angular momentum $L = 0$ near the $n = 2$ threshold. The coupled second-order integrodifferential equations coupling the 2s and 2p states then have the following form for $r \geq a$:

$$\begin{aligned}\left(\frac{\mathrm{d}^2}{\mathrm{d}r^2} + k_2^2\right) F_{2\mathrm{s}}(r) - \frac{6}{r^2} F_{2\mathrm{p}}(r) = 0,\\ \left(\frac{\mathrm{d}^2}{\mathrm{d}r^2} - \frac{2}{r^2} + k_2^2\right) F_{2\mathrm{p}}(r) - \frac{6}{r^2} F_{2\mathrm{s}}(r) = 0,\end{aligned} \tag{3.187}$$

where a is chosen such that non-local exchange and correlation potentials vanish for $r \geq a$ so that the following analysis applies for both singlet $S = 0$ and triplet $S = 1$ total spin states. Also in (3.187) we have neglected the diagonal r^{-3} potential in the 2p channel, since its presence does not significantly alter the following analysis. Comparing (3.187) with (3.167) we see that the coefficient of the r^{-2} term in (3.167) has the following matrix form

$$\boldsymbol{\ell}(\boldsymbol{\ell} + \mathbf{I}) + \boldsymbol{\alpha} = \begin{bmatrix} 0 & 6 \\ 6 & 2 \end{bmatrix}, \tag{3.188}$$

which can be diagonalized, as in (3.168), to yield the matrix

$$\boldsymbol{\lambda}(\boldsymbol{\lambda} + \mathbf{I}) = \begin{bmatrix} 1 + \sqrt{37} & 0 \\ 0 & 1 - \sqrt{37} \end{bmatrix}. \tag{3.189}$$

The corresponding diagonal elements of $\boldsymbol{\lambda}$ are then

$$\lambda_1 = -\frac{1}{2} \pm \left[\sqrt{37} + \frac{5}{4}\right]^{1/2},$$
$$\lambda_2 = -\frac{1}{2} \pm \mathrm{i}\left[\sqrt{37} - \frac{5}{4}\right]^{1/2}, \tag{3.190}$$

and the diagonalized form of (3.187) can be written as

$$\left(\frac{\mathrm{d}^2}{\mathrm{d}r^2} - \frac{\boldsymbol{\lambda}(\boldsymbol{\lambda}+\mathbf{I})}{r^2} + \mathbf{k}_2^2\right)\mathbf{A}^{-1}\mathbf{F}(r) = 0, \quad r \geq a, \tag{3.191}$$

where the orthogonal matrix $\mathbf{A}$ is defined by (3.168).

We now consider the zero-energy solution of (3.191) corresponding to the complex second eigenvalue λ_2, defined by (3.190). Writing $\mathbf{G} = \mathbf{A}^{-1}\mathbf{F}$ we see that the general solution of (3.191) corresponding to this eigenvalue can be written as

$$G_2(r) = d_1 r^{\lambda_2+1} + d_2 r^{-\lambda_2}, \quad r \geq a. \tag{3.192}$$

After substituting for λ_2 from (3.190) we can re-write (3.192) in the general form

$$G_2(r) = b r^{1/2} \sin(\mathrm{Im}\,\lambda_2 \ln r + \delta), \quad r \geq a. \tag{3.193}$$

where

$$\mathrm{Im}\,\lambda_2 = \left[\sqrt{37} - \frac{5}{4}\right]^{1/2} = 2.19835\ldots, \tag{3.194}$$

and where the coefficients b and δ in (3.193) are determined by fitting to the internal region solution of the coupled integrodifferential equations at $r = a$. We see that the solution $G_2(r)$, defined by (3.193), has an infinite number of oscillations in r in the range $a \leq r \leq \infty$, which corresponds to an infinite number of bound states supported by the angular momentum term in (3.191), which can be written in this case as

$$-\frac{\lambda_2(\lambda_2+1)}{r^2} = \frac{0.25 + (\mathrm{Im}\,\lambda_2)^2}{r^2}, \tag{3.195}$$

which is clearly attractive.

We next consider the solution of (3.191) for negative k_2^2. We first observe that an increase in the argument of the zero-energy solution (3.193) by π radians, corresponding to an additional node in the oscillation, occurs when the radius r increases by the ratio

$$\frac{r_2}{r_1} = \exp\left(\frac{\pi}{\mathrm{Im}\,\lambda_2}\right). \tag{3.196}$$

When k_2^2 is negative these oscillations are cut off for large r when the k_2^2 term in (3.191) dominates the angular momentum term. As the magnitude of k_2^2 decreases towards zero, additional oscillations are supported by the angular momentum term, each corresponding to an additional bound state. We then see from (3.191) and (3.196) that the ratio of the magnitudes of k_2^2 before and after the additional oscillation is supported is

$$R = \frac{(k_2^2)_{r=r_1}}{(k_2^2)_{r=r_2}} = \frac{r_2^2}{r_1^2} = \exp\left(\frac{2\pi}{\mathrm{Im}\,\lambda_2}\right). \tag{3.197}$$

In the present example we find, using (3.194), that the resonance spacing ratio

$$R = 17.429\ldots. \tag{3.198}$$

We note that (3.197) can be obtained directly from the multichannel effective range theory expansion for the T-matrix, given by (3.184), assuming the constancy of the M-matrix.

The infinite series of bound states predicted by this theory is reduced in practice to a finite number due to relativistic splitting of the $n = 2$ levels of atomic hydrogen, which removes the degeneracy of the levels with the same principal quantum number assumed in the above derivation. In addition, inclusion of coupling with the open 1s channel shifts the energies of the bound states into the complex energy plane where they give rise to a series of resonances, where the ratio of the widths of the neighbouring resonances also satisfies (3.197) and (3.198). The first resonance in this series with $^1S^e$ symmetry was found by Burke and Schey [160] at ~9.6 eV incident electron energy in a close coupling calculation including the 1s, 2s and 2p target states in expansion (2.57) and was first observed experimentally by Schulz [836].

The above analysis can be carried out for electron–hydrogen atom collisions for all total orbital angular momentum L and at all thresholds corresponding to principal quantum numbers $n \geq 2$, as discussed by Burke [151, 152] and Pathak et al. [720, 721]. We find that complex λ values leading to anomalous threshold behaviour are found at all thresholds with $n \geq 2$ for small L. We summarize the resonance spacing ratio R defined by (3.197) for $L \leq 6$ and for $n \leq 5$ in Table 3.1, where relativistic fine-structure splitting of the levels is neglected. We see that for some (L, n) values more than one resonance series occur. Also, as the principal quantum number n increases we find that resonance series occur for an increasing number of L values. We also find that for a given L, however large, resonance series will occur for sufficiently high n.

3.3.3 Excitation: Coulomb Potential

In this and the next section we extend our discussion of the threshold behaviour of excitation cross sections to treat many coupled two-body channels interacting through a Coulomb potential, corresponding to electron collisions with positive and

Table 3.1 Level spacing ratios R for electron–hydrogen atom resonances at thresholds corresponding to total orbital angular momentum $L \leq 6$ and principal quantum number $n \leq 5$ for both total spin angular momenta $S = 0$ and 1

n	$L=0$	$L=1$	$L=2$	$L=3$	$L=4$	$L=5$	$L=6$
2	17.429	29.334	4422.18	–	–	–	–
3	4.823	5.164	6.134	9.323	62.416	–	–
	–	16.752	80.552	–	–	–	–
4	2.982	3.047	3.197	3.485	4.070	5.608	16.698
	16.210	4.360	4.940	6.494	14.492	–	–
	–	27.299	18.777	8.516^{8}	–	–	–
	–	–	3226.6	–	–	–	–
5	2.312	2.334	2.382	2.463	2.594	2.812	3.213
	4.107	2.792	2.901	3.103	3.484	4.326	7.354
	–	4.224	4.091	4.892	7.396	59.907	–
	–	32.955	4.766	6.184	12.838	–	–
	–	–	9.577^{5}	25.479	–	–	–

The superscripts 5 and 8 are abbreviations for $\times 10^5$ and $\times 10^8$, respectively.

negative ions. In this section we obtain an effective range expression, first derived by Gailitis [357] using the analytic properties of the R-matrix, and we discuss the behaviour of the cross sections near threshold for an attractive Coulomb potential. Then in Sect. 3.3.4 we consider multichannel quantum defect theory (MQDT) introduced, developed and reviewed by Seaton [859], which is widely used in the analysis and calculation of electron collisions with positive ions and corresponding photoionization processes in the neighbourhood of threshold. Also, we summarize some of the most important extensions of MQDT to molecular collision processes.

3.3.3.1 Effective Range Theory

We consider the solution of n coupled second-order integrodifferential equations (3.2) describing the scattering of electrons by multi-electron positive or negative ions. We assume that the potential matrix $\mathbf{U}(r)$ in this equation, representing the local direct, non-local exchange and non-local correlation potentials, can be neglected for r greater than some radius a. Hence (3.2) then reduces to

$$\left(\frac{\mathrm{d}^2}{\mathrm{d}r^2} - \frac{\boldsymbol{\ell}(\boldsymbol{\ell}+\mathbf{I})}{r^2} + \frac{2(Z-N)}{r} + \mathbf{k}^2\right)\mathbf{F}(r) = 0, \quad r \geq a, \tag{3.199}$$

The general solution of (3.199) which vanishes at the origin has the following asymptotic form:

$$\mathbf{F}(r) = \mathbf{k}^{-1/2}\left[\mathbf{F}_{\boldsymbol{\ell}}(\boldsymbol{\eta}, \mathbf{k}r) + \mathbf{G}_{\boldsymbol{\ell}}(\boldsymbol{\eta}, \mathbf{k}r)\mathbf{K}\right], \quad r \geq a, \tag{3.200}$$

where $\mathbf{F}_\ell(\boldsymbol{\eta}, \mathbf{k}r)$ and $\mathbf{G}_\ell(\boldsymbol{\eta}, \mathbf{k}r)$ are diagonal matrices whose diagonal elements are the regular and irregular Coulomb wave functions, defined, respectively, by (1.58) and (1.59), where $\boldsymbol{\eta} = -(Z-N)/\mathbf{k}$ and $\mathbf{K}$ is the $n \times n$-dimensional K-matrix.

In order to determine the analytic properties of the K-matrix we proceed, as in our discussion of short-range potentials in Sect. 3.3.1, by relating the K-matrix to the analytic properties of the $n \times n$-dimensional R-matrix $\mathbf{R}(E)$, defined on the boundary $r = a$ by

$$\mathbf{F}(a) = \mathbf{R}(E)\left(a\frac{\mathrm{d}\mathbf{F}}{\mathrm{d}r} - b\mathbf{F}\right)_{r=a}, \tag{3.201}$$

We then set the arbitrary constant $b = 0$ in (3.201) and substitute the expression for $\mathbf{F}(a)$ given by (3.200) into (3.201). After re-arranging terms and using the Wronskian relation $\mathbf{F}'_\ell\mathbf{G}_\ell - \mathbf{G}'_\ell\mathbf{F}_\ell = \mathbf{I}$ we obtain

$$\mathbf{K}^{-1} = -\frac{\mathbf{G}_\ell}{\mathbf{F}_\ell} + \frac{\mathbf{I}}{\mathbf{F}'_\ell\mathbf{F}_\ell} + \boldsymbol{\rho}^{-1/2}\mathbf{F}'^{-1}_\ell\left(\mathbf{R}(E) - \boldsymbol{\rho}^{-1}\frac{\mathbf{F}_\ell}{\mathbf{F}'_\ell}\right)^{-1}\mathbf{F}'^{-1}_\ell\boldsymbol{\rho}^{-1/2}, \tag{3.202}$$

where the diagonal matrix $\boldsymbol{\rho} = \mathbf{k}a$ and the diagonal matrices $\mathbf{F}_\ell$, $\mathbf{F}'_\ell$, $\mathbf{G}_\ell$ and $\mathbf{G}'_\ell$ are defined by

$$\mathbf{F}_\ell = \mathbf{F}_\ell(\boldsymbol{\eta}, \mathbf{k}a), \quad \mathbf{G}_\ell = \mathbf{G}_\ell(\boldsymbol{\eta}, \mathbf{k}a), \quad \mathbf{F}'_\ell = \frac{1}{\mathbf{k}}\frac{\mathrm{d}\mathbf{F}_\ell}{\mathrm{d}r}\bigg|_{r=a}, \quad \mathbf{G}'_\ell = \frac{1}{\mathbf{k}}\frac{\mathrm{d}\mathbf{G}_\ell}{\mathrm{d}r}\bigg|_{r=a}. \tag{3.203}$$

We see that (3.202) has the same form as (3.160) obtained for short-range potentials and (3.175) obtained for dipole potentials. Hence, as in those cases, the analytic properties of the K-matrix in the complex energy plane can be obtained in terms of the analytic properties of the matrices $\mathbf{F}_\ell$, $\mathbf{F}'_\ell$ and $\mathbf{G}_\ell$ together with those of the R-matrix $\mathbf{R}(E)$.

The analytic properties of the Coulomb wave functions have been described in our development of an effective range expansion for potential scattering by a Coulomb potential in Sect. 1.4.3 and are given by (1.175) and the following equations. Using these results, we find that (3.202) yields the following multichannel effective range expression for the T-matrix:

$$\mathbf{T} = \mathbf{k}^{\ell+\frac{1}{2}}(2\boldsymbol{\ell}+\mathbf{I})!!\mathbf{C}_\ell(\boldsymbol{\eta})\frac{2\mathrm{i}}{\mathbf{M}(E) - \mathbf{k}^{2\ell+1}[(2\boldsymbol{\ell}+\mathbf{I})!!]^2\mathbf{p}_\ell(\boldsymbol{\eta})\boldsymbol{\tau}(2\boldsymbol{\ell}+\mathbf{I})^{-1}} \times \mathbf{C}_\ell(\boldsymbol{\eta})(2\boldsymbol{\ell}+\mathbf{I})!!\,\mathbf{k}^{\ell+\frac{1}{2}}, \tag{3.204}$$

where $\mathbf{C}_\ell(\boldsymbol{\eta})$, $\mathbf{p}_\ell(\boldsymbol{\eta})$ and $\boldsymbol{\tau}$ are diagonal matrices whose diagonal elements are defined by (1.60), (1.179) and (1.185), respectively. We can then show that the M-matrix in (3.204) is given by

$$\mathbf{M}(E) = \frac{(2\boldsymbol{\ell}+\mathbf{I})!!}{a^{\boldsymbol{\ell}+\frac{1}{2}}}\left\{-\frac{\boldsymbol{\Psi}_{\boldsymbol{\ell}}}{(2\boldsymbol{\ell}+\mathbf{I})\boldsymbol{\Phi}_{\boldsymbol{\ell}}} - \frac{\mathbf{k}^{2\boldsymbol{\ell}+1}\mathbf{p}_{\boldsymbol{\ell}}(\boldsymbol{\eta})a^{2\boldsymbol{\ell}+1}}{(2\boldsymbol{\ell}+\mathbf{I})}\right.$$
$$\times\left[\ln 2a + \frac{\mathbf{q}_{\boldsymbol{\ell}}(\boldsymbol{\eta})}{\mathbf{p}_{\boldsymbol{\ell}}(\boldsymbol{\eta})} - f(\boldsymbol{\eta})\right] + \frac{1}{\boldsymbol{\Phi}_{\boldsymbol{\ell}}\overline{\boldsymbol{\Phi}}_{\boldsymbol{\ell}}} - \frac{1}{\overline{\boldsymbol{\Phi}}_{\boldsymbol{\ell}}}\left[\frac{\boldsymbol{\Phi}_{\boldsymbol{\ell}}}{\overline{\boldsymbol{\Phi}}_{\boldsymbol{\ell}}} - \mathbf{R}(E)\right]\frac{1}{\overline{\boldsymbol{\Phi}}_{\boldsymbol{\ell}}}\Bigg\}$$
$$\times \frac{(2\boldsymbol{\ell}+\mathbf{I})!!}{a^{\boldsymbol{\ell}+\frac{1}{2}}}, \tag{3.205}$$

where

$$\overline{\boldsymbol{\Phi}}_{\boldsymbol{\ell}} = (\boldsymbol{\ell}+\mathbf{I})\boldsymbol{\Phi}_{\boldsymbol{\ell}} + a\frac{\mathrm{d}\boldsymbol{\Phi}_{\boldsymbol{\ell}}}{\mathrm{d}r}\bigg|_{r=a}. \tag{3.206}$$

Also in (3.205) we have written $\boldsymbol{\Phi}_{\boldsymbol{\ell}} \equiv \boldsymbol{\Phi}_{\boldsymbol{\ell}}(\boldsymbol{\eta}, \mathbf{k}a)$, $\boldsymbol{\Psi}_{\boldsymbol{\ell}} \equiv \boldsymbol{\Psi}_{\boldsymbol{\ell}}(\boldsymbol{\eta}, \mathbf{k}a)$ and $\overline{\boldsymbol{\Phi}}_{\boldsymbol{\ell}} \equiv \overline{\boldsymbol{\Phi}}_{\boldsymbol{\ell}}(\boldsymbol{\eta}, \mathbf{k}a)$, which are diagonal matrices whose diagonal elements Φ_ℓ, Ψ_ℓ and $\overline{\Phi}_\ell$ are entire functions of the energy. It follows from (3.205) that the M-matrix $\mathbf{M}(E)$ is a symmetric matrix which is real on the real energy axis and which is an analytic function of energy without threshold branch cuts. Hence $\mathbf{M}(E)$ can be expanded as a power series in energy

$$\mathbf{M}(E) = \mathbf{M}_0 + \mathbf{M}_1 E + \mathbf{M}_2 E^2 + \cdots, \tag{3.207}$$

where $\mathbf{M}_0, \mathbf{M}_1, \mathbf{M}_2, \ldots$ are real symmetric energy-independent matrices.

The multichannel effective range equation (3.204) was first derived by Gailitis [357]. We can show that it reduces to (1.187) for single-channel scattering by a Coulomb potential and to (3.163), obtained by Ross and Shaw [798], for multichannel scattering by short-range potentials. It follows that (3.204) enables the T-matrix to be extrapolated through thresholds, relating the cross sections above and below thresholds.

3.3.3.2 Cross Sections Near Threshold

We now obtain an equation relating the T-matrix and the cross sections above and below threshold for scattering by an attractive long-range Coulomb potential. We consider processes involving n coupled channels, corresponding to a given set of conserved quantum numbers, where the target states included are ordered in increasing energy so that (2.78) is satisfied. We determine the behaviour of the cross sections in the neighbourhood of the nth or highest threshold which we assume is non-degenerate.

We commence by observing that the M-matrix $\mathbf{M}(E)$ and the quantity $\mathbf{k}^{2\boldsymbol{\ell}+1}\mathbf{p}_{\boldsymbol{\ell}}(\boldsymbol{\eta})$ in (3.204) are analytic through the thresholds. We then obtain the following relation by evaluating (3.204) just above and just below the nth threshold

$$\left[\boldsymbol{\tau} + \mathrm{i}\mathbf{C}_0(\boldsymbol{\eta})\boldsymbol{\eta}^{-1/2}\mathbf{T}^{-1}\boldsymbol{\eta}^{-1/2}\mathbf{C}_0(\boldsymbol{\eta})\right]^a = \left[\boldsymbol{\tau} + \mathrm{i}\mathbf{C}_0(\boldsymbol{\eta})\boldsymbol{\eta}^{-1/2}\mathbf{T}^{-1}\boldsymbol{\eta}^{-1/2}\mathbf{C}_0(\boldsymbol{\eta})\right]^b. \tag{3.208}$$

The superscript a in (3.208) and later equations means that the quantity is evaluated in the limit $k_n^2 \to 0$ from above the nth threshold and the superscript b in this and later equations means that the quantity is evaluated in the limit $k_n^2 \to 0$ from below the nth threshold.

In order to relate $\mathbf{T}^a$ and $\mathbf{T}^b$ using (3.208) we consider the behaviour of the diagonal matrices $\mathbf{C}_0(\boldsymbol{\eta})\boldsymbol{\eta}^{-1/2}$ and $\boldsymbol{\tau}$ in the neighbourhood of the nth threshold. It follows from (1.61) that the first $(n-1)$ diagonal elements of $\mathbf{C}_0(\boldsymbol{\eta})\boldsymbol{\eta}^{-1/2}$ are continuous at the nth threshold. However, while the nth diagonal element is smoothly varying above this threshold, where the limit at threshold is

$$\left(\mathbf{C}_0^2(\boldsymbol{\eta})\boldsymbol{\eta}^{-1/2}\right)^a = -2\pi, \tag{3.209}$$

it is rapidly oscillating and discontinuous below this threshold. Also, it follows from (1.190) and (1.191) that while the first $(n-1)$ diagonal elements of the matrix $\boldsymbol{\tau}$ are continuous at the nth threshold, the nth diagonal element is discontinuous at this threshold. We find that

$$\tau_{jj}^a - \tau_{jj}^b = 0, \quad j = 1, \ldots, n-1 \tag{3.210}$$

and

$$\tau_{nn}^a - \tau_{nn}^b = -\mathrm{i}\pi - \pi \cot \frac{\pi z}{\kappa_n}. \tag{3.211}$$

Substituting these results into (3.208) and solving for the matrix $\mathbf{T}^b$, we find that the elements of the first $(n-1) \times (n-1)$ sub-matrix of $\mathbf{T}^b$ are given in terms of the $n \times n$ matrix $\mathbf{T}^a$ by

$$T_{jk}^b = \left[\left(\mathbf{T}^a\right)^{-1} - \boldsymbol{\Delta}\right]_{jk}^{-1}, \quad j,\ k = 1, \ldots, n-1, \tag{3.212}$$

where the only non-zero element of $\boldsymbol{\Delta}$ is

$$\Delta_{nn} = \frac{1}{2}\mathrm{i}\left(\cot \frac{\pi z}{\kappa_n} + \mathrm{i}\right) \equiv \frac{1}{2}\mathrm{i}(y + \mathrm{i}), \tag{3.213}$$

which defines y. On the right-hand side of (3.212), the inverse of the full $n \times n$ matrix $\left[(\mathbf{T}^a)^{-1} - \boldsymbol{\Delta}\right]$ is first determined, and then the $(n-1) \times (n-1)$ sub-matrix elements of this inverse matrix are equated to the $(n-1) \times (n-1)$ matrix elements on the left-hand side of (3.212). Owing to the special form of the matrix $\boldsymbol{\Delta}$, defined by (3.213), we can determine the inverse of $\left[(\mathbf{T}^a)^{-1} - \boldsymbol{\Delta}\right]$ explicitly in terms of the matrix elements of $\mathbf{T}^a$ and $\boldsymbol{\Delta}$. We find that (3.212) can be rewritten as

$$T_{jk}^b = T_{jk}^a - \frac{T_{jn}^a\, T_{kn}^a}{T_{nn}^a} + \frac{T_{jn}^a\, T_{kn}^a}{T_{nn}^a} \frac{2\mathrm{i}}{(y+\mathrm{i})\, T_{nn}^a + 2\mathrm{i}}, \quad j,\ k = 1, \ldots, n-1. \tag{3.214}$$

This equation expresses the T-matrix elements T^b_{jk} below threshold in terms of the slowly varying T-matrix elements T^a_{jk} above threshold, which can be taken to have their threshold values. We can see that the T-matrix elements below threshold are rapidly varying because of the factor $y = \cot(\pi z/\kappa_n)$, which has the same value at energies for which z/κ_n differs by an integer. By comparing (3.214) with (3.126) we see that the last term in (3.214) gives rise to a Rydberg series of resonances as $k_n^2 = -\kappa_n^2 \to 0$ from below the nth threshold. We can also show that the corresponding resonance widths Γ are related to the distances D between resonances by the expression

$$\frac{\Gamma}{D} = \frac{1}{2\pi}\left(2\mathrm{Re}\, T^a_{nn} - |T^a_{nn}|^2\right) = \frac{1}{2\pi}\sum_{j=1}^{n-1}|T^a_{jn}|^2, \tag{3.215}$$

which is constant for all resonances in the series.

We can also obtain a relation between the cross sections above and below the nth threshold. We observe that the resonances become very close together as we approach the nth threshold from below. Hence the quantity of interest just below the threshold is the partial wave cross section averaged over resonances, defined by

$$\overline{\sigma}(j \to k) = \frac{1}{D}\int_{E-D/2}^{E+D/2}\sigma(j \to k)\mathrm{d}E = \frac{1}{\pi}\int_{-\infty}^{\infty}\sigma(j \to k)\frac{\mathrm{d}y}{1+y^2}, \tag{3.216}$$

where the cross section is defined in terms of the T-matrix by (2.132) for non-relativistic collisions and by (5.129) for heavy ionic targets where relativistic effects become important. Using (3.214) and (3.216) we obtain the following expression relating the partial wave cross sections above and below the nth threshold:

$$\overline{\sigma}^b(j \to k) = \sigma^a(j \to k) + \frac{\sigma^a(j \to n)\,\sigma^a(n \to k)}{\sum_{k'=1}^{n-1}\sigma^a(n \to k')}, \quad j,\ k = 1, \ldots, n-1. \tag{3.217}$$

We see from this expression that the averaged cross sections below the nth threshold decrease abruptly at the threshold as the energy increases through this threshold. We also see that the total cross section, obtained by summing (3.217) over k, the open channels below the nth threshold, gives

$$\sum_{k=1}^{n-1}\overline{\sigma}^b(j \to k) = \sum_{k=1}^{n-1}\sigma^a(j \to k) + \sigma^a(j \to n), \quad j,\ k = 1, \ldots, n-1. \tag{3.218}$$

Hence, the total partial wave cross section is continuous across the nth threshold for all initial states. Also, the total cross section, obtained by summing over all conserved quantum numbers, is continuous across thresholds. The continuity of the

total cross section across a new threshold was first proved by Baz [83] and by Fonda and Newton [336, 337] by averaging the imaginary part of the scattering amplitude, which is related to the total cross section through the optical theorem.

The above theory has been generalized by Gailitis [357] to the situation where several degenerate channels open at the highest threshold. This occurs, for example, when several degenerate channels are coupled to a target state with non-zero angular momentum. When the cross sections for excitation of target states belonging to the highest threshold are small, corresponding to narrow resonances below this threshold, then the generalization of (3.217) can be written as follows:

$$\overline{\sigma}^b(j \to k) = \sigma^a(j \to k) + \sum_l \frac{\sigma^a(j \to l)\, \sigma^a(l \to k)}{\sum_{k'} \sigma^a(l \to k')}. \tag{3.219}$$

In this equation, j and k correspond to the channels which are open below the highest degenerate threshold, k' is summed over the open channels below this threshold and l is summed over the degenerate channels corresponding to the highest threshold. Hence, as in the case of one threshold channel, the averaged cross sections below the highest degenerate threshold decreases abruptly as the energy increases through this threshold. Also, we find by summing (3.219) over k, corresponding to the open channels below the highest degenerate threshold, that as in (3.218) the total cross section is continuous across this threshold. Again, this result can be obtained by averaging the imaginary part of the scattering amplitude.

Finally, the application of R-matrix theory in the analysis of the behaviour of electron–ion collision cross sections in the neighbourhood of thresholds has also been considered by Lane [565]. In this work the relationship with multichannel quantum defect theory, reviewed in the next section, was discussed.

3.3.4 Multichannel Quantum Defect Theory

In this section we conclude our discussion of the threshold behaviour of excitation cross sections by considering electron collisions with multi-electron positive ions using multichannel quantum defect theory (MQDT) introduced and developed by Seaton [851, 852, 854–856, 858] who also comprehensively reviewed this theory [859]. We then summarize some of the most important developments in the application of MQDT to molecular collision processes.

In our discussion of atomic MQDT it is convenient to introduce z-scaled radial and energy variables defined by

$$\rho = zr, \quad \epsilon = \frac{2E}{z^2}, \tag{3.220}$$

where $z = Z - N$ is the ionic charge, Z being the nuclear charge number and N the number of target electrons. Also, in (3.220), E is the energy of the colliding electron

in atomic units. It is also convenient to define the z-scaled wave number k and the quantity ν^2 by the equations

$$k^2 = \epsilon, \quad \epsilon \geq 0\,; \qquad \epsilon = -\frac{1}{\nu^2}, \quad \epsilon < 0. \tag{3.221}$$

The radial Schrödinger equation describing single-channel electron–ion collisions in the external region $r \geq a$, when the local direct, non-local exchange and non-local correlation potentials are negligible, then becomes

$$\left(\frac{\mathrm{d}^2}{\mathrm{d}\rho^2} - \frac{\ell(\ell+1)}{\rho^2} + \frac{2}{\rho} + \epsilon\right) G(\rho) = 0, \quad \rho \geq za. \tag{3.222}$$

It is clear that (3.199) reduces to (3.222) when only one channel is coupled, where we have written $F(r) \equiv G(\rho)$.

Functions f, g and h which are solutions of (3.222) have been defined by Ham [440] and Seaton [859]. The functions f and g are analytic functions of energy through threshold such that

$$f(\epsilon, \ell; \rho) = \sum_{n=0}^{\infty} \epsilon^n f_n(\ell; \rho), \quad g(\epsilon, \ell; \rho) = \sum_{n=0}^{\infty} \epsilon^n g_n(\ell; \rho). \tag{3.223}$$

Also the function h can be written as

$$h = -(g + \mathcal{G} f), \tag{3.224}$$

where $\mathcal{G}$ is defined by the asymptotic expansion

$$\mathcal{G}(\epsilon, \ell) = \frac{\epsilon A(\epsilon, \ell)}{\pi} \left[\sum_{p=0}^{\ell} \frac{p}{1 + p^2\epsilon} + \frac{1}{12}\left(1 + \frac{\epsilon}{10} + \frac{\epsilon^2}{21} + \frac{\epsilon^3}{20} + \cdots\right)\right], \tag{3.225}$$

with

$$A(\epsilon, \ell) = \prod_{p=0}^{\ell} (1 + p^2\epsilon). \tag{3.226}$$

For small ϵ, a good approximation for $\mathcal{G}$ is obtained by retaining a finite number of terms in the expansion in powers of ϵ. Hence $\mathcal{G}$ and thus h are "nearly analytic functions" of ϵ. The asymptotic forms of the functions f and h when $\epsilon \geq 0$ are given by

$$f(\epsilon, \ell; \rho) \underset{\rho \to \infty}{\sim} \left(\frac{2}{\pi k}\right)^{1/2} \left(\frac{1 - \exp(-2\pi/k)}{A(k^2, \ell)}\right)^{1/2} \sin\theta \tag{3.227}$$

and

$$h(\epsilon, \ell; \rho) \underset{\rho\to\infty}{\sim} \left(\frac{2}{\pi k}\right)^{1/2} \left(\frac{A(k^2, \ell)}{1 - \exp(-2\pi/k)}\right)^{1/2} \cos\theta, \tag{3.228}$$

where

$$\theta = k\rho - \frac{1}{2}\ell\pi + \frac{1}{k}\ln(2k\rho) + \arg\Gamma(\ell + 1 - \mathrm{i}/k). \tag{3.229}$$

The asymptotic forms of the functions f and h when $\epsilon < 0$ are given by

$$f(\epsilon, \ell; \rho) \underset{\rho\to\infty}{\sim} (-1)^\ell \nu^{\ell+1} \left(\frac{\sin(\pi\nu)\Gamma(\nu - \ell)}{\pi}\xi - \frac{\cos(\pi\nu)}{\Gamma(\nu + \ell + 1)}\theta\right) \tag{3.230}$$

and

$$h(\epsilon, \ell; \rho) \underset{\rho\to\infty}{\sim} (-1)^\ell \nu^{\ell+1} A(\epsilon, \ell) \left(\frac{\cos(\pi\nu)\Gamma(\nu - \ell)}{\pi}\xi + \frac{\sin(\pi\nu)}{\Gamma(\nu + \ell + 1)}\theta\right), \tag{3.231}$$

where

$$\xi(\epsilon, \rho) \underset{\rho\to\infty}{\sim} \left(\frac{2\rho}{\nu}\right)^{-\nu} \exp\left(\frac{\rho}{\nu}\right), \quad \theta(\epsilon, \rho) \underset{\rho\to\infty}{\sim} \left(\frac{2\rho}{\nu}\right)^{\nu} \exp\left(-\frac{\rho}{\nu}\right). \tag{3.232}$$

We now use the analytic properties of the functions f and h to derive MQDT equations relating the K-matrix and the S-matrix above and below thresholds. We first observe that the n coupled second-order integrodifferential equations (3.2) reduce to (3.199) when $r \geq a$. Also, we adopt the normalization defined by (3.200) for the solutions which vanish at the origin. When all the channels are open the general solution of (3.2), which defines the $n \times n$-dimensional K-matrix, can then be written as follows:

$$\mathbf{F}(r) = \left(\frac{\pi}{2z}\right)^{1/2} [\mathbf{f} + \mathbf{hK}], \quad r \geq a, \tag{3.233}$$

where $\mathbf{f}$ and $\mathbf{h}$ are diagonal $n \times n$-dimensional matrices, whose diagonal elements have the asymptotic forms defined by (3.227) and (3.228).

We now consider the solution of (3.2) when n_a channels are open and n_b channels are closed, where $n = n_a + n_b$. We can analytically continue the solution defined by (3.233) to this energy region yielding the solution

$$\boldsymbol{\mathcal{F}}(r) = \left(\frac{\pi}{2z}\right)^{1/2} [\mathbf{f} + \mathbf{h}\boldsymbol{\mathcal{K}}], \quad r \geq a, \tag{3.234}$$

where, in the n_b closed channels, the corresponding diagonal elements of $\mathbf{f}$ and $\mathbf{h}$ now have the asymptotic forms defined by (3.230) and (3.231), respectively. Also the $n \times n$-dimensional K-matrix $\mathcal{K}$ in (3.234) is the analytic continuation of the physical K-matrix, defined by (3.233). However, because the functions $\mathbf{f}$ and $\mathbf{h}$ in (3.234) now diverge exponentially in the closed channels, because of the ξ terms in (3.230) and (3.231), the corresponding solution, and hence the K-matrix $\mathcal{K}$, is non-physical.

In order to obtain physical solutions when n_a channels are open, we take linear combinations of the n solutions defined by (3.234), which eliminate the exponentially diverging terms in the closed channels. Hence we write

$$\mathcal{F}(r)\mathbf{C} = \left(\frac{\pi}{2z}\right)^{1/2} [\mathbf{f} + \mathbf{h}\mathcal{K}]\mathbf{C}, \quad r \geq a, \tag{3.235}$$

where $\mathbf{C}$ is an $n \times n_a$-dimensional matrix and where the matrices $\mathcal{F}$, $\mathcal{K}$ and $\mathbf{C}$ are partitioned into open- and closed-channel sub-matrices as follows:

$$\mathcal{F} \equiv \begin{bmatrix} \mathcal{F}_{oo} & \mathcal{F}_{oc} \\ \mathcal{F}_{co} & \mathcal{F}_{cc} \end{bmatrix}, \quad \mathcal{K} \equiv \begin{bmatrix} \mathcal{K}_{oo} & \mathcal{K}_{oc} \\ \mathcal{K}_{co} & \mathcal{K}_{cc} \end{bmatrix}, \quad \mathbf{C} \equiv \begin{bmatrix} \mathbf{C}_{oo} \\ \mathbf{C}_{co} \end{bmatrix}. \tag{3.236}$$

The $n_a \times n_a$-dimensional open-channel sub-matrix of $\mathcal{F}(r)\mathbf{C}$ is then

$$[\mathcal{F}(r)\mathbf{C}]_{oo} \equiv \left(\frac{\pi}{2z}\right)^{1/2} [(\mathbf{f}_o + \mathbf{h}_o\mathcal{K}_{oo})\mathbf{C}_{oo} + \mathbf{h}_o\mathcal{K}_{oc}\mathbf{C}_{co}], \tag{3.237}$$

and the $n_b \times n_a$-dimensional closed-channel sub-matrix of $\mathcal{F}(r)\mathbf{C}$ is

$$[\mathcal{F}(r)\mathbf{C}]_{co} \equiv \left(\frac{\pi}{2z}\right)^{1/2} [\mathbf{h}_c\mathcal{K}_{co}\mathbf{C}_{oo} + (\mathbf{f}_c + \mathbf{h}_c\mathcal{K}_{cc})\mathbf{C}_{co}], \tag{3.238}$$

where in these equations $\mathbf{f}_o$ and $\mathbf{h}_o$ are the diagonal open-channel components of $\mathbf{f}$ and $\mathbf{h}$, and $\mathbf{f}_c$ and $\mathbf{h}_c$ are the diagonal closed-channel components of $\mathbf{f}$ and $\mathbf{h}$, respectively. We then choose $\mathbf{C}_{oo} = \mathbf{I}_{oo}$, where $\mathbf{I}_{oo}$ is the $n_a \times n_a$-dimensional unit matrix, so that the matrix multiplying $\mathbf{f}_o$ in $[\mathcal{F}(r)\mathbf{C}]_{oo}$ is diagonal and we choose the $\mathbf{C}_{co}$ so that the divergent terms in $[\mathcal{F}(r)\mathbf{C}]_{co}$ involving ξ, which arise in $\mathbf{f}_c$ and $\mathbf{h}_c$ defined by (3.230) and (3.231), are eliminated. This last condition yields

$$\mathbf{A}\cos(\pi\nu_c)\mathcal{K}_{co}\mathbf{C}_{oo} + [\sin(\pi\nu_c) + \mathbf{A}\cos(\pi\nu_c)\mathcal{K}_{cc}]\,\mathbf{C}_{co} = 0. \tag{3.239}$$

After setting $\mathbf{A} = \mathbf{I}$, which we see from (3.226) is valid in the neighbourhood of threshold, we find that

$$\mathbf{C}_{co} = -\frac{1}{\mathcal{K}_{cc} + \tan(\pi\boldsymbol{\nu}_c)}\mathcal{K}_{co}, \tag{3.240}$$

where $\boldsymbol{\nu}_c$ is an $n_b \times n_b$-dimensional diagonal matrix in the closed channels, whose diagonal elements are defined by (3.221). It follows that we can write

$$[\boldsymbol{\mathcal{F}}(r)\mathbf{C}]_{oo} = \left(\frac{\pi}{2z}\right)^{1/2} [\mathbf{f}_o + \mathbf{h}_o \mathbf{K}_{oo}], \quad r \geq a, \tag{3.241}$$

where

$$\mathbf{K}_{oo} = \boldsymbol{\mathcal{K}}_{oo} - \boldsymbol{\mathcal{K}}_{oc} \frac{1}{\boldsymbol{\mathcal{K}}_{cc} + \tan(\pi \boldsymbol{\nu}_c)} \boldsymbol{\mathcal{K}}_{co}. \tag{3.242}$$

The $n_a \times n_a$-dimensional K-matrix $\mathbf{K}_{oo}$ defined by (3.242) is the physical K-matrix in the open channels, which can be used to determine the S-matrix, T-matrix and cross sections, as described in Sect. 2.5. We see that it is expressed in terms of the elements of the $n \times n$-dimensional non-physical K-matrix $\boldsymbol{\mathcal{K}}$ which can be analytically continued through thresholds.

We can obtain a similar expression for the $n_a \times n_a$-dimensional S-matrix $\mathbf{S}_{oo}$. When all channels are open the $n \times n$-dimensional physical S-matrix is defined in analogy with (3.233) by

$$\mathbf{G}(r) = \left(\frac{\pi}{2z}\right)^{1/2} [(\mathbf{h} - \mathrm{i}\mathbf{f}) - (\mathbf{h} + \mathrm{i}\mathbf{f})\mathbf{S}], \quad r \geq a, \tag{3.243}$$

where it follows from (3.227) and (3.228) that $(\mathbf{h} - \mathrm{i}\mathbf{f})$ and $(\mathbf{h} + \mathrm{i}\mathbf{f})$ are ingoing and outgoing waves, respectively. We now analytically continue the solution, defined by (3.243) to an energy region where n_a channels are open and n_b channels are closed, yielding in analogy with (3.234) the solution

$$\boldsymbol{\mathcal{G}}(r) = \left(\frac{\pi}{2z}\right)^{1/2} [(\mathbf{h} - \mathrm{i}\mathbf{f}) - (\mathbf{h} + \mathrm{i}\mathbf{f})\boldsymbol{\chi}], \quad r \geq a, \tag{3.244}$$

where the $n \times n$-dimensional unphysical S-matrix $\boldsymbol{\chi}$ is the analytic continuation of the physical S-matrix defined by (3.243). In order to obtain the physical solution when n_a channels are open, we take linear combinations of the n solutions defined by (3.244) which eliminate the exponentially diverging terms in the closed channels. Hence we write

$$\boldsymbol{\mathcal{G}}(r)\mathbf{D} = \left(\frac{\pi}{2z}\right)^{1/2} [(\mathbf{h} - \mathrm{i}\mathbf{f}) - (\mathbf{h} + \mathrm{i}\mathbf{f})\boldsymbol{\chi}]\,\mathbf{D}, \quad r \geq a, \tag{3.245}$$

where $\mathbf{D}$ is an $n \times n_a$-dimensional matrix. We then partition $\boldsymbol{\mathcal{G}}$, $\boldsymbol{\chi}$ and $\mathbf{D}$ into open- and closed-channel sub-matrices as follows:

$$\boldsymbol{\mathcal{G}} \equiv \begin{bmatrix} \boldsymbol{\mathcal{G}}_{oo} & \boldsymbol{\mathcal{G}}_{oc} \\ \boldsymbol{\mathcal{G}}_{co} & \boldsymbol{\mathcal{G}}_{cc} \end{bmatrix}, \quad \boldsymbol{\chi} \equiv \begin{bmatrix} \boldsymbol{\chi}_{oo} & \boldsymbol{\chi}_{oc} \\ \boldsymbol{\chi}_{co} & \boldsymbol{\chi}_{cc} \end{bmatrix}, \quad \mathbf{D} \equiv \begin{bmatrix} \mathbf{D}_{oo} \\ \mathbf{D}_{co} \end{bmatrix}. \tag{3.246}$$

The $n_a \times n_a$-dimensional open-channel sub-matrix of $\mathcal{G}(r)\mathbf{D}$ is then

$$[\mathcal{G}(r)\mathbf{D}]_{oo} \equiv \left(\frac{\pi}{2z}\right)^{1/2} \left\{\left[(\mathbf{h}_o - \mathrm{i}\mathbf{f}_o) - (\mathbf{h}_o + \mathrm{i}\mathbf{f}_o)\boldsymbol{\chi}_{oo}\right]\mathbf{D}_{oo} - \left[(\mathbf{h}_o + \mathrm{i}\mathbf{f}_o)\boldsymbol{\chi}_{oc}\right]\mathbf{D}_{co}\right\}, \tag{3.247}$$

and the $n_b \times n_a$-dimensional closed-channel sub-matrix of $\mathcal{G}(r)\mathbf{D}$ is

$$[\mathcal{G}(r)\mathbf{D}]_{co} \equiv \left(\frac{\pi}{2z}\right)^{1/2} \left\{-\left[(\mathbf{h}_c + \mathrm{i}\mathbf{f}_c)\boldsymbol{\chi}_{co}\right]\mathbf{D}_{oo} + [(\mathbf{h}_c - \mathrm{i}\mathbf{f}_c) - (\mathbf{h}_c + \mathrm{i}\mathbf{f}_c)\boldsymbol{\chi}_{cc}\right]\mathbf{D}_{co}\right\}. \tag{3.248}$$

We then choose $\mathbf{D}_{oo} = \mathbf{I}_{oo}$ so that the matrix multiplying $(\mathbf{h}_o - \mathrm{i}\mathbf{f}_o)$ in $[\mathcal{G}(r)\mathbf{D}]_{oo}$ is diagonal, and we choose $\mathbf{D}_{co}$ so that the divergent terms in $[\mathcal{G}(r)\mathbf{D}]_{co}$ involving ξ, defined by (3.232), are eliminated. This yields

$$\mathbf{D}_{co} = -\frac{1}{\boldsymbol{\chi}_{cc} - \exp(-2\pi\mathrm{i}\boldsymbol{\nu}_c)}\boldsymbol{\chi}_{co}. \tag{3.249}$$

It follows that we can write

$$[\mathcal{G}(r)\mathbf{D}]_{oo} = \left(\frac{\pi}{2z}\right)^{1/2} [(\mathbf{h} - \mathrm{i}\mathbf{f}) - (\mathbf{h} + \mathrm{i}\mathbf{f})\mathbf{S}_{oo}] \ , \quad r \geq a, \tag{3.250}$$

where

$$\mathbf{S}_{oo} = \boldsymbol{\chi}_{oo} - \boldsymbol{\chi}_{oc}\frac{1}{\boldsymbol{\chi}_{cc} - \exp(-2\pi\mathrm{i}\boldsymbol{\nu}_c)}\boldsymbol{\chi}_{co}. \tag{3.251}$$

The $n_a \times n_a$-dimensional matrix $\mathbf{S}_{oo}$ defined by (3.251) is the physical S-matrix in the open channels, which enables the cross sections to be determined, as described in Sect. 2.5. We see that it is expressed in terms of the elements of the non-physical S-matrix $\boldsymbol{\chi}$, which can be analytically continued through the thresholds.

Equation (3.251) can be obtained directly from the $n \times n$-dimensional non-physical K-matrix $\mathcal{K}$, defined by (3.234). In the energy region where n_a channels are open we define an $n \times n$-dimensional matrix $\boldsymbol{\mathcal{S}}$ by the equation

$$\boldsymbol{\mathcal{S}} = \frac{\mathrm{i}\mathbf{I} - \mathcal{K}}{\mathbf{t} + \mathcal{K}}, \tag{3.252}$$

where $\mathbf{t}$ is an $n \times n$-dimensional diagonal matrix with diagonal elements

$$\begin{aligned} t_{jj} &= \mathrm{i}, \quad \text{open channels} \quad j = 1, \ldots, n_a, \\ t_{jj} &= \tan\pi\nu_j, \quad \text{closed channels} \quad j = n_a + 1, \ldots, n. \end{aligned} \tag{3.253}$$

We then express the non-physical $n \times n$-dimensional K-matrix $\mathcal{K}$ in (3.252) in terms of the non-physical $n \times n$-dimensional S-matrix $\boldsymbol{\chi}$ using the equation

$$\boldsymbol{\chi} = \frac{\mathbf{I} + \mathrm{i}\mathcal{K}}{\mathbf{I} - \mathrm{i}\mathcal{K}}, \tag{3.254}$$

which is the analytic continuation of the usual expression relating the K-matrix to the S-matrix when all channels are open, discussed in Sect. 2.5. Substituting the expression for $\mathcal{K}$ in terms of $\boldsymbol{\chi}$ obtained from (3.254) into the right-hand side of (3.252) and separating out the $n_a \times n_a$-dimensional open-channel component of this equation yields

$$\mathcal{S}_{oo} = \boldsymbol{\chi}_{oo} - \boldsymbol{\chi}_{oc} \frac{1}{\boldsymbol{\chi}_{cc} - \exp(-2\pi \mathrm{i}\boldsymbol{\nu}_c)} \boldsymbol{\chi}_{co}. \tag{3.255}$$

We see that the right-hand sides of (3.251) and (3.255) are identical and hence the open-channel component of $\mathcal{S}$, defined by (3.252) and (3.253), corresponds to the physical S-matrix when n_a channels are open. It follows from this analysis that the open-channel K-matrix and S-matrix can be expressed in terms of matrices $\mathcal{K}$ and $\boldsymbol{\chi}$ which can be analytically continued through thresholds.

In concluding our discussion of atomic MQDT we observe that there have been many applications of this theory following its introduction and development by Seaton. These include a series of early applications to the following atomic collision processes: scattering of electrons by He^+ by Bely [89]; absorption of radiation by Ca atoms by Moores [657]; autoionizing and bound states of neutral beryllium atoms by Moores [658]; extrapolation along isoelectronic sequences by Doughty et al. [268]; resonances in the collision strengths for O^+ by Martins and Seaton [638]; complex quantum defects for the e^-–Be^+ system by Norcross and Seaton [695]; photoionization by Dubau and Wells [273] and complex quantum defects for the e^-–He^+ system by Dubau [272]. This series of papers together with many later papers have established MQDT as an essential component of the analysis of atomic resonance and threshold behaviour.

3.3.4.1 Molecular MQDT

Multichannel quantum defect theory has also been extended to describe resonance and threshold behaviour of electron collisions with positive molecular ions as well as near-threshold molecular photoionization and photoabsorption processes. In the remainder of this section we summarize some of the most important developments in this area.

In the pioneering work on molecular collision processes, Fano [303] extended and applied MQDT to the analysis of high-resolution photoabsorption spectra of H_2 near threshold reported by Herzberg [458] and in two Comments [305, 306] discussed the evolution of quantum defect methods. The work on H_2 was later extended by Jungen and Atabek [517], who developed and applied MQDT to ro-vibronic interactions in the photoabsorption spectrum of H_2 and D_2, and by Jungen

and Dill [518], who studied rotational and vibrational preionization channels of H_2 obtaining good agreement with photoionization data of Dehmer and Chupka [255]. Also, Giusti [376] extended molecular MQDT to describe dissociation into two atoms in electron collisions with molecular ions, and Giusti-Suzor and Jungen [377] adapted molecular MQDT to treat the simultaneous vibrational preionization and electronic predissociation in NO observed in the photoabsorption and photoionization spectra. Jungen [516] also developed a unified MQDT treatment of dissociation and ionization processes which was applied to preionized and predissociated resonances in the H_2 spectrum and Stephans and Greene [887] presented an MQDT procedure to calculate the broadening of preionization resonances due to competing predissociation in the ionization continuum of H_2. A review of the earlier developments and applications of molecular MQDT was written by Greene and Jungen [421]. In more recent work, a non-iterative eigenchannel R-matrix approach combined with MQDT was developed by Gao et al. [360] and applied to predissociation of H_2 and a unified MQDT treatment of both molecular ionization and dissociation was developed by Jungen and Ross [519].

We conclude this section by mentioning a major series of dissociative recombination studies of the triatomic ion H_3^+ which has been carried out by Kokoouline and Greene [543, 544] and by dos Santos et al. [267], and which has been extended by Kokoouline and Greene [544, 545] to dissociative recombination of the triatomic ions D_3^+, H_2D^+ and D_2H^+. We will also consider in Sect. 11.1.7.4 intermediate energy electron–H_3^+ collision calculations carried out using R-matrix theory. Dissociative recombination of H_3^+ ion is a fundamental process in diffuse interstellar clouds and, as the simplest triatomic ion, detailed theoretical studies can be seen as a prototype for the study of electron collisions with more complex polyatomic molecules and molecular ions. Also, in contrast to dissociative attachment/recombination in diatomic molecules and ions there is an additional three-body dissociative pathway for H_3^+ where the molecule dissociates into three hydrogen atoms. The theoretical approach developed by Kokoouline and Greene [543, 544] for treating this process combined MQDT to represent the closed channels, the hyperspherical coordinate approach, discussed in Sect. 3.2.6, to represent the motion of the nuclei and inclusion of outgoing wave Siegert [876] pseudostates to represent the vibrational continuum. These pseudostates, which are analogous to the pseudostates introduced in intermediate-energy collisions in Sects. 6.1 and 6.2, are included to let dissociative flux escape if it reaches the hyper-radial boundary. In the later work by dos Santos et al. [267], accurate vibrational wave functions were used and a large number of rotational states of the H_3^+ ground vibrational state were included in the calculation. This resulted in good agreement with dissociative recombination measurements using the Stockholm (CRYRING) and the Heidelberg (TSR) ion storage rings [734], showing the importance of Jahn–Teller coupling between the electronic and vibrational motion. In conclusion, this work has shown that recent state-of-the-art ab initio calculations on dissociative recombination of simple polyatomic molecules using MQDT and a hyperspherical coordinate representation of the collision process are now capable of accurately describing this complex process.

3.3.5 Threshold Behaviour of Ionization

In this section we consider the threshold behaviour of the single ionization process

$$e^- + A \rightarrow A^+ + e^- + e^-, \tag{3.256}$$

where an electron is incident on a neutral atom or positive ion target which we denote by A and an electron is ejected from the target. The foundations of this subject were laid by Wannier [954] who, using an elegant classical analysis, showed that the ionization cross section $\sigma_{\rm ion}$ satisfies the threshold law

$$\sigma_{\rm ion} = aE^m. \tag{3.257}$$

In this equation a is a constant, E is the sum of the kinetic energies of the two outgoing electrons in (3.256) which is zero at threshold and m is defined by

$$m = \frac{1}{4}\left[\left(\frac{100Z-9}{4Z-1}\right)^{1/2} - 1\right], \tag{3.258}$$

where in this case Z is the residual charge number of the ion denoted by A^+ in (3.256). When $Z = 1$, corresponding to ionization of a neutral atomic target, $m \approx 1.127$ and as the charge number of the ion $Z \rightarrow \infty$ we see from (3.258) that $m \rightarrow 1$. We note that in a later paper Wannier [955] extended the analysis to discuss the threshold law for multiple ionization.

Further developments in the classical theory of single ionization were made by Vinkalns and Gailitis [940], who investigated the dependence of the distribution of the ionization cross section on the angle θ_{12} between the final directions of the two outgoing electrons and found that this distribution has a sharp maximum at $\theta_{12} = \pi$ with a width which tends to zero as $E^{1/4}$ as the energy E tends to zero. The classical analysis was extended by Read [780] to small negative values of E and to study the energy partitioning of the two outgoing electrons in the ionization process using accurate trajectory calculations. Wannier's threshold law of ionization has also been derived using semiclassical theory by Peterkop [728–730] and Crothers [236, 237] and was shown by Rau [776] to follow from the two-electron Schrödinger equation. There have been many other important theoretical and computational investigations including studies by Fano [304], Rau [777], Klar and Schlecht [538], Klar [537], Greene and Rau [419, 420], Feagin [315], Altick [15], Kazansky and Ostrovsky [526], Macek and Ovchinnikov [622], Kato and Watanabe [522–524] and Bartlett and Stelbovics [59]. Experimentally, the validity of Wannier's threshold law was first clearly verified by Cvejanović and Read [239] and other early experiments confirming this law were carried out by Spence [884] and by Pichou et al. [735]. Finally, we mention earlier reviews of threshold behaviour of ionization written by Rau [778] and by Read [781] and a more recent review of collisions near threshold written by Sadeghpour et al. [804].

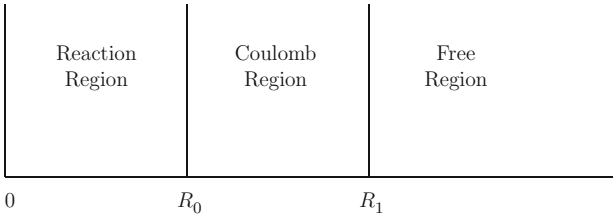

Fig. 3.8 Partitioning of configuration space into three regions in the Wannier theory of threshold ionization

Following Wannier [954], we now derive the threshold law of ionization using a classical analysis. We consider the process represented by (3.256), where the motion of the two electrons in the final state is described using hyperspherical coordinates discussed in Sect. 3.2.6 and defined by (3.128). In Wannier's analysis, configuration space is partitioned into three regions or zones, as illustrated in Fig. 3.8. These are an inner reaction region ($0 \leq R \leq R_0$), an intermediate Coulomb region ($R_0 \leq R \leq R_1$) and an outer free region ($R \geq R_1$). Following the fundamental paper by Wigner [970] on the behaviour of cross sections near threshold, Wannier observed that it is not necessary to know the detailed behaviour of the two electrons taking part in the ionization process in the reaction region. Instead, he assumed that the distribution in phase space of the two electrons is approximately uniform (i.e. quasi-ergodic) when they enter the Coulomb region. Wannier also assumed that for large enough R_0, the Coulomb potential varies sufficiently slowly for classical mechanics to be applicable in the Coulomb region, even when the total energy E of the two outgoing electrons in (3.256) tends to zero. This assumption can be seen to be valid since for a Coulomb potential the local de Broglie wavelength

$$\lambda(R) = \left(2E + \frac{2Z}{R}\right)^{-1/2} \tag{3.259}$$

is slowly varying for large R and the derivative $\mathrm{d}\lambda/\mathrm{d}R$ tends to zero as R tends to infinity. Finally, at very large R, where $R > R_1$, the magnitude of the Coulomb potential energy is less than the combined kinetic energies of the two outgoing electrons, so that these electrons move essentially freely. As $E \to 0$, then the radius $R_1 \to \infty$ and hence the Coulomb region extends to infinity. Hence the threshold behaviour of the ionization cross section is determined by the motion of the two electrons in the Coulomb region.

In order to determine the threshold behaviour of the ionization cross section, we consider the potential function $-C(\alpha, \theta_{12})$ defined by (3.130) and shown in Fig. 3.7. We have already observed that the valleys which occur at $\alpha = 0$ and $\pi/2$ correspond to the electron–nuclear attraction singularities. As a result, when $E \approx 0$ nearly all the classical trajectories end up in one or other of these valleys corresponding to single-electron escape. In order to consider the threshold behaviour of ionization we must consider the behaviour of the trajectories in the neighbourhood of the

saddle point at $\alpha = \pi/4$ and $\theta_{12} = \pi$. Near the saddle point the effective charge $\zeta(\alpha, \theta_{12}) = C(\alpha, \theta_{12})/2$ can be expanded as

$$\zeta(\alpha, \theta_{12}) = \zeta_0 + \frac{1}{2}\zeta_1 \left(\alpha - \frac{\pi}{4}\right)^2 + \frac{1}{8}\zeta_2(\theta_{12} - \pi)^2 + \cdots, \tag{3.260}$$

where

$$\zeta_0 = \frac{4Z - 1}{\sqrt{2}}, \quad \zeta_1 = \frac{12Z - 1}{\sqrt{2}}, \quad \zeta_2 = -\frac{1}{\sqrt{2}}. \tag{3.261}$$

It follows that the motion is stable in θ_{12} but unstable in α at constant R. Clearly, classical trajectories with $\alpha = \pi/4$ and $\theta_{12} = \pi$ lead to double-electron escape since as $R \to \infty$ both r_1 and r_2 tend to infinity.

Following Wannier, we consider the case where the total orbital angular momentum L of the two electrons is equal to zero which dominates the ionization cross section close to threshold. The motion of the electrons can then be described by three variables R, α and θ_{12}. The classical equations of motion then take the form

$$\frac{\mathrm{d}^2 R}{\mathrm{d}t^2} = R\left(\frac{\mathrm{d}\alpha}{\mathrm{d}t}\right)^2 + \frac{1}{4}R\sin^2 2\alpha \left(\frac{\mathrm{d}\theta_{12}}{\mathrm{d}t}\right)^2 - \frac{\zeta}{R^2}, \tag{3.262}$$

$$\frac{\mathrm{d}}{\mathrm{d}t}\left(R^2 \frac{\mathrm{d}\alpha}{\mathrm{d}t}\right) = \frac{1}{2}R^2 \sin 2\alpha \cos 2\alpha \left(\frac{\mathrm{d}\theta_{12}}{\mathrm{d}t}\right)^2 + \frac{1}{R}\frac{\partial \zeta}{\partial \alpha}, \tag{3.263}$$

$$\frac{\mathrm{d}}{\mathrm{d}t}\left(R^2 \sin^2 2\alpha \frac{\mathrm{d}\theta_{12}}{\mathrm{d}t}\right) = \frac{4}{R}\frac{\partial \zeta}{\partial \theta_{12}}, \tag{3.264}$$

and the energy of the system is given by

$$E = \frac{1}{2}\left(\frac{\mathrm{d}R}{\mathrm{d}t}\right)^2 + \frac{1}{2}R^2\left(\frac{\mathrm{d}\alpha}{\mathrm{d}t}\right)^2 + \frac{1}{8}R^2 \sin^2 2\alpha \left(\frac{\mathrm{d}\theta_{12}}{\mathrm{d}t}\right)^2 - \frac{\zeta}{R}. \tag{3.265}$$

We then write

$$\Delta\alpha = \alpha - \frac{\pi}{4} = u_1, \quad \Delta\theta_{12} = \theta_{12} - \pi = u_2, \tag{3.266}$$

and we assume that $\Delta\alpha$ and $\Delta\theta_{12}$ are small quantities. Retaining terms of the same order enables us to write (3.262)–(3.264) in the form

$$\frac{\mathrm{d}^2 R}{\mathrm{d}t^2} = -\frac{\zeta_0}{R} \tag{3.267}$$

and

$$\frac{\mathrm{d}}{\mathrm{d}t}\left(R^2\frac{\mathrm{d}u_i}{\mathrm{d}t}\right)=\frac{\zeta_i u_i}{R},\quad i=1,\ 2, \tag{3.268}$$

where we note that (3.268) are linear uncoupled equations for u_1 and u_2. It follows from (3.265) and (3.267) that the first integral for the velocity is given by

$$\frac{\mathrm{d}R}{\mathrm{d}t}=\left(2E+2\frac{\zeta_0}{R}\right)^{1/2}. \tag{3.269}$$

If we introduce the dimensionless variables

$$\rho=\frac{ER}{\zeta_0},\quad \tau=\frac{E^{3/2}t}{\zeta_0}, \tag{3.270}$$

then (3.268) and (3.269) can be written as

$$\frac{\mathrm{d}}{\mathrm{d}\tau}\left(\rho^2\frac{\mathrm{d}u_i}{\mathrm{d}\tau}\right)=\frac{\zeta_i/\zeta_0}{\rho}u_i,\quad i=1,\ 2 \tag{3.271}$$

and

$$\frac{\mathrm{d}\rho}{\mathrm{d}\tau}=\sqrt{2}\left(1+\frac{1}{\rho}\right)^{1/2}. \tag{3.272}$$

We remark that (3.270), (3.271) and (3.272) imply that the classical orbits are invariant under the transformation

$$R\to aR,\quad E\to a^{-1}E,\quad t\to a^{3/2}t,\quad u_i\to u_i, \tag{3.273}$$

which is sometimes referred to as the "similarity principle" [729, 954]. In particular we see that the quantities u_1 and u_2 depend on E only through the dimensionless variables ρ and τ. We note that the exact classical equations given by (3.262), (3.263) and (3.264) also satisfy this similarity principle.

Equation (3.272) can now be used to rewrite (3.271) in a form such that the independent variable is ρ instead of τ. We find that

$$2\rho(1-\rho)\frac{\mathrm{d}^2u_i}{\mathrm{d}\rho^2}+(3-4\rho)\frac{\mathrm{d}u_i}{\mathrm{d}\rho}=\frac{\zeta_i/\zeta_0}{\rho}u_i,\quad i=1,\ 2. \tag{3.274}$$

Since we are interested in the threshold behaviour $E\to 0$, the situation where $ER\ll\zeta_0$ (i.e. where $\rho\ll 1$) is of particular interest. Equations (3.274) then reduce to

$$\frac{\mathrm{d}^2 u_i}{\mathrm{d}\rho^2} + \frac{3}{2\rho}\frac{\mathrm{d}u_i}{\mathrm{d}\rho} = \frac{\zeta_i/\zeta_0}{2\rho^2} u_i, \quad i = 1,\ 2, \tag{3.275}$$

which have solutions of the form

$$u_1 = c_{11} R^{m_{11}} + c_{12} R^{m_{12}} \tag{3.276}$$

and

$$u_2 = c_{21} R^{m_{21}} + c_{22} R^{m_{22}}, \tag{3.277}$$

where we have reverted to the variable R and where c_{ij} are integration constants. The exponents m_{ij} in (3.276) and (3.277) are given by

$$m_{i1} = -\frac{1}{4} - \frac{1}{2}\mu_i, \quad m_{i2} = -\frac{1}{4} + \frac{1}{2}\mu_i, \quad i = 1,\ 2, \tag{3.278}$$

where

$$\mu_1 = \frac{1}{2}\left(\frac{100Z - 9}{4Z - 1}\right)^{1/2}, \quad \mu_2 = \frac{\mathrm{i}}{2}\left(\frac{9 - 4Z}{4Z - 1}\right)^{1/2}. \tag{3.279}$$

Since $Z \geq 1$ then μ_1 is real and $\geq 5/2$ and μ_2 is imaginary when $1 \leq Z < 9/4$ and is real and less than $1/2$ when $Z \geq 9/4$.

We consider first the dependence of u_2, defined by (3.277), on R and E, where we remember from (3.266) that $u_2 = \Delta\theta_{12}$. For sufficiently small values of E, (3.276) and (3.277) are valid at the inner boundary of the Coulomb region. Now from (3.278) and (3.279) we see that Re $m_{2i} < 0$ when $1/4 < Z < 9/4$ and m_{2i} is real and < 0 when $Z \geq 9/4$, for $i = 1, 2$. Hence when R increases, $\Delta\theta_{12}$ either oscillates with decreasing amplitude or falls off monotonically. This confirms that near threshold the two electrons escape in opposite directions where $\theta_{12} \approx \pi$.

The key equation that enables us to determine the threshold behaviour of ionization is (3.276), where we remember from (3.266) that $u_1 = \Delta\alpha$. We first observe that since μ_1 is real and $\geq 5/2$ when $Z > 1/4$, then m_{11} is real and < 0. Hence as R increases the term $c_{11} R^{m_{11}}$ in (3.276) will tend to zero. On the other hand, m_{12} is always positive and ≥ 1 and hence the term $c_{12} R^{m_{12}}$ will increase as R increases. Therefore, unless restrictions are placed on c_{12} this term will cause u_1 to increase and thus α to move away from the vicinity of $\pi/4$ and to fall into one of the potential wells at $\alpha = 0$ and $\pi/2$ in Fig. 3.7, corresponding to single-electron escape. Hence for ionizing trajectories the coefficient c_{12} must lie in a small interval, namely

$$|c_{12}| \leq c_{\max}, \tag{3.280}$$

where $c_{\max} \to 0$ as $E \to 0$. Moreover, according to the "similarity principle" defined by (3.273), u_1 can only depend on E through ER. We must therefore write

$$c_{12} = d_{12} E^{m_{12}}, \tag{3.281}$$

where d_{12} is a constant. Hence (3.276) becomes

$$u_1 = c_{11} R^{m_{11}} + d_{12} E^{m_{12}} R^{m_{12}}. \tag{3.282}$$

Since, in the neighbourhood of the boundary between the reaction region and the Coulomb region in Fig. 3.8 we have $E \ll Z/R$ we see that for variations of d_{12} of order unity, u_1 will remain small as R increases from R_0.

Wannier calculated the flux of phase space points which corresponds to double-electron escape for constant energy E and a given hyper-radius R. Making use of the quasi-ergodic hypothesis, he showed that this flux does not depend on the hyper-radius and that it varies with energy in the same way as $c_{\max}$. Since this flux is proportional to the total ionization cross section σ_{ion} it follows, using (3.280) and (3.281), that the Wannier threshold law of ionization is given by (3.257) where $m = m_{12}$ is defined by (3.278) and (3.279). Hence we find that m is given by (3.258).

As we pointed out in the introduction to this section, the Wannier threshold law of ionization has been confirmed using both semiclassical and quantum theory derivations. In addition, a number of detailed ab initio quantum theory calculations have been carried out which have provided strong support both for the threshold energy dependence of the ionization cross section and for its angular distribution predicted by Vinkalns and Gailitis [940]. These calculations include (i) an angle–Sturmian basis expansion of the wave function in hyperspherical coordinates by Macek and Ovchinnikov [622], (ii) the representation of hyperspherical channel functions using a smooth-variable-discretization method combined with an R-matrix propagator method by Kato and Watanabe [522–524], (iii) the application of the time-dependent close-coupling method by Colgan et al. [221, 225] and (iv) the use of a propagating exterior complex scaling (PECS) method by Bartlett and Stelbovics [59]. In this last calculation on electron–hydrogen atom ionizing collisions, Bartlett and Stelbovics found that for $L = 0$ singlet scattering $\sigma_{\text{ion}} \propto E^{1.122\pm0.015}$ and $(\pi - \theta_{12})_{\text{FWHM}} \approx 3.0 E^{1/4}$, and for $L = 1$ triplet scattering $\sigma_{\text{ion}} \propto E^{3.36\pm0.02}$, in excellent agreement with classical and semiclassical predictions. Further details of the PECS approach to electron–hydrogen atom collisions have been given by Bartlett [57, 58]. We will return to a discussion of electron impact ionization of atoms and atomic ions, including R-matrix calculations near threshold, when we consider intermediate-energy collisions in Chap. 6.